University of Southern Queensland

Faculty of Health, Engineering & Sciences

Design of a Portable Bushfire Attenuation Fence

Dissertation Submitted By
Bradley Fell

In fulfilment of the requirements of
ENG4111 and ENG4112 Research Project

Towards the degree of
Bachelor of Mechanical Engineering (Hons)

October 2016

Abstract

Bushfires are natural disasters that occur frequently in Australia, and are associated with substantial economic and human costs. Currently, methods of combating bushfire propagation rely predominantly on containment through the use of firebreaks; large open areas devoid of fuel to sustain the fire. However, ignited embers (firebrands) are often carried via wind across these spaces, leading to the fire spreading to the other side. Additionally, accumulation of these firebrands around buildings are responsible for a vast majority of homes destroyed in a bushfire event.

In this project, a novel new approach to preventing firebrand transmission is investigated. Fine aperture wire mesh screen barriers have been demonstrated in laboratory experiments to reduce the transmission of firebrand particles and prevent the subsequent accumulation on and ignition of flammable fuel beds. Therefore, the concept of constructing a large, portable fence comprising of this mesh material is investigated; with determination of required parameters and specifications carried out before a prototype computational design was developed and validated through the use of Finite Element Analysis.

In addition to the development of a preliminary design, an assessment criterion was developed in which the performance of a bushfire attenuation fence design could be evaluated, leading to the ability to qualitatively rank and refine designs based upon factors such as weight per unit length; cost per unit length and assembly time per unit length.

Investigation into the conditions associated with both close proximity to bushfires and the mechanics of their propagation lead to the selection of a maximum design wind speed of 28 m/s (100.8 km/h), a peak design temperature of 500^{o}C and a required fence height of 10 metres.

Feasibility analysis on various assembly and grounding methods lead to the selection of a combination of temporary ground screw anchors and guy wires as method of securing the fence, with the maximum fence span with this configuration being 10 metres.

Detailed design of individual fence components was then carried out, with the final design subjected to FEA validation under the imposed loads and conditions. The results of the final design specified was then evaluated against the assessment criteria developed, with the estimated results being 2.64 tonnes per 100 metres and assembly time estimates of between 25.5 to 38.7 metres per hour depending upon the assumptions used.

University of Southern Queensland
Faculty of Health, Engineering and Sciences
ENG4111/ENG4112 Research Project

Limitations of Use

The Council of the University of Southern Queensland, its Faculty of Health, Engineering & Sciences, and the staff of the University of Southern Queensland, do not accept any responsibility for the truth, accuracy or completeness of material contained within or associated with this dissertation.

Persons using all or any part of this material do so at their own risk, and not at the risk of the Council of the University of Southern Queensland, its Faculty of Health, Engineering & Sciences or the staff of the University of Southern Queensland.

This dissertation reports an educational exercise and has no purpose or validity beyond this exercise. The sole purpose of the course pair entitled “Research Project” is to contribute to the overall education within the student’s chosen degree program. This document, the associated hardware, software, drawings, and other material set out in the associated appendices should not be used for any other purpose: if they are so used, it is entirely at the risk of the user.

University of Southern Queensland
Faculty of Health, Engineering and Sciences
ENG4111/ENG4112 Research Project

Certification of Dissertation

I certify that the ideas, designs and experimental work, results, analyses and conclusions set out in this dissertation are entirely my own effort, except where otherwise indicated and acknowledged.

I further certify that the work is original and has not been previously submitted for assessment in any other course or institution, except where specifically stated.

Name: Brad Fell

Student Number: 0061042222

Signed: _____

Acknowledgements

I would first like to give my sincere gratitude and appreciation to my project supervisor, Dr Ahmad Sharifian, for not only offering me the opportunity to work on this project but also for his generosity with his time throughout the development phase of this project; his guidance has been invaluable to me during the course of the year.

I would also like to thank my parents, in particular my father, Russell Fell and his company Communications and Computer Support for providing me with access to a high performance computer to assist in the simulation phase of this project.

Finally, I would like to thank my friends and peers, for their help in bouncing ideas off of and helping to solve problems; as well as just for making the past four years a bearable and a memorable experience.

Contents

List of Figures

1.0 Introduction

1.1 Project Background

Bushfires are large scale fire events that occur frequently in Australia and other parts of the world with fuel dense forests and hot, dry climates. They are capable of causing widespread destruction of property, infrastructure, livestock and in extreme events have resulted in dramatic loss of life; as was seen in the 2009 Black Saturday Bushfires in Victoria, which killed 173 people and had an estimated economic impact of over a billion dollars (CFA 2012)(Australian Institute of Criminology 2009). With climate change anticipated to cause hotter and dryer conditions in bushfire prone areas, the occurrence and severity of future fires is likely to increase (Balston and Williams 2014). Therefore, there is significant interest from many parties in developing more effective methods of controlling and containing these natural disasters.

Due to the large size and intense heat generation of bushfires they cannot be directly extinguished through either smothering (removing available oxygen supporting combustion) or removing the generated heat. Instead, firefighters aim to contain large bushfires through techniques such as back burning and the construction of firebreaks. These measures are designed to reduce the available fuel in the path of the advancing fire, thus limiting its progress. However, bushfires can and often do jump these containment lines, posing a serious threat to the surrounding region.

The mechanism through which bushfires propagate and escape containment is multifaceted. In addition to fire spread through direct flame contact with new fuel, burning embers are also lifted by the fires convective effect and blown by the prevailing wind downstream of the main blaze. These 'firebrands' land on suitable fuel beds and can ignite new spot fires; complicating firefighting efforts and causing containment breaches. This phenomenon, also known as 'Ember Attack' is the primary cause of building ignition in bushfire events (Hashempour and Sharifian 2015).

Further affecting bushfire propagation is the intense heat radiated off from the fire, referred to as Radiant Heat Flux (RHF). The level of RHF in a large bushfire can reach as high as 100 kW/m^2, with values between 10 kW/m^2 and 80 kW/m^2 considered typical (Hashempour, Sharifian & Billingsley 2015). Such extreme heat flux assists the bushfire spread by thoroughly drying out vegetation and fuel ahead of the fire, decreasing ignition time and

causing spontaneous combustion above certain intensity levels. Radiant heat also prevents close access to the fire front, hampering combative measures. The majority of deaths that occur in bushfires are as a result of being trapped in close proximity to excess RHF.

Due to the abovementioned factors, controlling and containing bushfires is a difficult task fraught with danger. This has led to interest in developing new methods of approaching fighting bushfires. Recent research conducted at the University of Southern Queensland into a way of controlling bushfires has yielded promising results. Small aperture wire mesh has been investigated for its potential to reduce windborne firebrands and shield against excess levels of RHF.

The use of metal wire mesh as a protection measure against bushfires is currently used on a small scale. After the 2009 Black Saturday Bushfires in Australia, the Australian Standard AS 3959-2009, 'Construction of buildings in bushfire-prone areas' was revised, with one of the additions being the requirement of 2 mm or smaller aperture wire mesh screens to be installed across windows and other openings for the purpose of preventing the passage and subsequent accumulation of firebrands inside structures. Other jurisdictions in areas which experience wildfires have similar requirements mandated.

This project seeks to extend the concept of small aperture wire mesh as a bushfire defence measure through the construction of large fences using low porosity wire mesh. By placing such fences in the path of the bushfire, in conjunction with firebreaks, significant attenuation of the major causes of fire propagation could be achieved. Currently, there is no available literature on the use of fences or walls of fine wire mesh to retard bushfire attack.

1.2 Project Scope and Aim

This project aims to further develop the concept of the use of wire mesh as a method of retarding bushfire progress and better protecting man-made structures from bushfire attack. As this idea has not been trialled in a real bushfire situation, the concept has not been shown to be effective as of yet, although experimental results are promising.

As such, it is the aim of this project to investigate, through the use of computational simulation, the feasibility and consequently the design parameters for such a fence to be to be viable. However, as the concept is untested, the primary outcome of the project is not to develop the most effective fence. Rather, a design that is lightweight, easy to construct and requires low initial capital investment is the focus. Such a design could then be prototyped and tested on a small scale, and the effectiveness of the concept tested. As an initial trial, this project will focus on designing a fence capable of being erected on reasonably short notice without significant equipment, for the purpose of aiding the defence of a dwelling or individual building against bushfire attack.

Therefore, the objectives of this project can be summarised as such:

- Review the current research into the use of mesh screens as a barrier against fire embers and radiation to understand the relationship between mesh properties and potential fire protection properties.
- Investigate conditions created by bushfires in order to develop an understanding of the environmental limitations and subsequent design limitations faced.
- From the information compiled in the literature reviews, develop a series of design aims which address the factors which were identified as being important for the success of the bushfire fence.
- Develop a series of assessment criteria against which any particular design can be evaluated to quantify its adherence to the design aims from the previous point, in addition to developing a framework with a relevant benchmark future projects can measure against.
- Through the use of relevant engineering theory and data, evaluate the feasibility of various fence design options, determine the most appropriate and develop a preliminary computational design overview.

- Develop a computation model using the Finite Element Analysis Software ANSYS to determine design parameters such as maximum stress, deflection and support forces and reactions, refining and detailing the preliminary design further.
- Evaluate the final design developed against the assessment criteria previously created to assess the success in which the final design met the design goals.
- List recommendations for the direction which further work in this area should be directed, based upon the findings and information gained through the course of the research project.

1.3 Project Implications and Safety Considerations

Due to the nature of the area of research and the project aims; the preliminary design of a large mesh screen fence for use in bushfire events, there are significant implications in the outcome of the project to be considered. Due to the inherent danger associated with large fires, the extreme environment they create, and the dangers presented by structural failure of such a large object, care must be taken at each stage of design to ensure no oversights occur.

Thought must also be given not only to the direct factors affecting the effectiveness and structural integrity, but also to secondary issues that may be posed by the erection of a large impassable object. For example, while it is necessary for the fence to be effective to seal entire sections of land with mesh screens, this will also have the negative effect of preventing movement from one side to the other. This could have disastrous consequences for both wildlife and humans who may find themselves trapped between a fire and an impassable wall. Evidently, this should be taken into consideration during the design process to ensure that this danger is minimized for both animals and humans alike.

In a similar strain, the fence itself should never impair efforts to combat a bushfire. Its construction should be in such a way that its presence does not interfere with the speed in which firefighters and their equipment can be deployed to the necessary areas.

This project in itself however, does not pose any significant safety risks. As the methodology used in testing and designing is through the use of computer modelling and FEA, there is no contribution of risk from any associated experimental procedures or manufacturing.

2.0 Literature Review

This section of the report will explore the current literature available in the areas which have been deemed to be relevant to the design and implementation of a bushfire attenuation fence. The information presented in this section should provide the reader with a fair understanding of the knowledge which is applied in the development of the design in later chapters.

2.1 Conditions Inside a Bushfire

In order to successfully design a fence to aid in the defence against bushfire attack, the conditions that the structure will likely be subjected to must be identified. Without sufficient knowledge of the conditions, no useful design work can be undertaken.

The main issue presented in developing any design for use in close proximity to a bushfire is the extreme temperatures which are developed at the fire front. Elevated temperatures alter the mechanical properties of many materials, generally resulting in reduced stiffness and strength values; structural and stainless steels included. Therefore, a maximum temperature likely to be reached by the materials in the fence should identified to ensure the structural integrity of the fence in operation.

The heat released during a bushfire is transferred to the surroundings through two main methods; radiation and convection, with conduction having a near negligible effect in bushfires (Anderson 1969). However, due to the large temperature difference between the ambient air and the flame temperatures, much of the convective heat is directed vertically. Because of this, convection only plays a significant role in heat transfer to objects when direct flame contact occurs.

Like all heat transfer, radiation and convection is driven by a temperature difference between two objects (Kreith, Manglik & Bohn, 2011). As this temperature difference decreases, the rate of heat transfer between them also decreases, and reaches zero when the objects have the same temperature. Therefore, the maximum temperature which the materials in the fence could theoretically reach is equal to that of the flame temperature of the fire, regardless of heat transfer mechanism.

Research into the flame temperatures that occur in large scale bush and forest fires reveal that the observed temperatures are typically less than the adiabatic flame temperature (Poon, 2003). Additionally, the peak temperatures recorded in any given position often only lasted for between 10 to 30 seconds (Poon, 2003). Elevated temperatures remained for longer, on the order of around several minutes for test with higher fuel loading. Below is a figure taken from the results of a test consisting of a 56 200m x 200m plot of dense shrubbery. Measured heat flux during this test exceeded 7 MW/m (Poon, 2003).

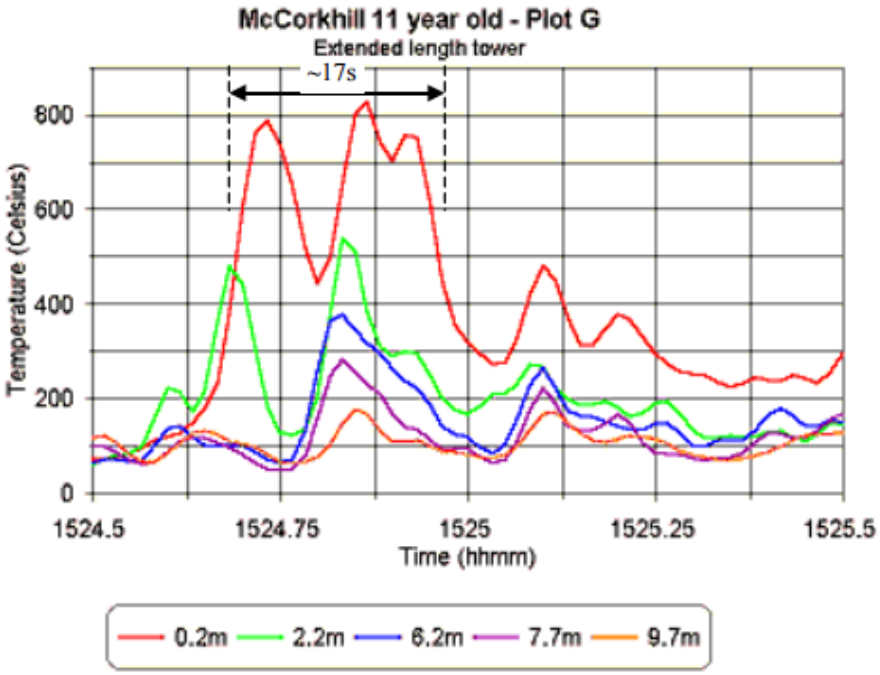

Figure 2-1 Graph Showing Flame Temperature vs Time for Different Heights above Ground Level in an Experimental Test (Poon, 2003)

From the figure above, which shows the recorded temperature vs time at a series of heights above ground level, it can be seen that the flame temperature only exceeded 500°C for around 17 seconds, with elevated temperatures remaining around 200°C to 300°C for several minutes afterwards.

Other experiments yielded similar results, with Mendez-Lopez reporting in his 2003 paper 'Flame characteristics, temperature–time curves, and rate of spread in fires propagating in a bed of Pinus pinaster needles', that small scale trials conducted observing flame temperatures did not exceed 600°C for greater than 30 seconds in any test. Additionally, the International Crown Fire Modelling Experiment (ICFME) conducted a large scale experiment using a 150m x 150m plot of 12m high Jack Pines. They recorded that 10m away from the forefront, the peak heat flux reached 46 kW/m for a duration of only 20 seconds, with a heat

flux of above 20 kW/m only lasting on the order of 1 minute. The figure below is shows the recorded heat flux vs time in the ICFME experiment.

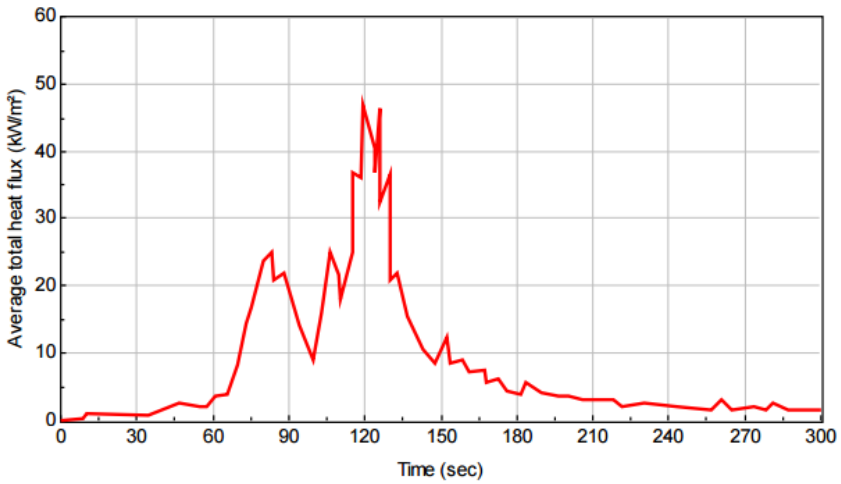

Figure 2-2 Measured Heat Flux vs Time for ICFME Test (Cohen, J. 2000)

In the 2003 review 'Predicting Radiation Exposure from an Advancing Bushfire Flame Front' conducted by Poon, it was explained that the reason for the short duration of peak flame temperature in any given location is due to the rapid consumption of fine fuels such as foliage and small branches. These fuels rapidly burn, releasing substantial amounts of heat quickly but do not last for long, whereas the denser fuels such as branches and trunks release heat at a slower rate. This explanation is in agreement with the aftermath of bushfires in Australia, where all of the foliage and small fuels are burnt but trunks and branches remain. This is illustrated in the picture below.

Figure 2-3 Image Showing Aftermath of a Victorian Bushfire (O'Neill, 2003)

From the above literature, it can reasonably be predicted that the maximum temperature the fence is likely to reach will always be less than the peak flame temperature. This is based upon two reasons.

Firstly, as the window of peak temperature is rather small, the fence is unlikely to have sufficient time in any one location to reach a steady thermal state. Secondly, excluding conditions in which the flames are engulfing the fence, the surrounding air temperature is going to be at a lower temperature than the fence. This will result in convective cooling of the fence, assisting in limiting the temperature rise of the fence.

In order to fully characterise the thermal behaviour of the fence in a bushfire, computational modelling of the fence design should be performed. To proceed with the design of the fence however, a conservative value will be chosen. As figure 1 shows and the associated studies show, the peak temperatures of fires typically do not exceed 500^{o}C for greater than around 30 seconds. Therefore, a maximum design temperature of 500^{o}C will be selected.

2.2 High Temperature Effects on Structural Steel Properties

Designing a structure to reliably withstand the conditions outlined in section 2.1 above requires a detailed understanding of how the mechanical properties of the construction materials change with elevated temperature. A literature review was then begun to identify suitable materials which could withstand the design temperature identified. This quickly revealed that many of the lightweight type materials commonly available were unsuitable, either due to poor high temperature performance such as in the case of aluminium and common fibre composite materials, or prohibitively expensive such as in the case of various specialized high temperature fibre composite resins. Remaining materials that met the required criteria were various grades of structural steel.

The effects of high elevated temperatures on structural steel have been well investigated, primarily for the same reason as this literature review; to understand the behaviour of structural members in the event of a building fire. The findings of several relevant documents on the mechanical properties of various grades are detailed below.

In a 2006 paper titled ‘Behaviour of high strength structural steel at elevated temperatures’, Chen et. al. conducted numerous tensile test experiments on both high strength structural

steel and mild structural steel at temperatures ranging from 20°C up to 940°C, and compared their findings with the Australian, American and British Standard models of mechanical properties reduction in steel structures at elevated temperatures.

The 'high strength structural steel' used in their testing was BISPLATE 80, a steel with a guaranteed minimum 0.2% Proof Strength of 690 MPa and ultimate tensile strength of 790 MPa. The 'mild structural steel' used in the paper was XLERPLATE Grade 350, with a guaranteed minimum yield stress of 360 MPa and ultimate tensile stress of 450 MPa. Both of these steels are manufactured in Australia and are in common use in Australian construction, and as such are a good representation of the grades of steel actually available for the fence construction.

The investigation found that the strength reduction factor (the ratio of elevated temperature stress divided by room temperature stress) for a 0.2% Proof Load was extremely similar for both the high strength steel and mild steel up to a temperature of 540°C. A comparison of their results with the models used in the various standards is shown in figure 2-4 below. Note the conservative nature of the AS4100 and ASCE standards in the temperature range of 300°C to 700°C.

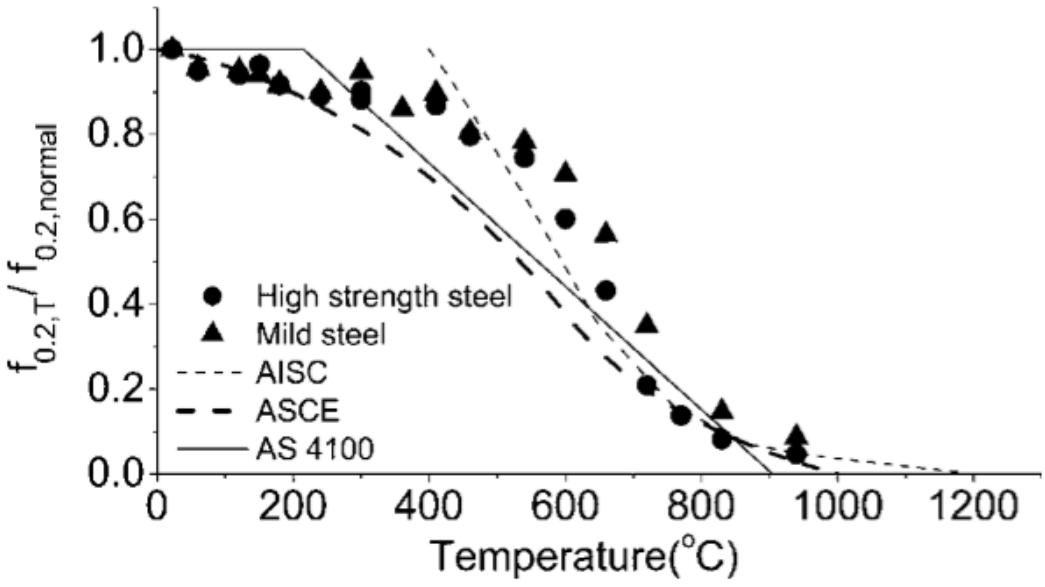

Figure 2-4 Graph Showing Steel Strength Reduction at Elevated Temperatures (Chen et. al. 2006)

A more interesting result was found when the behaviour of the modulus of elasticity was investigated. The reduction of the modulus of elasticity of the high strength steel was dependent upon whether the applied load was steady state or transient. The steady state reduction factors for both the high strength and mild steels were again very similar, and were in fact over predicted by the models used in the standards as can be seen in figure 2-5 below.

However, when a transient load was applied to the heated samples of the high strength steel, the measured modulus of elasticity reduction factor was noted to be much less than the steady state reduction at the same temperature. In fact, in the region between 100°C and around 500°C, the reduction in the modulus of elasticity was under predicted by all of the models used in the standards. Transient testing was not performed on the mild steel so it was not determined if this also occurs in this metal. This can also be seen in figure 2-5 below. As the likely loading case of the steel used in the construction of the fence is going to be transient, this result should be noted and care taken to account for this effect in the design.

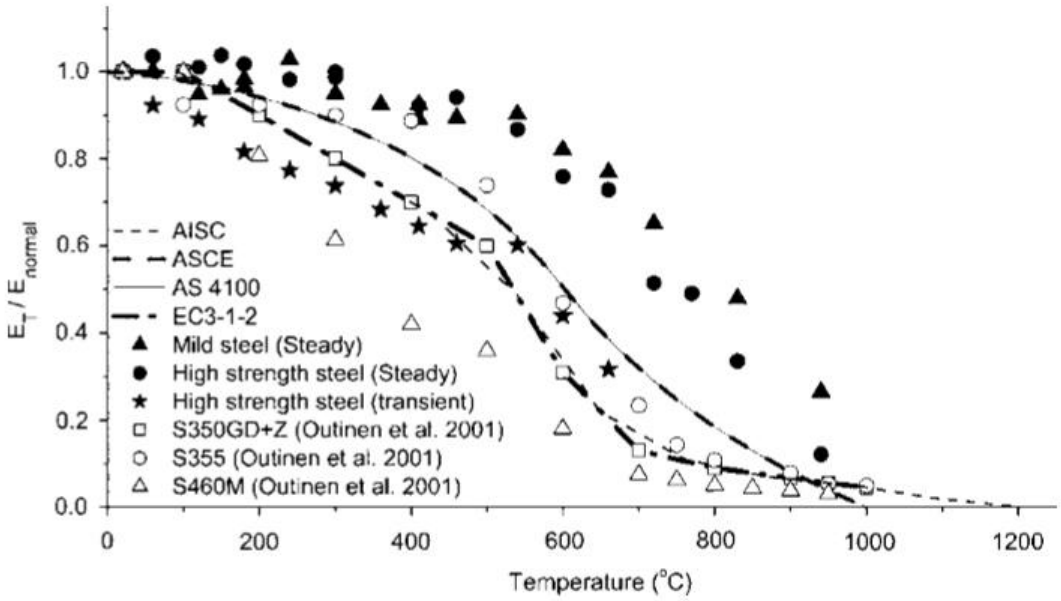

Figure 2-5 Figure Showing Reduction in Modulus of Elasticity at Elevated Temperatures (Chen et. al. 2006)

Knowing the accuracy and limitations of the models used in the standards in predicting the reduction factors for the material properties; the equations given by the Australian Standard AS4100 'Steel Structures', are given below:

The variation of yield stress with temperature should be taken as the following:

$$\frac{f_y(T)}{f_y(20)} = 1.0 \qquad \text{when } 0°C < T \le 215°C; \text{ and}$$

$$= \frac{905 - T}{690} \qquad \text{when } 215°C < T \le 905°C$$

Where $f_y(T)$ is the yield stress of the steel at a given temperature T°C, $f_y(20)$ is the yield stress of the steel at 20°C and T is the temperature of the steel in degrees Celsius.

The variation of the modulus of elasticity should be taken as follows:

$$\frac{E(T)}{E(20)} = 1.0 + \left| \frac{T}{2000\left[\ln\left(\frac{T}{1100}\right)\right]} \right| \qquad \text{when } 0°C < T \le 600°C; \text{ and}$$

$$= \frac{690\left(1 - \frac{T}{1000}\right)}{T - 53.5} \qquad \text{when } 600°C < T \le 1000°C$$

Where $E(T)$ is the modulus of elasticity of the steel at a given temperature T°C, $E(20)$ is the modulus of elasticity of the steel at 20°C and T is the temperature of the steel in degrees Celsius.

2.3 Types of Meshes

In Australia, the meshes used in bushfire protection applications must comply with AS 3959-2009; which mandates an aperture size of less than 2mm and must be corrosion resistant (AS3959-2009). Therefore, the most common material used in these meshes is Stainless Steel, usually grade 304 or 316. These grades of Stainless Steel exhibit good corrosion, high temperature properties and affordable cost, making them well suited to this type of application.

An assessment of the currently available suitable meshes found three main sizes. While the aperture size of these meshes is less than 2mm, there is significant variation in the 'open

area', or porosity, of the meshes available (SSWM 2016). A table showing typical dimensions of the types of meshes available are shown below.

Type	Nominal Aperture (mm)	Wire Diameter (mm)	Approx. Open Area (%)
Low Porosity	1.64	0.9	42
Medium Porosity	1.67	0.45	62
High Porosity	1.23	0.18	76

Table 2-6 Table Showing Typical Available Bushfire Mesh Sizes (SSWM 2016)

Note that the aperture size of a mesh is different to its porosity, and meshes with large apertures can have low porosities and vice versa. For example, in the available meshes above, the lowest aperture mesh had the largest porosity. Mesh porosity is a measure of the open area of a mesh, and is a function of the mesh aperture and wire diameter. This relationship is shown below.

$$p = (1 - \frac{d}{L})^2 \qquad 2.3.1$$

Where p is the mesh porosity, d is the wire dimeter and L is the span of the wires from centre to centre across one cell, i.e. the aperture plus the wire diameter.

While Stainless Steel meshes are the most common type of material used for these meshes, other materials could also work and may offer advantages over Stainless Steel in a bushfire attenuation fence application, such as weight, handling and storage. Glass fibre is one such example which is currently being investigated in a separate project.

An interesting property to note which is relevant when investigating meshes comprising of fine wires is that the wire material strength tends to increase as the diameter of each individual wire decreases. For wires made of 316L, an austenitic stainless steel, a correlation between wire diameter and ultimate tensile strength is shown below (Kraft, 2010).

$$S_{ut} = Ad^{-m} \qquad 2.3.2$$

Where S_{ut} is the ultimate tensile strength of the wire, A and m are material properties (1623.7MPa-mm^m and 0.149 respectively for SS316L) and d is the diameter of the wire.

The graph below shows the relationship between wire diameter and ultimate tensile strength for wires made of 316 L Austenitic Stainless steel.

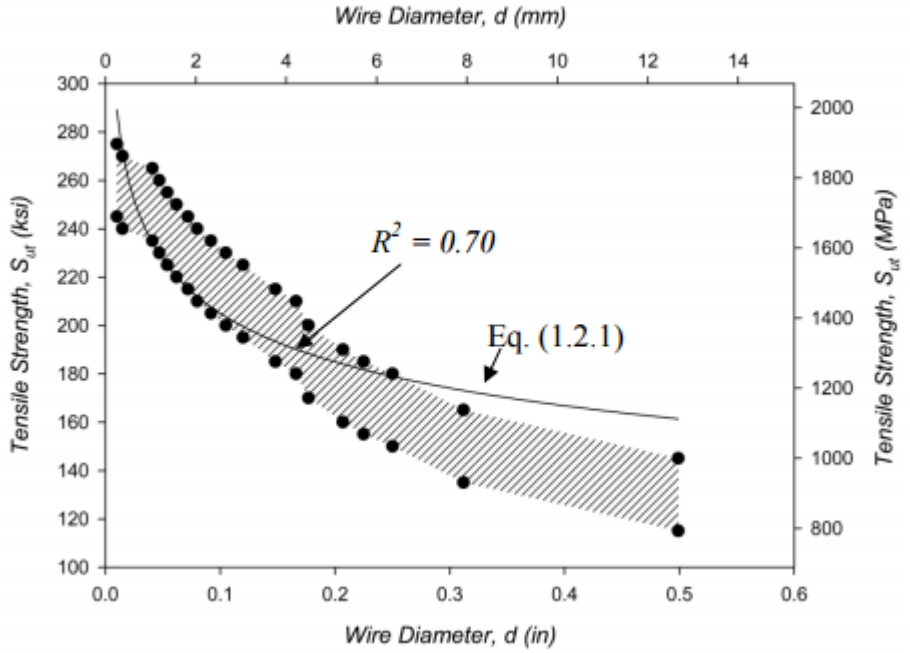

Figure 2-7 Graph Showing Strength of Stainless Steel Wire vs. Diameter (Kraft 2010)

From the graph it can clearly be seen that at a wire diameter of less than 1 mm, which all of the bushfire meshes listed in table 2-4 are, the ultimate tensile strength is around the order of 1600 to 2000 MPa. This is a useful property, particularly in this proposed application due to the likelihood of large stress concentrations due to the large wind loading.

2.4 Fire Retardant Properties of Wire Mesh

There are two main ways in which small aperture wire mesh can act to reduce bushfire propagation. These are:

- Reducing the transmission of airborne firebrands to potential fuel beds.
- Reducing the level of radiant heat flux that the bushfire emits, which subsequently reduces the amount of preheat and drying of available fuel in the path of the fire.

The effectiveness and performance of both these are dependent upon the physical properties of the mesh, and are further discussed below.

2.4.1 Wire Mesh Defence Against Firebrand Transmission

The creation, transfer and build-up of firebrands against flammable materials during bushfire events is a significant issue, and is responsible for the ignition of the majority of buildings lost along with contributing to the spread fire through the creation of additional spot fires (NIST 2016). An image depicting a simulated firebrand attack against a building is shown below.

Figure 2-8 Image Showing a Simulated Firebrand Attack Upon a Dwelling (Insurance Institute for Business and Home Safety, 2016)

The rationale behind using mesh screens to protect buildings and prevent the spread of bushfires is quite simple. By creating a barrier in the form of a small aperture mesh screen, the firebrands which would normally be able to move freely and accumulate are unable to pass through the openings of the mesh.

The performance of a mesh against firebrand attack is a complex phenomenon and depends upon wind speed, mesh geometry, average firebrand size and composition, e.g. wood, leaf, mulch etc.

Several papers have been published which investigate the behaviour of different wire mesh configurations and sizes against various firebrand attacks. The findings of these papers is discussed below.

Described in a personal communication, Hashempour and Sharifian used a specially designed wind tunnel to test the effect of various mesh parameters, including aperture size, on the transmission of myrtle leaf firebrands.

At the test wind speed of 14.5 m/s second used in the experiments, they noticed an interesting phenomenon. In contrast with the expected results, the penetration ratio was larger than one for all the meshes tested, showing a peak value of 3.65 at a mesh aperture of 2.8 mm before decreasing again as the mesh openings grew larger.

Upon reviewing their results, they identified that the cause of this effect was the fracturing of the approaching firebrands when they impacted upon the mesh. Rather than remain stuck in place on the mesh until they had reduced in size enough to allow them to pass through the mesh; the typical behaviour that had been observed in earlier, lower velocity trials such as the one by Manzello et. al. in 2011, they found that firebrands which were structurally weaker or which impacted the mesh at higher speeds had a tendency to break apart into smaller pieces that could pass through the mesh easily.

However, despite the presence of the mesh increasing the amount of firebrands leaving the mesh, they are of significantly smaller size after having passed through the mesh. In addition to contributing to an earlier burn out time due to a reduction in available fuel; Ellis, in his 2012 paper 'review of empirical studies of firebrand behaviour', states that the main method of heat transfer from glowing embers is via conduction. Therefore, a significant reduction in size of the firebrands is very likely to reduce the chance of ignition of fuel beds.

This result was confirmed by Hashempour in a secondary personal communication detailing further experiments into fuel bed ignition. Hashempour described two fuel beds consisting of oven dried cotton cloth was positioned approximately 4.5 m away from various mesh screens as they were subjected to firebrand attack in a similar manner to the above study, although at a lower speed of 10 m/s.

Again in this study, an increase in penetration ratio of between 1.23 to 1.28 was found to occur with mesh with an aperture of 1.61 mm. However, the percentage of firebrands that was recorded to impact upon the fuel beds was reduced from 74.7%, the result without any mesh screen, to 48.0% with the 1.61 mm screen.

Tests with 1 mm aperture mesh yielded even greater results, completely eliminating the impact of any firebrands on the fuel beds in one test. Figure 6, taken from the paper is shown below, revealing state of the fuel beds after one of the tests. Image A and B was with no mesh, C and D was with the 1.61 mm aperture and D and E was with 1 mm aperture mesh.

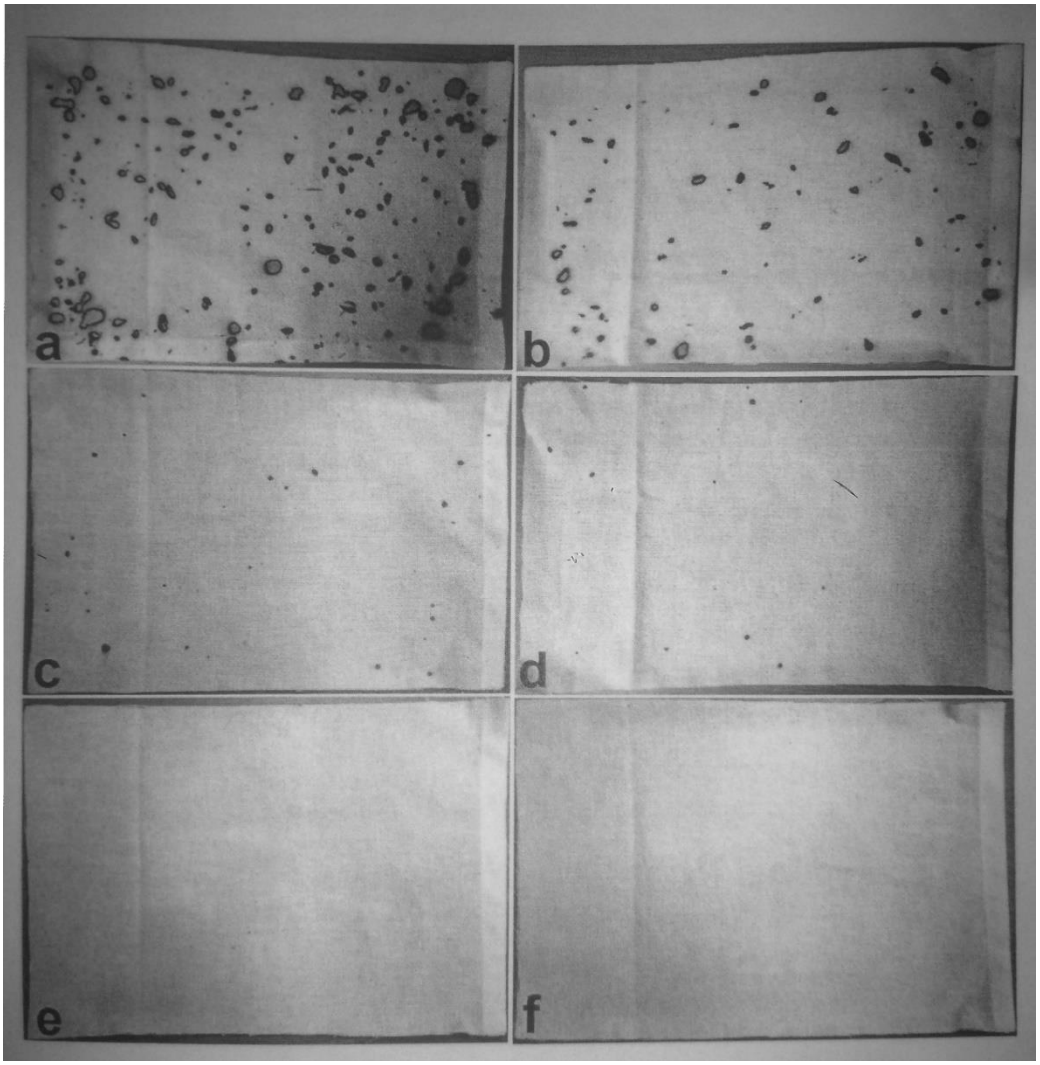

Figure 2-9 Image Showing Effect of Mesh Screen Upon Firebrand Ignition of Fuel Beds (Hashempour, J., pers. comm.)

From the above results, the authors concluded that the ability of the mesh screens to reduce firebrand transmission was dependent upon the aperture of the mesh. They also noted that the mesh alone did not completely prevent firebrands reaching the fuel beds, and that the mesh exhibited the best firebrand reduction when used in conjunction with a buffer zone clear of combustible materials, around the order of at least 4.5m; the buffer zone used in the study.

Therefore, it can be concluded that the effectiveness of the design of a bushfire attenuation fence at reducing firebrand transmission is likely to increase as the aperture size decreases, regardless of the porosity of the mesh. As the fence is intended to be erected in clear areas, the requirement of a buffer zone is not a large concern, although should be noted.

2.4.2 Wire Mesh Reduction of Radiant Heat Flux

Wire mesh screens also serve to reduce the amount of radiant heat flux that is transmitted from the fire front. Primarily, this is achieved by reducing the view factor of objects behind the mesh to the fire via the obstruction provided by the mesh wires.

Therefore, it follows that the lower the porosity of the mesh, the greater the reduction in radiant heat flux that would be achieved. This result has been verified by experimental models in the work of Hashempour et. al (2016).

An interesting result that was identified in their paper 'Experimental measurement of direct thermal radiation through single-layer square-cell plain woven screens' was that the level of radiation measured to be passing through the mesh was actually less than that indicated by the porosity of the mesh. This was attributed a 'tunnel vision' phenomenon. As the incident angle relative to normal increases, the wires of the mesh cells come into alignment. This limits the amount of radiation that can pass each mesh cell, as incident radiation outside of this view angle is blocked.

Hasempour and Sharifian demonstrated, both analytically and experimentally, that for a simplified woven wire mesh this view angle is only a function of the mesh porosity, with low porosity meshes having a smaller view angle. This indicates that the advantage of the tunnel vision effect in reducing radiant heat flux is more prevalent at lower porosities. The experimental results of Hashempour et. al. (2016) confirms this; finding that the 'Passing Ratio' of incident radiation (the ratio of measured radiation through a mesh screen vs. without a screen) for each mesh porosity was always less than the porosity itself, although this difference was found to reduce as the porosity increased. This is shown in figure 7 below.

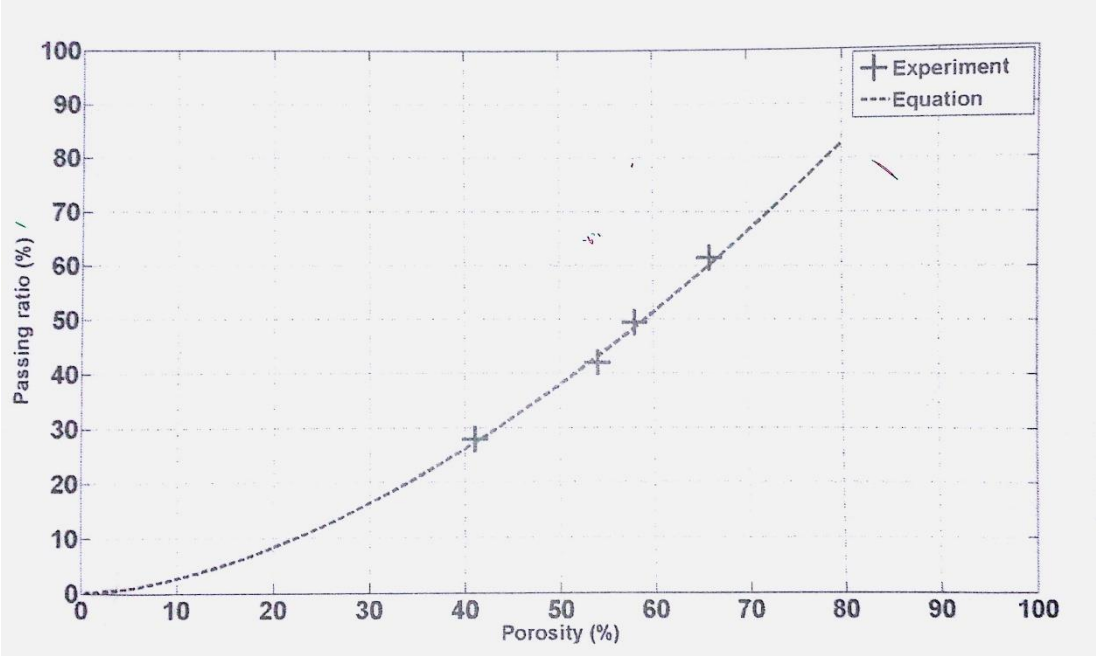

Figure 2-10 Graph Showing Radiation Passing Ratio vs Mesh Porosity with Predicting Function (Hashempour et. al. 2016)

2.5 Drag Force on Wire Mesh Screens

A major issue affecting the design of such a fence is the impact of drag force on the mesh screen. Due to the potential for very high wind speeds around bushfires, as mentioned in section 2.1, it is important to know the order of magnitude of the force that will be imposed on the fence by the wind loading.

Drag force of a fluid on an object is defined as the component of force that acts on a body parallel to the direction of relative motion, caused by the fluids interaction with the body. (Fox, Pritchard, & McDonald, 2010). Dimensional analysis shows that this force is a function of a bodies area relative to the flow, the density of the fluid and the velocity with which it is moving relative to the body. The derived formula for calculating drag force can be found in any Fluid Mechanics Textbook and is presented below:

$$F_D = \frac{1}{2} C_d . \rho . A . V^2 \qquad 2.5.1$$

Where F_D is the drag force, C_d is a dimensionless number called the drag coefficient, ρ is the fluid density, A is the area of the body and V is the fluid velocity relative to the object. By dividing both sides of this equation by the object area, an expression for the drag force per

unit area can be found. This is a more useful value as it allows for easy comparison between meshes for design purposes. The formula is:

$$\frac{F_D}{A} = \frac{1}{2} C_d . \rho . V^2 \qquad 2.5.2$$

In order to accurately calculate the drag force on the mesh screens using this formula, the value of the coefficient of drag for each configuration must be known. This number is difficult to determine for complex shapes and is often done by experimentation or simulation. The results of two papers that investigated the calculation of drag coefficients for wire mesh screens are examined below.

In their 2007 paper 'Computational Simulation of the Wind-force on Metal Meshes', Sharifian and Buttsworth used the CFD package FLUENT to simulate fluid flow at various Reynolds numbers around meshes of different sizes. Three mesh sizes were used, varying the Reynolds number between 10 and 1000. By calculating the drag coefficients for the meshes in each flow and comparing them to the theoretical drag coefficient for a single cylinder of the same respective diameter, they found that the Cd values for the wire mesh were related to, but always greater than that of the single cylinder. This was explained as a result of the constraining nature of the additional wires reducing the cross-sectional area available for airflow (Sharifian and Buttsworth 2007).

Consequently, they showed that the larger the mesh opening, the closer the drag force approached that of the single cylinder. From this, Sharifian and Buttsworth (2007) proposed the following correlation for the drag coefficient on a wire mesh as a function of Reynolds number and mesh porosity:

$$Cd = -0.491 + \frac{0.47}{p^{1.773}} - \frac{7.49}{Re^{0.661}} + \frac{6.475}{p^{2.244} Re^{0.661}} \qquad 2.5.3$$

Where Cd is the drag coefficient, corrected for overall mesh cross-sectional area, p is the mesh porosity and Re is the Reynolds number for the flow. The correlation is reported to be accurate to 6.5 % within the range of $10 \leq Re \leq 1000$ and $0.27 \leq p \leq 0.82$.

Another paper which addresses the prediction of drag coefficient imposed on mesh screens due to restriction of airflow is 'The Flow of Air Through Wire Screens', authored by G. De Vahl Davis. The paper, published in 1957, experimentally determined the drag coefficient of wire meshes with different porosities at different Reynolds numbers ranging from approximately 50 to 250.

Davis also noted the relationship between porosity and drag coefficient, in addition to noting that the Cd value begins to approach a constant value as the Reynolds number increases, much the same way to a cylinder in the range of 400 ≤ Re ≤ 200 000 (Fox, Pritchard, & McDonald, 2010). From this he proposed the following correlation:

$$Cd - Cd_0 = \frac{55}{Re} \qquad 2.5.4$$

Where Cd is the drag coefficient of the wire mesh, Cd_0 is the limit that Cd approaches as Reynolds number is increased, and Re is the Reynolds number of the flow through the mesh.

To approximate Cd_0, Davis assumed the flow to similar in behaviour to sudden expansion in a pipe flow. By estimating the pressure difference through the momentum equation and neglecting viscous effects, he found:

$$Cd_0 = \left[\frac{1-p.C}{p.C}\right]^2 \qquad 2.5.5$$

Where Cd_0 is the limit Cd approaches, p is the porosity of the mesh and C is a contraction coefficient to correct for the flow through the constrained area. Davis reports that the value of C was experimentally determined to be approximately 0.95, steady within the range of 100 ≤ Re ≤ 100 000.

In order to assess the level of agreement of these two correlations, and thus subsequently determine the most appropriate one to use in the estimation of drag force on the wire mesh screens, the drag coefficients for the three sizes of wire mesh discussed in section 2.2 was calculated for a series of Reynolds numbers which corresponded to a range of wind speeds from 1 to 28 m/s.

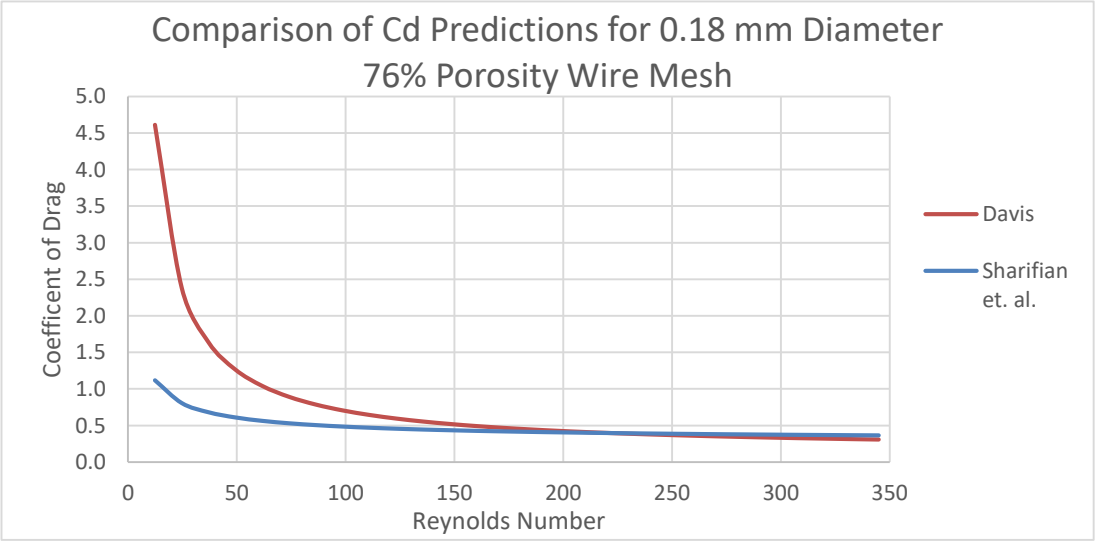

Figure 2-11 Graph Showing Cd values for Wire Mesh from Two Different Correlations

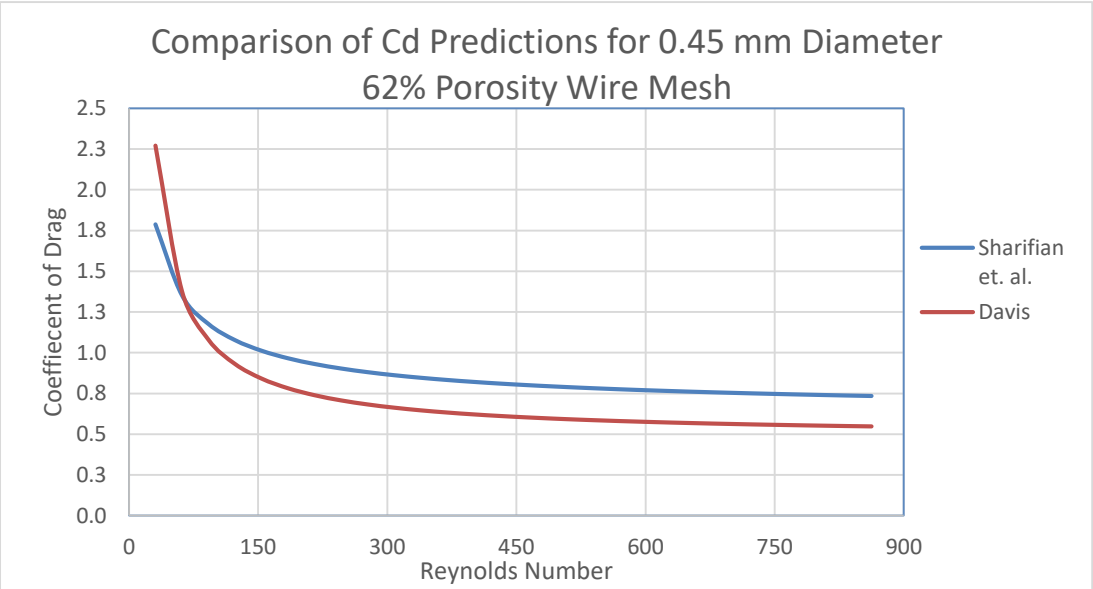

Figure 2-12 Graph Showing Cd values for Wire Mesh from Two Different Correlations

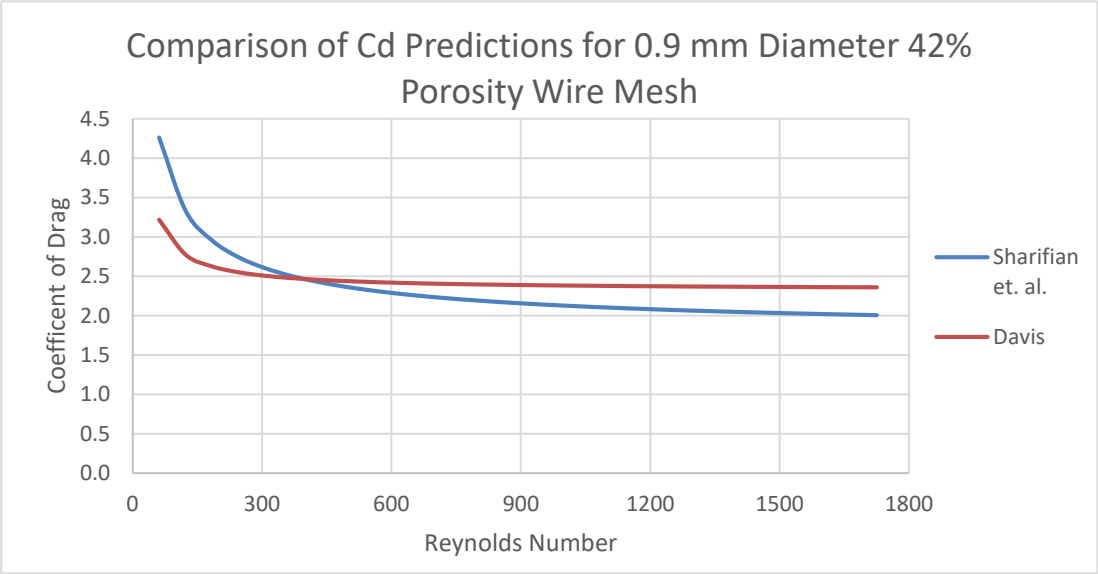

Figure 2-13 Graph Showing Cd values for Wire Mesh from Two Different Correlations

As the three charts above show, there is a reasonable level of agreement between the two models. While there is significant divergence at lower Reynolds numbers, most noticeable for the 76% porosity mesh, this large difference begins to disappear at a Re value of between 75 to 150. This discrepancy at low Re values is not of great concern however. As the drag force formula shows, drag force scales with the velocity squared; meaning that the greatest drag forces on the mesh will be encountered at high velocities and therefore higher Re values.

For the 76% and 62% porosity meshes, the correlation proposed by Sharifian and Buttsworth shows a higher Cd value than the one by Davis in the Re range of 150 onwards, with a

maximum percentage difference of 17.6% and 29.0% respectively at a wind speed of 28 m/s. However, the result of the 42% porosity shows the correlation proposed by Davis to be larger for Re values greater than approximately 400. The maximum percentage difference again occurred at 28 m/s, and was found to be 16.1%.

However, it should be noted that the correlation proposed by Davis was only drawing upon data for Reynolds numbers up to approximately 300. Therefore, the extrapolation of the formula is done under the assumption that the Cd value does indeed approach a constant value in the $300 \leq Re \leq 1800$ range. Likewise, the correlation of Sharifian and Buttsworth was only trialled within the $10 \leq Re \leq 1000$ range; while the range of Re for the 41% porosity mesh was up to 1725 for a wind velocity of 28 m/s.

Therefore, in order to maintain a conservative approach, for any given mesh the larger of the two Cd values will be used when estimating the drag force. This will ensure a greater level of confidence in the results of the simulations used in the design process.

2.6 Australian Standards for Temporary Fencing

Before any design work can be undertaken, any standards that are applicable to the proposed design need to be identified and assessed. This will ensure that no oversights occur during the design process that could invalidate the outcome of the project. The primary standard that has been identified as most relevant to the project is AS 4687-2007, Temporary fencing and hoardings. However, it is quite obvious that the intended application for this standard is much smaller fences designed for typical fencing type applications. Due to the requirements for effectiveness against bushfires outlined in the above sections, it is unlikely that all of the points mentioned below can be reliably met, although it was found to be a good reference to guide in the design.

The general requirements of the standard can be summarised as follows:

- The temporary fencing should remain stable and erect at all times.
- Movement and assembly of the fencing should be carried out by a competent and trained person in compliance with the manufactures directions.
- The design of any temporary fencing must take wind loading, impact loading and stability into account.
- All temporary fences must be at least 1500 mm in height.

Design specific requirements listed in the standard are summarised below:

- Fence infill materials, i.e. mesh screens must comply with their applicable Australian Standards.
- The material used in for the fencing frames must comply with AS 1163; Cold Formed Structural Steel Products.
- The maximum aperture, i.e. opening size of the fence infill material must be less than 75 mm.
- All clamps, hinges and other fittings used must comply with their relevant Australian Standards.
- Bracing must be manufactured and installed on the fence when necessary to prevent collapse and misalignment.
- Counterweights and base plates used should be designed for the life of the fence, and designed appropriately to withstand the performance requirements above.

Also included in the standard is the testing requirements and procedures that the design of any temporary fencing must meet. There are six tests that need to be performed to meet the requirements of the standard. These are detailed in the following subsections.

2.6.1 Simulated Climbing Test

The temporary fencing design must be shown to be able to withstand the forces and moments imposed by a person attempting to climb the fence. The standard stipulates that to test this, three 'panels' of fencing must be assembled, and a 65 kg load hung from the centre of the fence at the top, offset perpendicular from the fence by 400 mm. A diagram showing the arrangement is shown at right. The fence must be able to withstand the test for a period of 3 minutes.

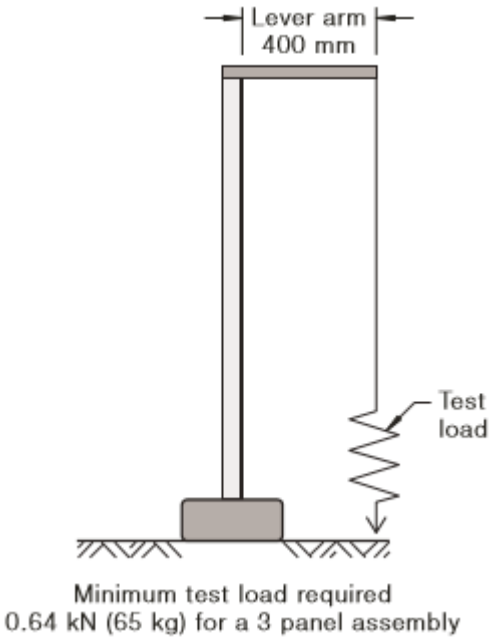

Figure 2-14 Diagram Showing Simulated Climbing Test Arrangement (Standards Australia 2009)

2.6.2 Impact Loading Test

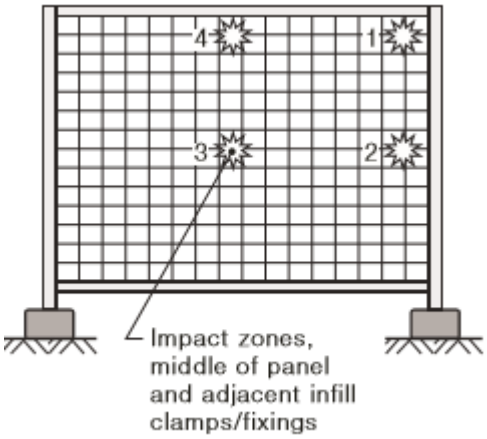

Figure 2-15 Diagram Showing Sites of Impact Testing (Standards Australia 2009)

In this test, a single panel of the fence will be subjected to a series of impact tests to assess the fences resistance to overturning, cracking, excessive deflection and other methods of failure in the event of a sudden impact. A 37 kg projectile with a kinetic energy of 150 J (2.85 m/s) must be impacted against four sections of the fence infill material, as shown in the diagram at left.

For the fencing to pass the test, the infill material must not show any signs of penetration or cracking, failure at the joint to the frame, deflect more than 300 mm at the site of impact or overturn the fence.

2.6.3 Infill Aperture Width Test

To pass this test, the aperture size of the fence infill material must not allow a 76mm x 76mm block through. As the mesh required to stop firebrands is many orders of size smaller, this test is not particularly relevant.

2.6.4 Infill Downforce Test

In this test, a downwards load of 1 kN is to be applied to the centre of the infill material and maintained for a minimum of 60 seconds. For the fencing to pass the test, the infill material must not deflect greater than 35 mm from its original position.

2.6.5 Wind Force Overturning Test

In this final test, which is arguably the most important criteria for this particular project, the fence must be subjected to a simulated wind force to ensure that it does not overturn. A single panel of the fencing must be subjected to the minimum calculated wind force at its centroid and must resist overturning.

The minimum wind velocity used in the calculation corresponds to the wind speed region in which the fence is to be deployed, and ranges from 15 m/s for region A to 24 m/s for region D.

3.0 Project Methodology

This chapter will examine in detail the methodology used throughout the duration of this project; covering aspects such as the basis of deciding the design criteria, development of the performance metrics against which the final design will be measured and the analysis methods used to validate the design.

3.1 Development of Design Specifications

Before any design work could begin, a series of decisions had to be made on how the design could best meet the specified project aims of:

- Reasonable effectiveness in preventing firebrand transmission and radiant heat flux from an approaching bushfire.
- Portable, lightweight construction that is capable of being assembled with minimal tools or machinery.
- Fast assembly to maximize protective coverage installed prior to fire approach.
- Low manufacture cost to create an attractive investment option.

As with any design project, different aims are often contraindicative of one another. In order to better understand the requirements posed by each design aim, the factors affecting each of the specific aims are examined in the relevant sections below. Where two aims were in direct conflict with one another, a decision was made as to which should be prioritized.

3.1.1 Effectiveness at Preventing Firebrand Transmission and Radiant Heat Flux

From section 2.4 in the literature review section, it is clear that the performance of wire mesh against firebrand transmission depends upon the opening size of the mesh used, along with the actual area blocked by the fence. This indicates that in order for the fence to demonstrate the best efficiency against firebrands, a mesh with a sufficiently small opening

size should be chosen. Additionally, the fence should be of a such a height that lofted firebrands and those generated by foliage from nearby trees in a bushfire are adequately constrained by the mesh.

While opening size is not necessarily related to porosity; meaning opening size is somewhat independent of drag, increasing the height of the fence does effect the drag force, increasing the frontal area of the mesh, while also shifting the centre of pressure further away from the base. This would result in higher stresses in the structural members by creating a larger bending moment.

In order to insure the effectiveness of the fence at limiting firebrand transmission, it was reasoned that the design height should be similar to that of the surrounding trees in order to prevent embers created in crown fires from passing over the fence. However, as the primary tree type in Australia and many other parts of the world where wildfires are a serious concern, e.g. California, are Eucalyptus (Gum Trees); and many species of eucalyptus tree can grow to heights of in excess of 20 metres, it was unlikely that this could practically be achieved.

In a document detailing fire risks in blue gum plantations, it was stated a fire hazard was not particularly posed by the trees in the plantation until around 3 to 4 years, when the trees were considered 'mid rotation' in the plantation cycle. Trees at age 4 years had an average height of 7 to 9 metres and those at 6 years which posed an even greater fire hazard had an average height of 14 to 18 metres (Mar & Adshead, 2011). Therefore, a minimum design height of 10 metres was chosen as this would offer a compromise between fire protection and the other listed design aims.

Also indicated in section 2.4 is that the effectiveness of wire mesh at blocking incident radiant heat flux is dependent upon the porosity of the mesh used, with lower porosity meshes offering an increasing protection through the reducing view factor.

However, the literature indicates that the drag force coefficient of the mesh grows quite substantially with decreasing porosity. This creates an issue as higher drag forces require stronger supports and structural members; making the aims of high portability, lightweight and ease of construction difficult to realize.

Given the evidence identified in the literature review suggesting that the main cause of fire spread and house fire ignition is the accumulation of firebrands and not radiant heat flux, the design aim of reducing firebrand transmission was given priority over that of blocking

radiant heat flux. Given the short duration of the radiant heat associated with the fire front versus the persistent nature of the firebrands, this was considered a pragmatic approach.

3.1.2 Portable Lightweight Construction Capable of Assembly with Minimal Tooling and Machinery

As this method of combating bushfires is still in its infancy, the aim of this project is to develop a serviceable design capable of being deployed in a variety of conditions and locations in order to field test the concept against actual bushfire conditions. Due to the often remote location of bushfires and the properties they threaten, portability and ease of construction are extremely important factors for allowing both testing of the overall concept and the defence of property. If the concept gains sufficient evidence in actual situations to support its widespread use, more permanent and elaborate designs requiring a higher level of mechanized equipment may be justified.

Portability in this case has been taken to mean the ability to both transport the components to and from the required location and assemble the design without necessitating any specialized vehicles, e.g. a crane or similar machine. The vehicles that are considered to be readily available are those such as utes, trailers and flat-bed trucks. Therefore, the design should not be larger or heavier than which would allow a reasonable sized section of fence to be easily carried by one of these vehicle types.

A logical extension of the requirement for portability is the minimization of the tools or machinery required in the assembly of the fence. Where possible, design decisions have been made to eliminate the necessity of equipment that is large, difficult to transport, prohibitively expensive or requiring additional infrastructure. Permitted was hand held tools which could be easily be carried; powered either through individual battery packs, connection to a vehicle fitted with an inverter, or a small portable generator.

Additionally, no single part of the design should be heavier than can safely be carried by a two-man team. Currently, under the Australian Work Health and Safety legislation there is no upper limit to the weight that a person or persons can carry, stating that this depends upon the physical capabilities of the individuals (Worksafe Australia, 2016). Therefore, as guidance on what could be considered as a reasonable weight, Piyush G. Chapla's 2004 paper 'How Much Weight is Too Much for Manual Lifting: Determining a Weight Limit Guideline for Team-effort Lifting Tasks' was consulted.

The final guidelines reported state that: up to 30.8 kg (68 lb) is the recommended maximum weight for a single person, between 31.3 kg to 72.6 kg (69 lb to 160 lb) is the recommended range for a two-person lift, between 73 kg to 90.7 kg (161 lb to 200 lb) the recommended maximum for 3 people and anything over 90.7 kg (200 lb) lifting in any team arrangement was not recommended.

Taking the middle of the range given for the maximum two man-team lift means that a maximum weight limit of approximately 50 kg should be should be applied to any given part of the design. However, where possible the weights of components will be minimized to reduce the effort required to assemble the fence.

3.1.3 Fast Assembly to Maximize Protective Coverage Prior to Fire

Due to the unpredictable and rapid way in which bushfires can develop, any defensive strategy must be able to respond in a quick manner to changing conditions and posed threats. Therefore, the proposed design for a bushfire defence fence must be such that an adequate level of coverage can be established in the relatively short period between the issue of a bushfire alert and the approach of the fire front, without endangering those people installing the fence.

This requirement is very hard to quantify as the factors affecting it are highly variable. The period between the issuing of a bushfire alert to its impending approach can vary between hours and days. What might be deemed an acceptable level of coverage depends upon the specific application for the fence. For the defence of a single property, a perimeter of approximately 200 metres may suffice, while for a more organized effort for fire containment by firefighters may require a stretch of fencing along a firebreak of up to several kilometres.

As this project is the first of its kind, and aims to develop a design suitable for use as a proof of concept, the fence design must be capable at least of being installed as a defensive measure for a single property; or several properties in close proximity. This should be capable of being achieved within the period of a single day, at most 6 to 8 hours.

3.1.4 Low Capital Cost to Attract Market Investment

Given the financial and human costs that are associated with bushfires, significant interest is anticipated in wire mesh fencing as a bushfire defence strategy once its efficacy has been suitably demonstrated. Given the lack of large scale testing of the concept at this stage

however, there may be some hesitation to invest large sums of money into such a project with no guaranteed success.

The design should keep this in mind and aim to minimize costs associated with the fence materials, manufacture and related equipment in order to maintain appeal to investors and other interested parties. This will encourage widespread testing of this bushfire defence concept and pave the way for more involved designs requiring higher levels of organization and investment.

3.2 Development of Design Assessment Criteria

Given the listing of the specific design aims above, a series of performance metrics was established in order to measure how well the final design met these design aims and to create a baseline assessment against which potential future designs could be compared.

3.2.1 Efficacy of Firebrand Transmission Prevention

As the primary purpose of the fence is to retard bushfire progress through reducing firebrand transmission into a protected zone, the fences success in performing this task is one of the most important performance metrics to be considered. However, it is also one of the most difficult to assess at a design stage.

This is due to the large amount of unknown variables and the untested nature of the concept. While empirical data exists from the preliminary trials of various sizes of wire mesh and their ability to reduce fuel bed ignition, all of these trials were conducted in specialized devices where the firebrands had no choice but pass into the mesh.

In actual application however, the success of the fence depends upon several other factors. Height of the surrounding trees and lofted firebrands is a big consideration; as was mentioned in section 3.1.1 it is unlikely a design meeting all the aims would be of the same height as the surrounding foliage. The impact this is likely to have on the performance is unknown and makes assessing the design difficult from a theoretical approach.

Another unknown which could affect the performance is the potential for the creation of high pressure region in front of the fence due to the impeded airflow, which could result in an updraft carrying the firebrands up and over the fence. This potential phenomenon has

not been investigated and could impact the performance of the fence. Again, this makes assessing the real world performance of the design difficult from a theoretical approach.

In view of these factors, the performance of the design against firebrand transmission will just be taken as the preliminary testing performance of the size and style of mesh used. Primarily, the percentage reduction in fuel bed ignition criteria will be used. However, due to the variation in buffer zone size and other parameters in the different papers on firebrand transmission, this metric will simply be a qualitative ranking rather than quantitative, i.e. a smaller mesh opening size will be taken to be more effective if trials show a reduction in fuel bed ignition spots.

3.2.2 Efficacy of Radiant Heat Flux Reduction

Assessing the performance of a design in reducing the amount of radiant heat flux from the fire that can pass through is more straightforward. From the experimental work of Hashempour that was discussed in section 2.4.2, the passing ratio of radiation through the mesh can be predicted based upon the porosity. While other factors such as the emissivity of the wire mesh material would affect the total amount of re-radiation from the fence, this factor is considered to be small compared to the incident radiation. Therefore, the performance of the fence in terms of reducing radiant heat flux will be measured by the passing ratio of the mesh used, given in figure 7.

3.2.3 Measurement of Portability and Weight of Design

As was detailed in section 3.1.2 above, individual components of the structure need to be less than 50 kg per section, and compact and light enough that they can easily be transported by the listed vehicles. Given that each individual part of the fence is of an acceptable weight to manoeuvre, the main factor affecting the portability is the total weight of material required.

Therefore, the metric that has been decided upon to measure the portability of the design is mass per unit length. This will allow a fair comparison between future designs of different construction styles and also gives useful information for the purposes of logistics and planning.

Because the primary focus of this design is on a relatively small scale assembly for the purpose of defending a single house or property, the units used will be tonnes per 100 metres, units corresponding roughly to the anticipated scale of the design.

3.2.4 Measurement of Speed of Assembly

As with several of the other performance metrics discussed here, determining the speed with which a proposed design could be assembled is a difficult endeavour, based upon numerous simplifying assumptions. However, as was discussed in section 3.1.3 the rate at which the fence can be assembled is an important criterion in determining the practicality and effectiveness of a design.

The measurement unit which has been selected to quantify the assembly speed is metres of fence per hour (m/hr). Similar to the units used in the measurement of portability, t / 100 m, the units chosen here correspond to the anticipated rate of assembly. Again, the chosen unit of metres / hour serve a practical purpose in logistics and planning as well as comparing different design performances.

When the final design is assessed for speed of assembly, the procedure used will be as follows:

- A list of all tasks required in the assembly of a section of the fence will be listed, and a reasonable estimate of the time that each task is anticipated to take will be made. A rationale behind each time estimate will be given to attempt to standardize the method of assigning the times, i.e. allow others understand the reasoning used.
- The order of these tasks will then be examined and any task that is required to be completed immediately before a specific task can be begun will be recorded against that task, i.e. a precedence table will be created.
- A network diagram will then be constructed from this precedence table.
- The critical path of this network, i.e. the quickest time that the fence section can be assembled, is calculated. However, should more tasks occur in parallel than workers assembling the fence, the additional time required to complete the extra tasks will be calculated and added to the total.
- This time will then be converted to hours.

- The speed of assembly of the fence will then be approximated by dividing the length of the section of fence used in the above calculations by the time in hours to assemble it.

3.2.5 Measurement of Cost

The final metric used to measure the proposed design is that of cost per unit length. Again, the specified length used is 100 metres, in order to maintain homogeneity with the portability metric. This is calculated by dividing the cost of a section of fencing by its length in metres then multiplying this result by 100.

In order to determine the cost of a section of fence, the influential factors have been examined. Initial expenditure associated with creation of a bushfire defence fence can be broadly split into two main categories; material costs and labour costs. These investigated in detail below.

Material costs are the easiest to quantify. Prices of materials such as wire mesh, steel sections etc. are readily available. While these prices may depend upon order quantity and supplier, a reasonably accurate estimation of the cost can be established by determining the amount of material required to construct a single fence section and multiplying by a standard material price.

Labour costs associated with the initial fence price are mainly due to the manufacturing process, which varies with the complexity of the design. In addition, labour costs often are equal to or in excess of the material costs, however, manufacturing costs tend to decrease with an increased production volume in accordance with the economies of scale. This makes estimating the manufacturing costs a difficult exercise to perform and as such was excluded from the scope of the project.

3.3 Development Procedure of Fence Design

The methodology used in the development of the fence design consisted of three major components. These were:

- Idea generation.
- Feasibility analysis through fundamental calculations.

- Modelling and simulation using Finite Element Analysis to develop and refine the design.

These three components comprised an iterative cycle through which the individual aspects of the final design were conceived, refined and completed. Each component is discussed in further detail below.

3.3.1 Idea Generation

Idea generation is one of the most important steps in the design process, yet also the most difficult to quantify. Solutions to problems can sometimes be obvious, sometimes elusive. The most obvious solution may not in fact be the most appropriate. Consultation with peers and university staff was a major technique used in this stage of the design process.

3.3.2 Feasibility Analysis Through Fundamental Calculations

The next stage in the design methodology is assessing the feasibility of an idea. Primarily, this was achieved through determining the relevant factors affecting the outcome, e.g. wind loading magnitude, bending stresses, overturning moment etc. and then using basic equations from engineering texts relating these factors to calculate the feasibility.

The basic procedure used in this approach was as follows:

- Identification of the appropriate formula from a reputable engineering textbook.
- A general calculation was carried out by hand to rearrange and solve the equation or equations and a sample calculation performed.
- A Microsoft Excel document was created using the general hand calculation to allow numerous calculations to be performed in a rapid and iterative manner.
- These results were then compared against available data to evaluate the suitability of the proposed solution.

This approach saved much time in evaluating ideas and gave a solid starting foundation for the next step in the design process.

3.3.2 Modelling and Simulation Using Finite Element Analysis

Once an idea had been proved feasible and an estimate of the appropriate sizing had been identified from the basic engineering calculation, a solid model of the proposed component

or assembly was created using the modelling package Autodesk Inventor. Once drafted, the model was then imported into the software package ANSYS Workbench and simulated using the 'static structural' analysis; a FEA package which meshes the geometry and can simulate the effects of various types of contact between multiple bodies, large deformation effects and thermal stresses. All of these effects are important in obtaining accurate results from the simulations of the models.

4.0 Preliminary Design Parameter Development

This chapter details the processes undertaken to develop an initial overarching approach to the design from the requirements identified in section 3.1. Exact design parameters are determined from further analysis and reasoning based on relevant available literature.

4.1 Calculation of Mesh Drag Force

Basic engineering judgement clearly demonstrates that the largest issue associated with the construction of such a fence is the drag force that will be imposed upon the structure by the wind. Due to the design limitations discussed in section 3.1, the magnitude of this wind loading will be the primary factor dictating the overall parameters such as fence height and span between supports.

Identified in section 2.6.5, the maximum wind speed that the fence is required to withstand as per the Australian Standard is 24 m/s (86.4 km/h). However, as bushfire risk increases with wind speed, and speeds of 100 km/h reported as contributing to the intensity Black Saturday fires, the design wind loading calculations presented here use 28 m/s as the wind speed (100.8 km/h). This will also go some way to accounting for high speed gusts, i.e. dynamic loading of the fence structure, which has not been considered in the scope of this project.

While there is numerous different variation of stainless steel wire mesh available on the market, the drag forces will only be calculated for the three typical sizes of bushfire mesh listed in section 2.3. This is reasonable as it was discussed in 2.5 of the literature review that the drag force is largely a function of the mesh porosity. This means that other meshes with slight variations in wire diameter and opening size but with the same porosity will have very similar drag forces, within an acceptable margin of difference.

To calculate the drag force per unit area, equivalent to pressure, on the mesh the drag coefficient of each mesh needs to be calculated. In order to do this, the Reynolds number of the flow around each of the meshes has to be calculated. It is found using the following formula:

$$Re = \frac{\rho V D}{\mu} \qquad 4.1.1$$

Where Re is Reynolds number, ρ is the density of the air in kg/m^3, V is the velocity of the airflow in m/s, D is the diameter of an individual strand of the wire used in the mesh in m and μ is the dynamic viscosity of the air in Pa.s. In these calculations a value of 1.225 kg/m^3 for ρ and 17.83 x 10^{-6} Pa.s for μ was used (Dixson, J.C, 2007).

These values of Reynolds number were then used to calculate the drag coefficient for each of the meshes at the design speed of 28 m/s. This was done by using both of the equations found in the literature review and selecting the larger of the two values. From these drag coefficients, the drag force per unit area was calculated using formula 2.5.2. The results of the three meshes are shown in the table below.

Diameter (mm)	Mesh Porosity (%)	Reynolds No.	Cd	Drag Force (N/m^2)
0.9	42	1731	2.3	1105
0.45	62	866	0.735	353
0.18	76	346	0.368	177

Table 4-1 Results of Calculations of Re, Cd and Drag Force for Three Porosities of Mesh

Examining the values for drag force per unit area of each mesh, it is apparent that the drag force for the 62% porous mesh is approximately twice that of the 76% porous mesh, while the 42% porous mesh has a drag force per square metre approximately 6.25 times that of the 76% porosity mesh. The 42% porosity mesh had approximately 3.13 times larger drag force than the 62% mesh.

These values for drag force are the values that were used in the next stage of the design process.

4.2 Implications of Drag Force on Fence Sizing

4.2.1 Total Drag Force and Overturning Moment for Various Fence Sizes

Using the drag forces for the three meshes identified in section 4.1, the total wind loading for a range of different fence heights and main support spans was estimated. A schematic demonstrating the loading configuration used in these calculations is shown below.

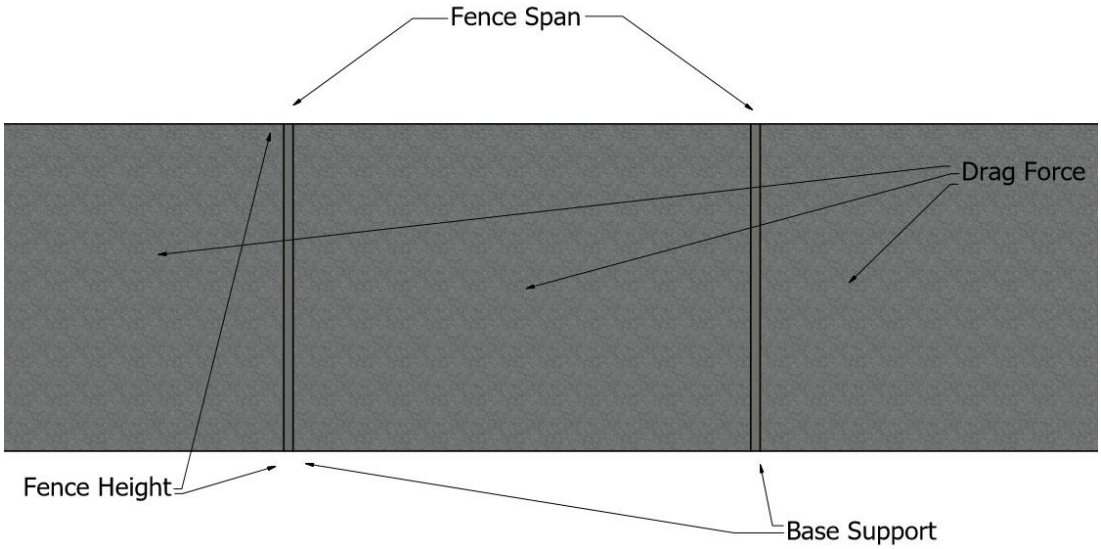

Figure 4-1 Image Showing Basic Fence Configuration

The magnitude of the drag force acting on a single support was approximated by multiplying the height of the fence by the span between support to find the total mesh area effectively supported by a single support and then multiplying this by the drag force per unit area for each respective mesh.

$$F_D = Span \times Height \times \frac{Drag}{m^2} \qquad 4.2.1$$

Assuming that this load was acting at the centroid of the fence, the overturning moment at each of the supports was also estimated. The overturning moment for each support was estimated by applying this load at half the height of the fence, using the following formula.

$$Overturning\ Moment = \frac{1}{2} \times F_D \times Height \qquad 4.2.2$$

Several tables showing the results of these calculations are presented below.

76 % Porosity Mesh								
Fence Height								
	10 m		12 m		14 m		16 m	
Span	Drag kN	Moment kN.m	Drag kN	Moment kN.m	Drag kN	Moment kN.m	Drag kN	Moment kN.m
2 m	3.5	17.7	4.2	25.5	5.0	34.7	5.7	45.3
4 m	7.1	35.4	8.5	51.0	9.9	69.4	11.3	90.6
6 m	10.6	53.1	12.7	76.5	14.9	104.1	17.0	135.9
8 m	14.2	70.8	17.0	102.0	19.8	138.8	22.7	181.2
10 m	17.7	88.5	21.2	127.4	24.8	173.5	28.3	226.6
12 m	21.2	106.2	25.5	152.9	29.7	208.2	34.0	271.9
14 m	24.8	123.9	29.7	178.4	34.7	242.8	39.6	317.2
16 m	28.3	141.6	34.0	203.9	39.6	277.5	45.3	362.5

Table 4-2 Table Showing Drag Force and Overturning Moment for Various Fence Configurations with 76% Porosity Mesh

62 % Porosity Mesh								
Fence Height								
	10 m		12 m		14 m		16 m	
Span	Drag kN	Moment kN.m	Drag kN	Moment kN.m	Drag kN	Moment kN.m	Drag kN	Moment kN.m
2 m	7.1	35.3	8.5	50.8	9.9	69.2	11.3	90.4
4 m	14.1	70.6	16.9	101.7	19.8	138.4	22.6	180.7
6 m	21.2	105.9	25.4	152.5	29.7	207.6	33.9	271.1
8 m	28.2	141.2	33.9	203.3	39.5	276.8	45.2	361.5
10 m	35.3	176.5	42.4	254.2	49.4	345.9	56.5	451.8
12 m	42.4	211.8	50.8	305.0	59.3	415.1	67.8	542.2
14 m	49.4	247.1	59.3	355.8	69.2	484.3	79.1	632.6
16 m	56.5	282.4	67.8	406.7	79.1	553.5	90.4	722.9

Table 4-3 Table Showing Drag Force and Overturning Moment for Various Fence Configurations with 62% Porosity Mesh

Note however that these are simply estimates of the total drag force and moment assuming

42 % Porosity Mesh								
Fence Height								
	10 m		12 m		14 m		16 m	
Span	Drag kN	Moment kN.m	Drag kN	Moment kN.m	Drag kN	Moment kN.m	Drag kN	Moment kN.m
2 m	22.1	110.5	26.5	159.1	30.9	216.6	35.4	282.9
4 m	44.2	221.0	53.0	318.2	61.9	433.2	70.7	565.8
6 m	66.3	331.5	79.6	477.4	92.8	649.7	106.1	848.6
8 m	88.4	442.0	106.1	636.5	123.8	866.3	141.4	1131.5
10 m	110.5	552.5	132.6	795.6	154.7	1082.9	176.8	1414.4
12 m	132.6	663.0	159.1	954.7	185.6	1299.5	212.2	1697.3
14 m	154.7	773.5	185.6	1113.8	216.6	1516.1	247.5	1980.2
16 m	176.8	884.0	212.2	1273.0	247.5	1732.6	282.9	2263.0

that

Table 4-4 Table Showing Drag Force and Overturning Moment for Various Fence Configurations with 42% Porosity Mesh

only the mesh is responsible for the drag force. As such, they are likely to represent an unconservative estimate as the drag on the fence supports themselves has not been calculated; in addition, the drag on the mesh is likely to be slightly higher in the final design due to the presence of restraints to hold the mesh to the fence.

4.2.2 Analysis of Total Drag and Overturning Moment Estimations

Several trends were noticed in the estimations of drag force and overturning moment for each of the mesh porosities which would affect the design. As was expected, increasing both the height and span of the fence increased the drag force and overturning moment. However, for any given support span, as the height of the fence was raised the overturning moment grew faster than the drag force, at an increasing rate. This was not unexpected as an increase in height not only increases the area of wind loading but raises the centre of action of the force; as a result, the moment is proportional to the height squared.

At a constant fence height, increasing the span between supports increased both the drag force and consequently the overturning moment, however, this increase was linearly proportional to the increase in span.

What this means from a design perspective is that increasing the height of the fence has a much higher cost in regards to the design aims of high portability and speed of assembly. Raising the height of the fence by any given amount will require larger supports and stronger support footings than the same increase in support span.

As the only potential benefit associated with increasing the height of the fence is to improve the performance of firebrand reduction; a relationship which is still unclear due to a lack of experimental data, it is more productive from a design sense to limit the height of the fence to maximize the support span that can be used. A larger support span will directly correspond to increased portability and speed of assembly through reducing the amount of supports that need to be transported and assembled for any given fence length. Therefore, a fence height of 10 metres, the lowest height deemed acceptable to meet the design aims, was selected in order to minimize the created moment and maximize the span of the fence.

4.3 Fence Support Footing Design Selection

One of the primary challenges posed by the high level of drag force experienced by the fence is securing the supports firmly to the ground such that they do not slide or tip when under the design load; this would constitute a structural failure of the fence. As each fence support is effectively supporting the area of a single span, the required reaction forces for any fence dimensions should be sufficient to counteract the drag force and overturning moment for that particular configuration, with the inclusion of an appropriate safety factor.

Several options were investigated as methods of securing and restraining the fence supports into place. These were:

- Weighted blocks at base of fence supports.
- Drilling post holes to bury the supports into the ground.
- Using ground anchors to secure the fence support.

Each of these methods were assessed for their feasibility and alignment with the design aims, before a decision was made. The details of the assessment of each method is presented in the following sections.

4.3.1 Use of Weighted Blocks to Secure Fence Supports

The first method which was considered to secure the fence supports was the use of some type of weight, such as concrete blocks, at the base of each support. This method of support is used in other fencing applications, such as the assembly of temporary barriers at motor racing street circuits; shown in the figure below.

Figure 4-2 Picture Showing Use of Concrete Blocks as Fence Support (McGinnis 2013)

While it was evident that the required weight of these blocks would be large, the option was considered attractive due to its simplicity in assembly and was therefore investigated to determine if the required weight would be feasible amount.

The mechanism through which a weighted block secures the fence support has two components; the reaction against the drag force and the counteraction of the overturning moment.

In order to stop the fence support from sliding backwards due to the drag force, the weighted block relies upon the friction created between itself and the ground to stop the sliding. Therefore, the maximum frictional force possible in any conditions must be larger than the maximum design drag force, by the selected factor of safety. This means that the lateral restraint capacity is dependent upon both the coefficient of friction between the block and ground and the weight of the block.

Preventing the fence from tipping over however, depends upon the weight of the block as well as its physical geometry. As the drag force on the fence increases, the 'location' at which the normal force from the ground acts will shift away from the centre of gravity and towards the rear, such that the moment created by the drag force is balanced by the moment created by the now offset normal force. Therefore, the maximum moment that can be supported by the weighted block is the product of its weight multiplied by half of its length in the direction of the wind loading.

To evaluate the feasibility using weighted blocks as a support footing, an Excel spreadsheet was created to calculate the weight that would be required to support each of the 10-metre-high fence configurations from section 4.2.1 for a block with a length of 2 metres in the direction of wind loading.

This was done by taking the larger of the results from the formulas below for each fence configuration. Note that a coefficient of friction between the block and the ground of 0.25 was chosen to represent a conservative estimate for the friction between the block and the ground (Transportation Research Board, 2010).

	Support Span							
Porosity	**2 m**	**4 m**	**6 m**	**8 m**	**10 m**	**12 m**	**14 m**	**16 m**
76%	1,804 kg	3,609 kg	5,414 kg	7,218 kg	9,023 kg	10,827 kg	12,632 kg	14,436 kg
62%	3,590 kg	7,198 kg	10,797 kg	14,396 kg	17,994 kg	21,593 kg	25,192 kg	28,791 kg
42%	11,266 kg	22,531 kg	33,797 kg	45,062 kg	56,328 kg	67,593 kg	78,859 kg	90,124 kg

Table 4-5 Table Showing Theoretical Mass Required to Support Fence

Upon reviewing the results of the required support block weights shown in the table above, it was immediately apparent that this method of fence restrain was unsuitable for this application. The required block weight for the 76 % porous mesh with a support spacing of 2 metres was over 1800 kg, without including a safety factor against the overturning moment. Therefore, this method of support was not perused any further.

4.3.2 Planting of Fence Supports into Ground via Post-Hole Digger

The second method investigated for securing the fence supports was burying the base of the posts into the ground at a sufficient depth to resist the applied lateral force and overturning moment. This is the typical method used in the construction of more permanent fences and walls.

Digging post-holes for the supports will require the use of drilling machinery, as it is unfeasible to dig the necessary number of holes in the time and to the depth required. This is in contrast to the design aim to minimize the amount of requisite machinery. However, post hole digger attachments for tractors are readily available for a reasonable price, and are capable of drilling holes quite quickly. This is in line with the design aims of assembly speed and cost and was therefore investigated.

The mechanism in which this method of footing works is through the soil pressure created against the buried section when a force applied to the support attempts to displace the earth surrounding it. Therefore, the magnitude of the support reactions that this type of footing can provide is dependent upon the soil properties, support size and buried depth.

This was demonstrated by Mason, Gates and Moore in their 2012 paper 'Determining forces required to override obstacles for ground vehicles'. In this report, they derived a formula for the force required to push over posts buried into the ground, before conducting empirical testing to confirm its validity. The derived equation is shown below.

$$F = \frac{2\gamma DL}{3\left(h+\frac{L}{2}\right)} \qquad 4.3.3$$

Where F is the force required to overturn the post in Newtons, γ is the dry bulk density of the soil in N/m^3, D is the effective diameter of the post in metres, L is the buried depth of the post in metres and h is the height in metres above the surface of the soil at which the overturning force is applied.

In order to evaluate the feasibility of this method of support, an Excel document using the above formula was created to calculate the overturning force for a variety of post support diameters and burial depths. These results, shown in table 4.3.2 below, were then compared to the estimated wind loading for the different fence configurations in table 4.2.1.

Note that in these calculations, a soil specific weight of 12753 N/m^3 (corresponding to a density of 1.3 g/cm^3) was used as this represents a reasonable estimation of average soil density (Argonne National Laboratory, 2010).

	Post Diameter				
Post Depth	**100 mm**	**200 mm**	**300 mm**	**400 mm**	**500 mm**
1 m	0.155 kN	0.309 kN	0.464 kN	0.618 kN	0.773 kN
2 m	0.283 kN	0.567 kN	0.850 kN	1.134 kN	1.417 kN
3 m	0.392 kN	0.785 kN	1.177 kN	1.570 kN	1.962 kN

Table 4-5 Overturning Force of Various Footing Depth and Diameter Configurations

Comparing these results with the drag force estimates, it is clear to see that this method of support is unsuited to the application as it simply cannot support the drag force. Most results differ by two orders of magnitude.

While a larger and more permanent style of footing may be suitable for future designs, a simple backfilled post-hole is not adequate for the required load. Consequently, further investigation into this method of support was not continued.

4.3.3 Restraint of Fence Supports with Ground Anchors

The third approach to restraining the fence supports investigated was using temporary ground anchors. Ground anchors are devices that are driven into the earth to support large tensile loads; they are commonly used in the construction of towers, utility poles and other similar applications to tie supporting guy wires to the ground.

Because they can typically only support a tensile load, guy wires will be necessary in a design which uses ground anchors to restrain the fence supports. This is not a disadvantage, however, as this allows the location of the support reaction to be shifted further up the post. By increasing the lever arm of the support reaction, the overturning moment created by the drag force can be reduced substantially. As it was the excessive size of the overturning moments which made the previous two methods investigated unfeasible, rather than the drag force itself, eliminating the moment is a definite improvement.

Another advantage to using ground anchors is flexibility in the design. If required, several anchors and guy wires can easily be used on a single support. This allows the total load to be shared, meaning that larger fence support spans can be used than would be possible with a single anchor, likely leading to increases in assembly speed and reductions in weight. It also means that in the event of poor soils, the fence design can still be safely installed, simply requiring additional anchors rather than being unsuitable.

There are several different types of earth anchor design, however temporary reusable anchors are most commonly a 'screw' style. As the name suggests, these feature a helical thread which is drilled into the ground. An image showing one particular make is below.

Figure 4-3 Image of Several Temporary Earth Anchors (Rittenhouse, 2016)

Due to the interaction between the soil and the anchor, the maximum load that a ground screw can support depends upon various factors such as the type of soil, size of the anchor, placement depth and the tensioning torque applied.

While earth anchors are available in extremely large sizes, larger sizes typically require the use of heavy machinery such as an excavator or tractor with a drilling attachment to install and remove. For more moderate sizes, hand-held hydraulic installers are available at a reasonable price, allowing for rapid, portable installation.

In line with the design aims of maximizing assembly speed and portability, sizes of ground anchors that could be installed using such an installer were investigated further to determine the magnitude of load that they could support.

Preliminary searches of available temporary ground anchor products fitting this criterion found that there were numerous different companies offering similar competing products. Not all of these firms offered estimates of the load capacity of their products, however, the values from those that did was in reasonable agreement, when comparing similar soil types and anchor sizes.

The maximum load values that were selected for the purpose of feasibility investigation and subsequent design work were those taken from the website of the company *ANCA Structural Anchors*, a firm based in South Yorkshire, England. This was because they offer a complete

ground anchor solution, including ground screws, hand-held portable installers, in addition to an apparatus for proof testing the strength of installed anchors (ANCA, 2016).

The nominal holding strength of their 'System 2000' ground anchors is given as 2000 kg (19.6 kN), similar to that of a comparably sized anchor from Hubbell Power Systems, which has maximum load of 5000 lb (22.3 kN) in typically encountered soils (Hubbell, 2016).

To assess the feasibility of using ground anchors to secure the fence posts, an Excel spreadsheet was made, calculating the maximum drag force that an arrangement using the ground anchors specified above could withstand. As the anchors have to be loaded in tension to work effectively, an anchor angle of 45° to the horizontal was chosen. The results are shown in table 4-3 below.

Number of Load Bearing Anchors	Maximum Drag Force
1	**13.86 kN**
2	**27.72 kN**
3	**83.16 kN**

Table 4-6 Maximum Lateral Support Force for Various Number of Ground Anchors

From the results in the table, it can be seen that the use of ground anchors is suitable to secure the fence as these results overlap with several of the calculated drag forces for different configurations outlined in section 4.2.1. Therefore, ground screw anchors were selected for use in the design.

4.4 Support Spacing and Mesh Porosity Selection

Having selected an appropriate method to secure the fence posts, the type of mesh and fence span and height configuration was determined.

To ensure the structural integrity of the fence at the design conditions, a factor of safety is required to account for all uncertainties in the loads or supports. However, an overly conservative safety factor will adversely impact upon the design aims unnecessarily.

As the exact load capacity of the ground anchors is variable, a suitable safety factor should be chosen to maintain a safe margin against failure. As detailed in the above section, soil type plays a major part in determining their strength. However, the availability of the portable proof testing tripod with the ground anchors goes some way to reducing this

concern. By testing a sample of anchors at the site of assembly, reliable values can be collected and additional ground anchors used if deemed necessary. As this safety factor at this stage is simply assisting in determining an appropriate fence size, a safety factor of 1.5 was chosen.

Applying the safety factor of 1.5 to the values in table 4-3, it can be seen that with one anchor, a maximum drag of 9.24 kN was permissible, two anchors 18.48 kN and three 27.72 kN. However, it was decided that only two anchors should be nominally used in the design. Because anchors would have to be installed on both sides of the fence, this is a total of four per post. By only specifying two, extra capacity is allowed for poor soil conditions, whereas is three were specified and an additional required, eight anchors would be required per post, simply too many.

Comparing the results above against the drag force tables in section 4.2.1, it is clear that 42% porosity mesh is unsuitable, as two anchors do not even cover a 2 metre span. Between the 62% mesh and the 76%, the 62% mesh could have a span of approximately 5 metres whereas the 76% mesh could have a span of 10 metres.

From the information outlined in section 2.4.2 of the literature review, lower porosity meshes blocked more Radiant Heat Flux, at an amount greater than the porosity itself would suggest. However, from figure 2-7 it appears that this 'tunnel vision' effect is negligible in the range between 62% to 76% porosity.

In light of this information, it was decided that the 76% porous mesh would be used in the fence design. By using 76% mesh in the design, the fence support spacing could be doubled compared to that of the 62% mesh. This would relate nearly directly to a doubling of the fence assembly speed; halving of the weight per unit length and also reduce material costs, all for the price of a 14% increase in Radiant Heat Flux transmission.

4.5 Fence Construction Method Selection

Another issue requiring consideration at this stage of the design process is the method of assembly of the fence. As was detailed in section 3, the final design must be both portable and able to be assembled rapidly with minimal requirement for machinery or tooling.

Due to the large height of the fence, this issue is complicated. Several different approaches to assembling the fence are listed below.

- The entirety of the fence is assembled lying on the ground and then the whole fence is stood up as one unit.
- Small sections of the fence such as a single support span are assembled lying on the ground and then stood up in segments.
- The fence posts are assembled and stood up first, and then the mesh is strung up between the posts.

The advantages and disadvantages of each approach are detailed in the sections below, before a decision on the final approach to be taken is decided.

4.5.1 Entire Fence Assembled on Ground and Erected as Single Unit

The first method of fence assembly investigated was the complete assembly of the fence sections in position, lying on the ground such that the fence simply requires 'standing up' by rotating about its base into a vertical position.

This method has its advantages, primarily the ease with which the fence can be assembled. By positioning and attaching the mesh infill material to the fence supports on the ground, access to the full length of the fence posts is ensured without the requirement for any lifting device such as a scissor lift or cherry picker. This allows a simpler attachment method of attaching the mesh infill to the posts to be used.

A major disadvantage to this approach however, is the necessity for the entire fence to be stood up as one unit in one step. Because the length of mesh between each fence is fixed, each post has to be elevated at the same rate as the ones beside it. If the posts are not lifted together, the effective length between the top of the posts will grow, straining the infill material and will pull the neighbouring posts out of alignment.

This is an issue for two reasons. Firstly, the longer the length of fence that is being stood up, the more people will be required, as at a minimum one person will be required per post if the use of machinery is excluded. A length of 100 metres will therefore require at least eleven people to construct (one per fence support), which does not suit the design aims of a simple, fast assembly.

Secondly, in the event that the fence was being lifted into the direction of a substantial wind, the drag force imposed would likely be too great to be overcome without some type of heavy machinery. Again, this does not suit the design aims specified in section 3.

4.5.2 Assembly and Construction in Single Support Span Sections

The second method investigated was similar to the first which is detailed above. Rather than constructing large spans of the fence as a single unit however, this approach would concentrate on raising a single 10 metre span with the two supports on each end in one movement. This would result in the fence design comprising of many separate 10 metre sections, all individual units.

This approach retains the advantages of easy positioning and component assembly outlined in the above approach due to the easy access from the ground. It also avoids the issue of having to raise the entire fence as a single unit, the major problem with the first approach.

However, new issues are also posed by this method. Firstly, due to the requirement of having a fence post on each end of the mesh infill being raised, a 'doubling up' of fence supports will occur on centre sections as each support is only attached to mesh on one side. This will increase the total weight and assembly time of the fence, due to the requirement to transport and assemble more posts for the same length of fence.

Secondly, unless the two posts from the neighbouring sections are securely joined together after the sections are raised, each individual fence post will require additional ground anchoring in the direction parallel to the fence. This is to counteract the tendency of the mesh to pull the fence supports together when wind loading is applied. As the infill material cannot support a bending moment, equilibrium is achieved through tensile forces, and the shallow angle at the supports means these forces are several times larger than the applied load.

These tensile forces are less of an issue when mesh is connected to both sides of the support, or if individual supports are used, they are securely joined to one another. In this configuration, the tensile force created is either counteracted by the same tensile force from the neighbouring mesh section or transmitted through the infill material to the rest of the posts, avoiding the need for individual longways restraint on each post.

However, joining the two individual posts together all the way to the top securely enough to transmit these lateral loads from one to another is an issue due to their large height. To avoid the need for lifting equipment, any joining method much be easy to implement and reverse remotely without introducing alignment problems. The joints must also must be strong enough to adequately transmit the tensile loads; not an easy problem to solve.

4.5.3 Fence Post Construction Followed by Hoisting Mesh

The third approach to constructing the fence that was investigated was assembling and lifting the fence posts into position individually, before the mesh infill is hoisted into position between the respective posts with a separate lifting arrangement.

Several advantages over the other methods are presented in this method of fence construction. Firstly, by lifting the fence posts individually, without any mesh infill attached, the force required to raise each post is minimized. This is because both the total weight being lifted at any point is reduced, in addition to eliminating any potential drag force on the mesh opposing the lifting process. Furthermore, by hoisting the mesh infill material vertically between the already erected fence posts, the capability of the fence to be constructed in windier conditions is improved. Barring any potential friction at the restraints, the direction of motion is perpendicular to the applied wind loading and as such should minimize any issues in construction.

Again, this approach introduces new issues. Obviously, by moving away from a design where the mesh is fixed into a set position while on the ground to a design where the mesh is hoisted up the post, an additional lifting mechanism is required introducing additional complexity along with extra weight.

Secondly, as the mesh is being mounted onto the posts after they have been lifted rather than on the ground, extra care is required in the positioning of the posts to ensure that they are separated by the correct spacing. If the spacing between two posts is too great, the mesh will be unable to be installed onto that span, and the post will have to be deconstructed and shifted into the correct position.

4.5.4 Final Fence Construction Method Selection

Weighing up the advantages and disadvantages for each approach to the fence construction outlined in the above sections, a decision for the method to be used in the final design was chosen.

The method selected was the third approach listed; assembling and constructing the fence posts first, before hoisting the mesh in a similar manner to a flag between the posts. After consideration, it was decided that this method presented the least obstacles to implementation when weighted against the other options. Therefore, further design decisions were made with this method of construction in mind.

4.6 Final Design Parameter Summery

Below is a table summarizing the design parameters that were determined in this chapter.

Fence Height	**10 m**
Fence Span Between Supports	**10 m**
Mesh Type	**76 % Porosity with 1.23 mm Aperture**
Max. Design Wind Speed	**28 m/s**
Drag Force at 28 m/s	**17.7 kN**
Drag Force per m^2	**177 N**
Support Method	**19.6 kN Earth Screw Anchors**
Fence Construction Method	**Posts Positioned & Mesh Hoisted into Position**

Table 4-7 Summary of Design Parameters

5.0 Final Design Development and Validation

This chapter covers the development of the final fence design. This includes the identification of factors requiring consideration in the development of the design, the methodology used in developing each aspect of the design and validation of the final design in the form of FEA analysis results.

5.1 Fence Post Sizing and Selection

After preliminary investigations, several key factors requiring consideration in the design of the fence posts were identified. These were:

- Post material and geometry
- Location of guy wire / ground anchor attachment points
- Bending moment induced stress along post height
- Buckling considerations
- Maximum length and weight requirements

Ultimately, the aim was to develop a design for the fence posts which was lightweight, portable, cheap, made from readily available steel sections and featured a good factor of safety at the design temperature of 500°C. The process through which this was achieved is detailed in the sections below.

5.1.1 Fence Post Material Selection

The first stage of designing the fence posts was to select and size the material and geometry to be used as the base structure, and to identify the optimum locations to attach the guy cables. The optimum design objectives of this stage of the process was to:

- Use commonly available steel sections to ensure availability and reduce cost
- Minimize the total weight of the posts
- Have an acceptable factor of safety at the design temperature of 500°C
- Keep total post deflection under design load to an acceptable level

A review of the commonly available steel sections which could be suitable found that the main selection options were either Rectangular Hollow Section (RHS), Square Hollow Section (SHS) or Circular Hollow Section (CHS).

After consideration of the various options, Circular Hollow Section was rejected. It was found that while CHS offered the best second moment of area in all directions for a given amount of material, the strength was primarily required in the direction of the wind loading, and therefore other geometry was better suited. It was also deemed to pose more difficulties in the implementation of the mesh attachment and hoisting as outlined in section 4.5.

Both RHS and SHS were determined to be suitable for the design of the fence posts. However, the final decision made was to first investigate and if possible use SHS. This was done for several reasons. Firstly, SHS provides an equal I value in both axis directions, providing better rigidity in both directions over RHS while maintaining a roughly similar weight per metre for comparable sizes. Secondly, the equal sized faces would allow for easier affixing of the required guy wire attachment points and other required items.

5.1.2 Steel Properties at 500°C

Reviewing the material properties of commonly available SHS in Australia found that the grade of steel used in a majority of SHS sections was AS/NZS 1163 Grade C450L0 (OneSteel, 2010). From AS/NZS 1163, the grade C450L0 has a guaranteed minimum yield strength of 450 MPa, with a guaranteed minimum tensile strength of 500 MPa (Standards Australia, 2016). The modulus of elasticity is 200 GPa. Note that all values are with reference to room temperature.

Rearranging equation 2.2 to calculate the yield stress at 500°C of C450L0 gives:

$$f_{y\,500} = f_{y\,20} \times \frac{905 - T}{690}$$

$$f_{y\,500} = 264.13 \text{ MPa}$$

For the reduction in the modulus of elasticity, the formula provided by the Australian Standard was not used, as it was shown to under predict the reduction under transient loading. Therefore, the reduction factor read off figure 2.5 at 500° was used. This corresponded to a value of 0.6, therefore:

$$E_{500} = 0.6 \times E_{20}$$

$$E_{500} = 120 \text{ GPa}$$

As such, these are the material properties that will be used in the design case of 500°C.

5.1.3 Metal Fatigue Considerations

In addition to considering the reduction in yield strength of the steel sections at the anticipated maximum design temperature of 500°C, the effect of metal fatigue resulting from cyclic loading should be considered. Due to the gusty nature of wind, the stress levels in the fence post will constantly be rising and falling with the fluctuations of the wind velocity.

To ensure the structural integrity of the fence over a long timeframe, the endurance limit of CL450L0 steel from which the SHS sections are manufactured was estimated.

According to Juvinall and Marshek in their 2012 text 'Fundamentals of Machine Component Design', the endurance limit of a metal can be estimated using the following formula:

$$S_n = S'_n . C_L . C_G . C_S . C_T . C_R \qquad 5.1.1$$

Where the terms are as follows:

- S'_N is the R.R. Moore Reversed Bending Stress Endurance Limit; Juvinall and Marshek report that for steel this can be approximated as half of the ultimate tensile strength. For a steel with an ultimate tensile of strength of 500 MPa, this corresponds to a value of 250 MPa.
- C_L is a load factor corresponding to the type of loading; bending loads; the major load type of the fencepost, have a value of 1,
- C_G is a stress gradient factor; for samples with an equivalent diameter greater than 10 mm, this is given as 0.9 for bending loads, which is what the loading of the fencepost predominantly is.
- C_S corresponds the surface finish of the material. As fatigue failure begins at the site of an existing crack or microscopic flaw in the material, the surface finish of the material affects the number of flaws present on the material for this process to begin (Juvinall and Marshek, 2012). A figure showing the relationship between ultimate tensile strength, surface finish and the surface finish factor is shown in figure 5.1 below. For a hot rolled section with ultimate tensile strength of 500 MPa, the surface factor is 0.68.
- C_T is a temperature factor relating to the temperature at which the metal is constantly subjected to. For temperatures less than 449°C (840° F) this value is 1. For temperatures over 449°C an equation is provided for evaluating C_T. Despite the maximum design temperature of the fence being 500°C, the value for C_T in

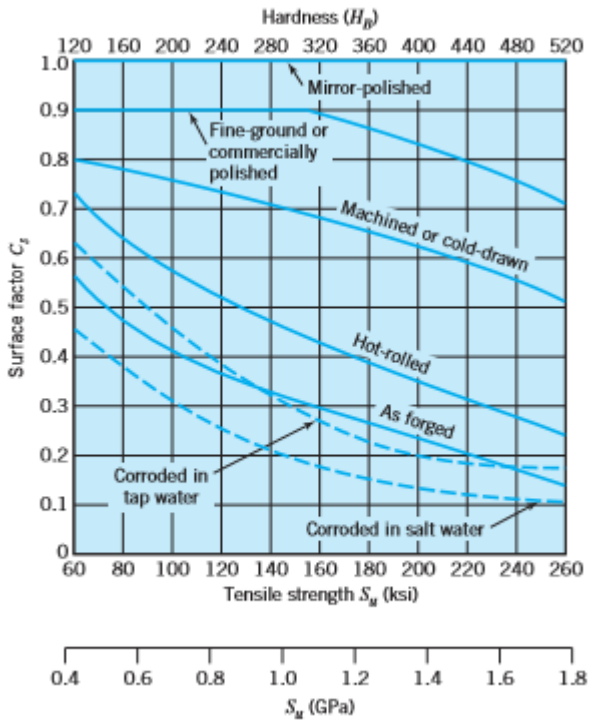

Figure 5-1 Figure Showing Relationship Between Fatigue Surface Factor, Tensile Strength and Surface Finish (Juvinall & Marshek, 2012)

calculating the endurance limit will be taken as 1, as the vast majority of the cyclic loading will take place well under 449°C.

- C_R is a reliability factor which corresponds to an 8% standard deviation of the endurance limit. As such, a 50% reliability is the mean result and thus has a value of 1; 90% reliability is 1.2875 Standard Deviations away from the mean and thus has a value of 0.897, etc.

As the fence is not being designed for permanent assembly, and periodic inspection can easily be carried out in between fence deployments, a reliability factor of 1, corresponding to 50% reliability was selected.

Substituting the values determined above into equation 5.1.1 gives the following expression:

$$S_n = 250 \times 1 \times 0.9 \times 0.68 \times 1 \times 1$$

$$S_n = 153 \text{ MPa}$$

While the true loading condition of the fence is more likely to conform to a combination of alternating load levels around a steady average level, rather than a fully reversed loading, uncertainty about the loading profile prohibits this further analysis. As a conservative approach, keeping the maximum stress levels below the endurance limit above will most likely at least guarantee a 10^6 cycle life, effectively infinite in this application.

Given that this value is less than the yield stress at of the steel at 500°C, the endurance limit above was compared against the maximum allowable stress in the design calculated using an appropriate safety factor, and the lower of the two values was used as the limiting stress level in the design of the fence post.

5.1.4 Fence Post SHS Sizing Methodology

As was discussed in section 4.2, the major problem posed by high drag forces applied at elevated heights is the moment produced. Not only does this moment attempt to overturn the structure, it also creates significant bending stresses in the fence post material.

In order to keep the weight of the fence post to a minimum, the bending moment created in the material must be minimized. The most effective way of achieving this is to position the guy wire supports at varying heights up the post, providing restraint at several different locations thereby reducing the length able to develop a large bending moment. This approach is applied in the construction of tall thin structures such as radio towers, shown in figure 5.1 at right.

Figure 5-2 Image Showing Guy Wire Placement on Radio Tower (Zhejing Guanming Power Transmission Material Corp. 2016)

This configuration also provides lateral restraint to reduce the occurrence of long column buckling.

However, this results in a statically indeterminate loading case, as the base of the post is supported, with a number of separate guy wire attachment points at varying locations up the post.

An investigation into available techniques for solving statically indeterminate loading cases revealed that the best suited method to carry out the required iterations was 2D beam element modelling using the ANSYS Mechanical software. Simple beam elements corresponding to a given beam cross section profile and material properties could be created and equivalent loading and support conditions to the actual situation could be applied, giving the reaction forces, bending moment diagram and deflections for that particular configuration.

Preliminary investigations using 2D beam analysis in ANSYS revealed little change of bending moment and reaction force results for different beam cross sections and Young's Modulus.

Therefore, to determine the number of ground anchors and guy wires required, the optimum location for the guy wire attachments to the post, and the required section size of the SHS, the following methodology was used.

- A 2D beam of 10 metre length and an arbitrarily selected cross section of 200mm x 200 mm x 5 mm thickness was modelled in ANSYS Static Structural.
- A UDL of 1770 N/m was applied to the entire length of the beam, to model the effect of the maximum design wind loading on the post.
- Fixed displacement supports were positioned on the beam to mimic the effects of the base and guy wire connections. The displacement supports for the guy wires however only restricted the displacement of the post in the axis of the applied load.
- Numerous simulations were run to determine the number of guy cables and locations which gave the most desirable reaction forces and bending moment distribution along the beam.
- After determining this configuration, an appropriate size of SHS was estimated by calculating the maximum bending stress associated with the maximum bending moment for a variety of SHS sections using the following formula:

$$\sigma = \frac{M}{Z} \qquad 5.1.3$$

  Where M is the maximum bending moment and Z is the Elastic section modulus for a given SHS section.

- This selection was used in the design and validated through FEA simulation of a 3D model.

In determining the optimum number and placement of guy wires and ground anchors to be used, certain criteria had to be met to ensure the viability of the design. These are summarized listed below.

- The support reaction forces at the guy wire attachments had to be less than the maximum allowable. As the displacement restraints only give the horizontal reaction force required, the corresponding tension in the guy wire was estimated by dividing the horizontal reaction by the cosine of 45 degrees, as the design angle for the guy wires is 45^{o}, for reasons explained below. As the nominal pull out strength of the ground anchors is 19.6 kN (see section 4.3.3), applying a minimum safety factor of 1.5 to this value gives a maximum guy wire tension of approximately 13 kN. Therefore, the calculated guy wire tension for a suitable configuration must be less

than 13 kN. Note that 1.5 was decided to be a suitable safety factor due to the ability to use additional anchors if required.

- While the base of the fence features smaller screw ground anchors to assist in securing it in place (see section 5.2), it was decided that they should be a redundancy in this particular loading configuration, as ground anchors are much weaker in lateral loading than in tension. Lateral restraint from the ground anchors provide a factor of safety only.

  Any lateral load on the base of the fence post therefore needed to be less than the frictional force which would be created by the vertical components of the guy wire forces. To maximize both the vertical and horizontal components of the guy lines, a design angle of 45 degrees was chosen. In addition, a value for the coefficient of friction between the base and ground of 0.25 was chosen. This corresponds to the smallest recorded value for the coefficient of friction between steel and the type of ground that the fence is likely to be deployed upon. (Transportation Research Board, 2010).
- The maximum bending stress calculated for the selected SHS section must be either lower than the endurance limit calculated in section 5.1.3, or have at least a factor of safety of 1.5 with respect to the calculated yield strength of the material at 500^{o}C, depending upon the smaller of the two. As figure 2.4 demonstrates the formula in AS 4100 for yield strength reduction is conservative at 500^{o}C, the safety factor of 1.5 was determined to be an appropriate safety factor for the high temperature scenario.

The results of the investigation process outlined above are presented in the section below.

5.1.5 Fence Post Sizing Results

Following the methodology outlined above, the optimum number of guy cable supports, guy wire attachment locations and SHS size was determined. It was found that two ground anchors and two guy wires was the minimum required to meet the specified criteria. Note that this means a total of four anchors and cables are required per post, as the two specified in the sizing are on the same side of the post.

The optimum locations of guy wire attachment identified was one at a height of four metres and the second at a height of eight metres. This configuration resulted in the minimum

bending moment at any location along the post. A Bending Moment Diagram for this arrangement with an applied UDL load of 1770 N/m is shown in the figure below.

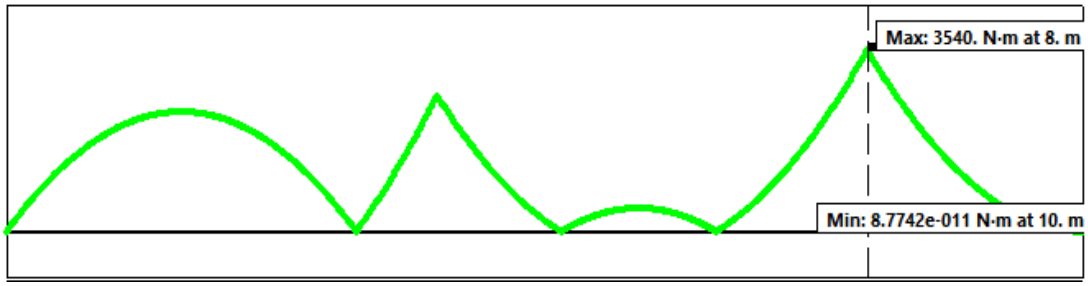

Figure 5-3 Absolute Bending Moment Diagram of Fence Post with Guy Wire Supports at 4m and 8m Respectively

In addition to the bending moment diagram, the force reactions at the base and each guy cable attachment was also found. From these, the tension force in guy wire was calculated as described in the section above, using the following formula:

$$T = \frac{Horizontal\ Reaction}{\cos 45} \qquad 5.1.4$$

The vertical reaction from the guy wire downforce and corresponding maximum lateral friction value was also calculated to ensure the design criteria was met. This was done using the following formulas:

$$Vertical\ Reaction = T_1 . \sin 45 + T_2 . \sin 45 \qquad 5.1.5$$

Where Vertical Reaction is the normal force at the base of the post and T_1 and T_2 are the tensions in each guy wire, respectively. The frictional force was calculated using:

$$Max\ Friction = 0.25\ \times Vertical\ Reaction \qquad 5.1.6$$

Where 0.25 is the conservative coefficient of friction selected in section 5.1.3. The final results are shown in the table below:

Horizontal Reaction of Cable 1 Attachment	**7521.7 N**
Tension in Cable 1 (T_1)	**10637.3 N**
Horizontal Reaction at Cable 2 Attachment	**7301.7 N**
Tension in Cable 2 (T_2)	**10326.2 N**
Vertical Reaction at Post Base	**14823.4 N**
Horizontal Reaction at Base	**2876.7 N**
Maximum Frictional Force with μ = 0.25	**3705.9 N**

Table 5-1 Results of Inital 2D FEA Analysis of Fence Post

As the maximum frictional force is greater than the horizontal reaction at the base, and the tension in both guy lines is less than the maximum allowed of 13 kN, corresponding to the minimum safety factor, this configuration is suitable to use in the design. Therefore, the maximum bending moment of 3540 N.m was used to size the SHS used in the fence post design.

Using formula 5.1.3 to estimate the bending stress with the elastic section modulus of various different SHS sections taken from the OneSteel catalogue, it was found that a 100mm x 100mm x 2mm section was the lightest section per linear metre (6.07 kg/m) that fell within the required stress requirements. With an elastic section modulus of 24.6 x 10^3 mm^3, the estimated bending stress calculated was 143.9 MPa; less than both 153 MPa and 176 MPa, the endurance limit and the minimum required stress for a safety factor of 1.5 with respect to the 500^{o}C yield strength respectively.

To validate this selection, a 3D model of the post was created and a full FEA analysis was run, both at ambient conditions and 500^{o}C, to assess the additional impact of thermal stresses and self-weight upon the reaction forces, maximum von-Mises stress and deflection levels.

As the mesh attachment system had not yet been designed, simulation of the drag force loading was achieved by applying a uniformly distributed load corresponding to the half the total calculated drag force of 17700 N to each side of the post, so as to apply the load in a similar configuration to where the mesh will be attached.

Similarly, as the guy wire attachments had not been designed either, simulation of the guy wires was achieved by a combination of displacement constraints and applied forces directly applied to a 20 mm x 100 mm section of the front face of the post.

As the ground anchor/guy wire angle was to be 45^o, the vertical reaction is equal to the horizontal reaction. As the horizontal reaction forces at the guy wire displacement restraints differed slightly from the 2D predicted values, an iterative process was used, where the applied forces simulating the vertical load of the guy wires was set equal to the horizontal reaction force of the last iteration until the results stabilized.

The results from the FEA simulations for both ambient (22^{o}C) and maximum design temperature (500^{o}C) are shown below. Note that due to the large size of the post, only the areas of interest are shown, i.e. the base restraint, guy wire restraints or any other regions of interest.

Note that in the results shown below, the graphical deflection depicted has been considerably scaled to better show the deformed shape; the true level of deformation is difficult to detect on an image covering the entirety of the fence post.

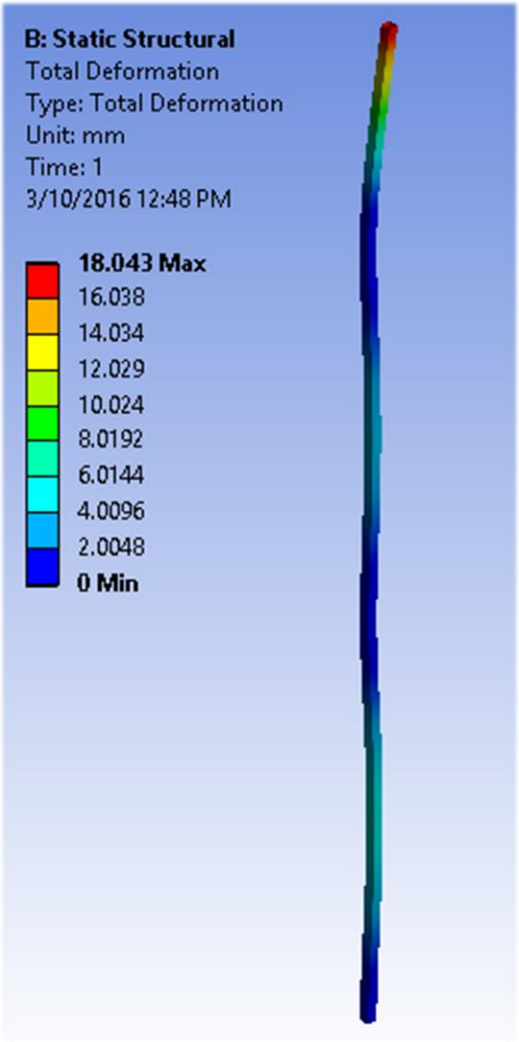

Figure 5-5 Image Showing FEA Results for Total Deflection of Fence Post at 22°C

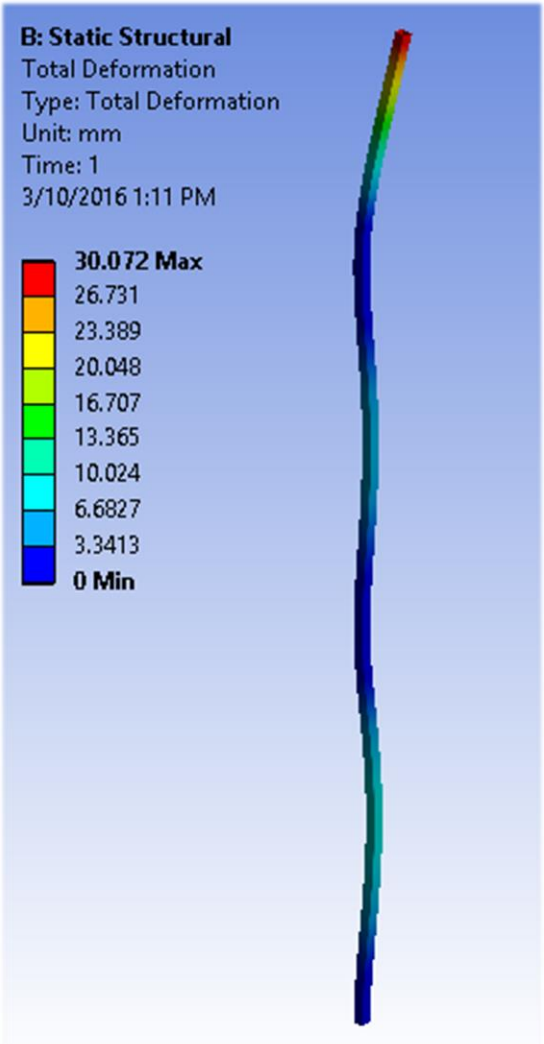

Figure 5-4 Image Showing FEA Results for Total Deflection of Fence Post at 500°C

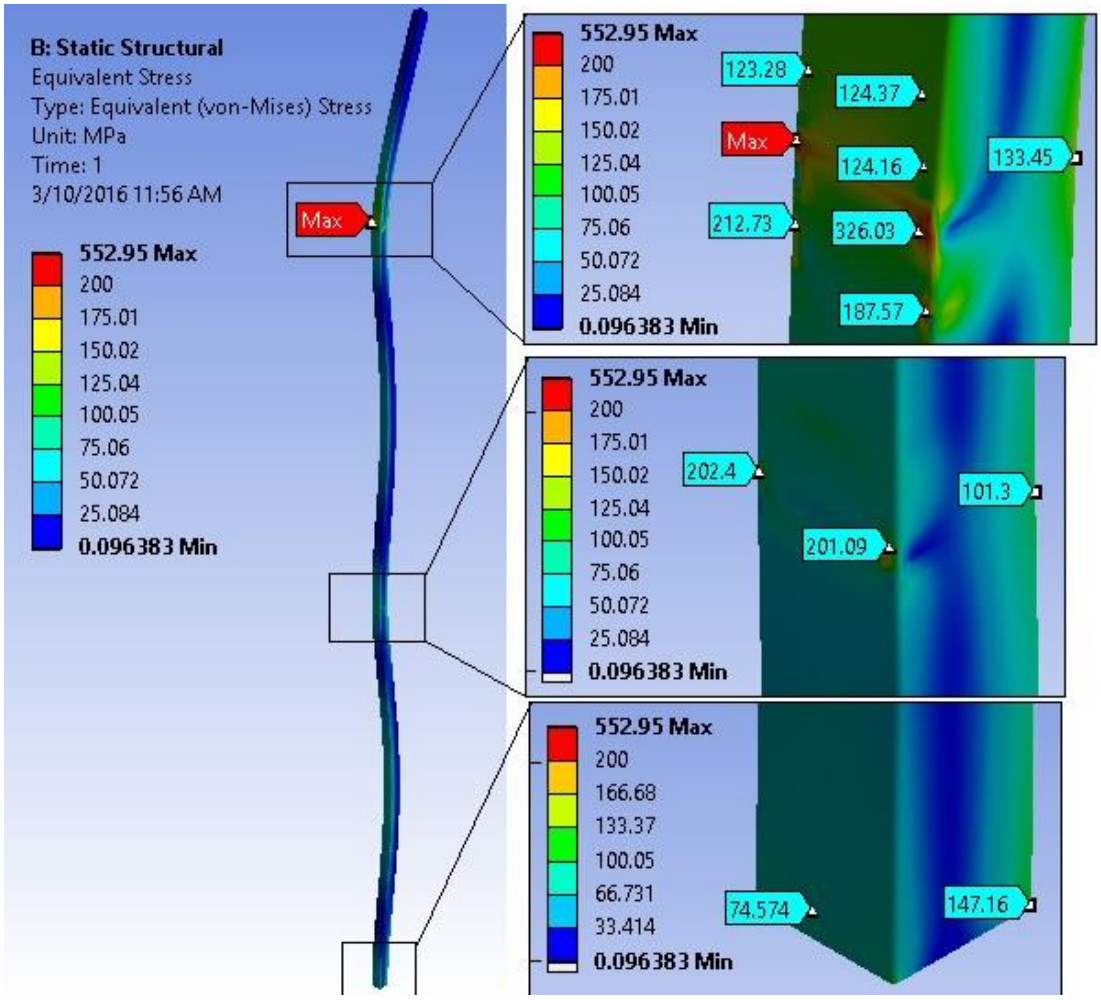

Figure 5-6 Image Showing FEA Results for Von-Mises Stress on Fence Post at both 22°C and 500°C

Horizontal Reaction at Top Guy Wire	**7160.5 N**
Vertical Reaction at Top Guy Wire	**7160.5 N**
Total Tension in Top Guy Wire	**10,126.5 N**
Horizontal Reaction at Lower Guy Wire	**6895.4 N**
Vertical Reaction at Lower Guy Wire	**6895.4 N**
Total Tension in Lower Guy Wire	**9751.6 N**
Horizontal Reaction at Base	**3644.1 N**
Vertical Reaction at Base	**14604 N**
Maximum Frictional Force at Base	**3651 N**

Table 5-7 Table Showing Force Reaction Results for 3D FEA Analysis of Fence Post at both 22°C and 500°C

Several interesting results were noted during the analysis of the FEA findings shown above. Primarily, the stress results mirrored those of the 2D beam analysis, showing that the stress in the mid sections between all the supports was limited to under 70 MPa.

However, the 3D analysis revealed the presence of significant stress concentrations occurring around each of the supports, with the most pronounced being at the location of the top guy wire connection point. They are localized to the immediate vicinity of the supports however, and as such can be overcome by appropriate design of the guy wire attachment points.

Another interesting result of note was that the stress levels throughout the post did not change between the simulations between 22^{o}C and 500^{o}C, despite the large change to the Young's Modulus of the material. This is because in a linear FEA analysis, stress is calculated using Hook's law, which depends upon strain, Young's modulus and Poisson's ratio. As the modulus of elasticity is used in calculating the strain, the stress remains constant over the temperature change. While Poisson's ratio does change slightly with temperature, which would theoretically alter the stress, this effect was found to be negligible.

Additionally, the results for the magnitudes of the reaction forces at each support differ slightly from those calculated with the 2D beam analysis. Most notable is that the horizontal support reaction at the base increased from 2876.7 N to 3644.1 N; an increase of 767.4 N. Correspondingly, this resulted in a reduction of the load at the guy wire supports, with the horizontal reaction at the top support decreasing from 7521.7 N to 7160.5 N; a change of 361.2 N, and from 7301.7 N to 6895.4 N for the bottom guy wire; a change of 406.3 N.

These changes in guy wire tensions also reduced the vertical reaction force at the base, however, the inclusion of gravitation force in the 3D analysis minimized this impact; the total reaction force only decreasing by 219.4 N.

Recalculating the maximum frictional force that could be supplied by the interaction between the base and the ground, again using the coefficient of friction of 0.25, found that the difference between the max friction and the horizontal reaction had diminished and the two were roughly equal. Therefore, this design concept is still workable, but the ground anchors used in the base design must be sized sufficiently to provide a considerable safety factor, given the uncertainty associated with the coefficient of friction estimation used.

The deflection results for both the 22^{o}C and 500^{o}C revealed no major issues with the current selection of SHS section. The maximum deflection in both cases occurred at the very top of

the post, and was relatively minor relative to the beam span. A deflection of this magnitude is unlikely to compromise the fence functionality or structural integrity.

5.1.6 Portability and Weight Requirements

As was mentioned in section 5.1.5, the weight per metre of the 100 mm x 100 mm x 2 mm SHS section chosen for the fence post is 6.07 kg/m (OneSteel, 2016). Multiplying this by the fence design height of 10 metres gives an approximate total fence post weight of 60.7 kg.

As part of the requirement for portability, section 3.1.2 of the design methodology chapter stated that no part of the fence should be heavier than 50 kg, in order to allow a two-man team to be able to carry the fence sections comfortably. It was also stated that the design of the fence should be able to be transported either on trailers attached to regular vehicles or flatbed trucks.

Therefore, the fence post needs to be split into multiple sections to both reduce to weight of each part and to aid in the transportation of the fence. However, while aiding in the ease of mobility, increasing the number of individual sections of the fence will have a negative impact upon the speed of assembly, as each additional piece that requires joining will slow down the assembly process.

To balance these competing aims, the fence posts will split into only two separate pieces. This gives both sections a length of 5 metres, with an approximate weight of 30.35 kg; 19.65 kg under the maximum allowable weight. This also allows for the additional weight that has not been accounted for at this stage associated with the guy wire and mesh attachment and restraint systems.

5.1.7 Joining of Fence Post Sections

Due to the long length of the fencepost and the large forces applied to it, the method used for joining the two sections of post together is important to consider. Primarily, the joint needs to have the following properties:

- Simple and fast assembly and disassembly that can easily be performed onsite without requiring careful alignment of the sections or special tooling.
- Not interfere with the other functions of the fence post such as the mesh attachment mechanism.

- Safely transmit the forces between the sections without compromising the strength or structural integrity of the post.

Considering the loading condition of the fencepost, the joint will have to handle all three internal beam reactions of shear force, axial force and bending moment.

In addition to the internal beam reactions above, the effect of the joint on the fence posts buckling load must also be considered due to its length and magnitude of axial and lateral loads.

To determine the most appropriate method of joining the two sections, a review into the literature of connecting columns in civil construction was conducted. Known in civil construction as a 'splice', several different methods were found to be commonly used in joining column sections. Primarily, these were through a welded connection; obviously unsuitable in this application, through the use of bolted gusset plates on the flange and web of the sections, or through the use of bolted butt plates attached on the ends of the steel sections.

Of these two bolted connections, the most suited to this particular application was the bolted butt plates, as the use of gusset plates would require plates to be positioned on all sides of the section, which would interfere with the installation of the mesh attachment arrangement. As such, the use of butt plates to join the sections was chosen. See figure 5.8 for an image of this type of arrangement.

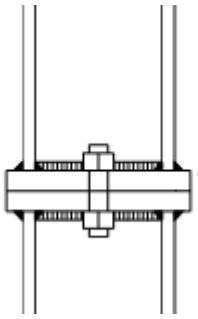

Figure 5-8 Image of Butt Plate Column Splice (Snijder and Hoenderkamp, 2006)

From the review of the literature, it became evident that the reduction in stiffness associated with splice connections results in changes to the buckling resistance of a column. As buckling is a major failure method in compressively loaded sections, often occurring at forces less than the yield stress, the impact of a butt plate splice on column buckling load was investigated further.

In their 2006 paper titled 'Experimental Tests On Spliced Columns for Splice Strength and Stiffness Requirements', Snijder and Hoenderkamp investigated the impact upon different splice configurations to determine the changes to buckling load for pin ended columns.

They report that for a butt plate splice that had been tensioned to supply a moderate rotational stiffness, there was a negligible effect upon the load capacity of the column

section, even when tensile forces were present at the splice location (Snijder & Hoenderkamp, 2006). Therefore, this is an acceptable type of joint to use for joining the sections.

In order to appropriately size the butt plate connection, the shear and axial forces in addition to the bending moment at the joint location in the fencepost had to be determined.

As the joint is to be placed at 5 metres along the post, the values of bending moment and shear force at that location was taken from the shear and bending moment diagrams produced by ANSYS in the 2D beam analysis performed on the post in section 5.1.5. The axial force was simply taken as the vertical component of the top guy wire cable. The results obtained are shown in the table below.

Axial Force	**7160.5 N**
Shear Force	**1557.2 N**
Bending Moment	**220.0 N.m**

Table 5-2 Internal Beam Reactions at Proposed Fence Post Joint

Given that the axial force is acting in the compressive direction rather than as a tensile force, the bearing force of the plates will support this load; leaving only the shear force and bending moment that the bolts have to overcome.

As the butt plates should not extrude past the sides of the SHS where the mesh attachment mechanism will be placed, the plates will need to be joined on the front and back sides of the fence post only. While the major bending forces are predominately about this axis due to the wind loading, a total of four bolts should be used, two on each side, to offer additional bending support in the out of plane direction.

Assuming that the centre to centre distance between the bolts on either side of the SHS is to be 150 mm, i.e. the bolt hole centres are 25 mm away from their respective side of the SHS, the required force to supply the couple to overcome the bending moment can be calculated as such:

$$Bending\ Moment = F \times d \qquad 5.1.7$$

Therefore, the maximum force found was 1466.7 N. As there are two bolts on each side, the minimum force required for each bolt to overcome the bending moment is half of this value; 733.35 N.

As bolts should avoid being loaded in shear, the axial force in the bolts should be enough to provide sufficient frictional force to transmit the shear load. Neglecting the contribution from the axial compressive load, the total bolt tension force required can be calculated using as follows:

$$Shear\ Force = \mu \times F \qquad 5.1.8$$

Taking a coefficient of friction of 0.2 for untreated steel surfaces, taken from teaching material published by the Institute for Steel Development and Growth, 2011, the force required is 7786 N.

As this load is shared over all four bolts, the required force in each bolt is 1946.5 N. As this force is larger than that of the bending moment requirement, this force will be used to size the bolts.

According to Juvinall and Marshek in Fundamentals of Machine Component Design, the force from the initial tightening of a bolt is given by the equation:

$$F = K \times A \times S \qquad 5.1.9$$

Where F is initial tension, K is the percentage of proof strength the bolt is tightened to, A is the tensile strength area of the thread and S is the proof strength of the bolt. Assuming an initial tension coefficient K of 0.6 to allow for possible under tightening that may occur during field assembly, it was found that SAE class 5.8 M10 bolts, with a tensile area of 58.0 mm^2 would provide approximately 15428 N per bolt (Juvinall and Marshek, 2012). This gives a safety factor of over 7.9, and as such was selected for use in the design.

5.1.8 Design of Guy Wire Attachment Points

While overall the size of SHS chosen (100 mm x 100 mm x 2 mm) was shown to be appropriate for use as the fence post in the above section, the existence of significant stress concentrations was noted at both guy wire attachment locations; in particular, around the upper guy cable.

Therefore, care had to be taken in the design of the attachment points to ensure that the total stress levels remained beneath the endurance limit of the steel, estimated as 153 MPa, as this was the lower than the allowable stress based off the 500°C yield point with a 1.5 safety factor.

For full functionality of the fence, the guy wire attachment points had to meet the following criteria:

- Allow for easy connection and disconnection of guy cables
- Support a wide range of guy wire yaw angles, allowing for variation in anchor location placement required at changes of fence direction and ends.

In order to allow for easy connection and disconnection, it was decided that the guy wires have attachment hooks at the post connection end. As such, the post attachment assembly just had to consist of a 'loop' around which a hook could be installed.

The further away from the post the contact point of the 'loop' with the hook is, the greater the bending moment created by the vertical component of the force is. Therefore, to minimize this, the loop should be as close to the post as possible. In order to properly size the opening, the required size of hook had to be determined.

Determined using the maximum guy wire tension determined in section 5.1.5 of 10.13 kN and applying a safety factor of 2, the Working Load Limit (WLL) of the hooks used must be at least 20.3 kN. As most hooks and lifting attachments list the WLL in tonnes, the required WLL of the hook is 2.07 tonnes.

A review of available hooks similar to the intended design found an Australian company, All Lifting had a 'Grade 100 Eye Sling Hook with Latch', shown in figure 5.9 below, with a WLL of 2.5 tonnes.

Figure 5-9 Picture Showing Type of Hook Used for Guy Cable Attachment to Post (All Lifting, 2016)

The pertinent dimensions of the hook are the latch opening size of 28 mm, the depth around the 'top' of the hook section (shown down the bottom of the picture in figure 5.8) of 23 mm and the thickness around the 'top' of 20 mm (All Lifting, 2016).

Therefore, the opening size of post attachment has to at least be 20 mm by 23 mm, with a thickness of the main 'latching point' less than 28 mm.

For the second requirement; allowing for a wide range of yaw angles, it was determined that the orientation of the 'latching point' of the hook onto the post should be vertical, not

horizontal. Because the line of action of the force should pass straight through the hook, the hook must be able to rotate to align itself with the guy wire. A horizontal latching point would not allow this, while a vertical one does as shown in figure 5.9 below.

From this, a preliminary design of the attachment point on the fence post was 3D modelled, as shown in figure 5.10. Engineering judgement was used in the initial sizing, which was then subjected to FEA analysis in ANSYS at 22°C with the same loading conditions as in section 5.1.5.

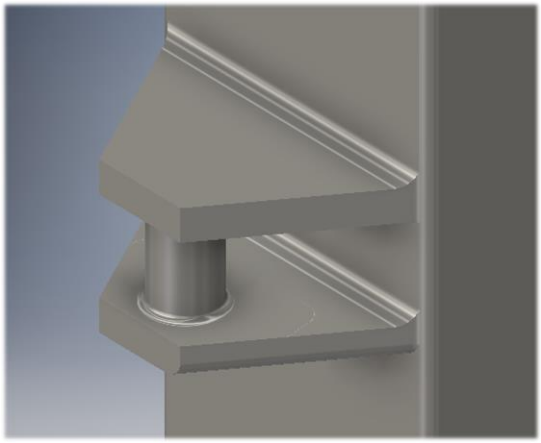

Figure 5-10 Image Showing Preliminary Guy Cable Attachment Point Design

As expected, the results of the initial FEA revealed significantly larger stresses on the post directly above the attachment point than in the rest of the post, shown in figure 5.11.

In order to reduce the stress levels to the levels required, the areas of high stress needed to be reinforced and the geometry smoothed to allow better stress 'flow' in the case of the stress concentrations. This was done through an iterative process, where the geometry of the attachment point was altered and reanalysed until the stress levels fell to acceptable levels. The results from the FEA performed on the initial model assisted in pinpointing the areas which required modification.

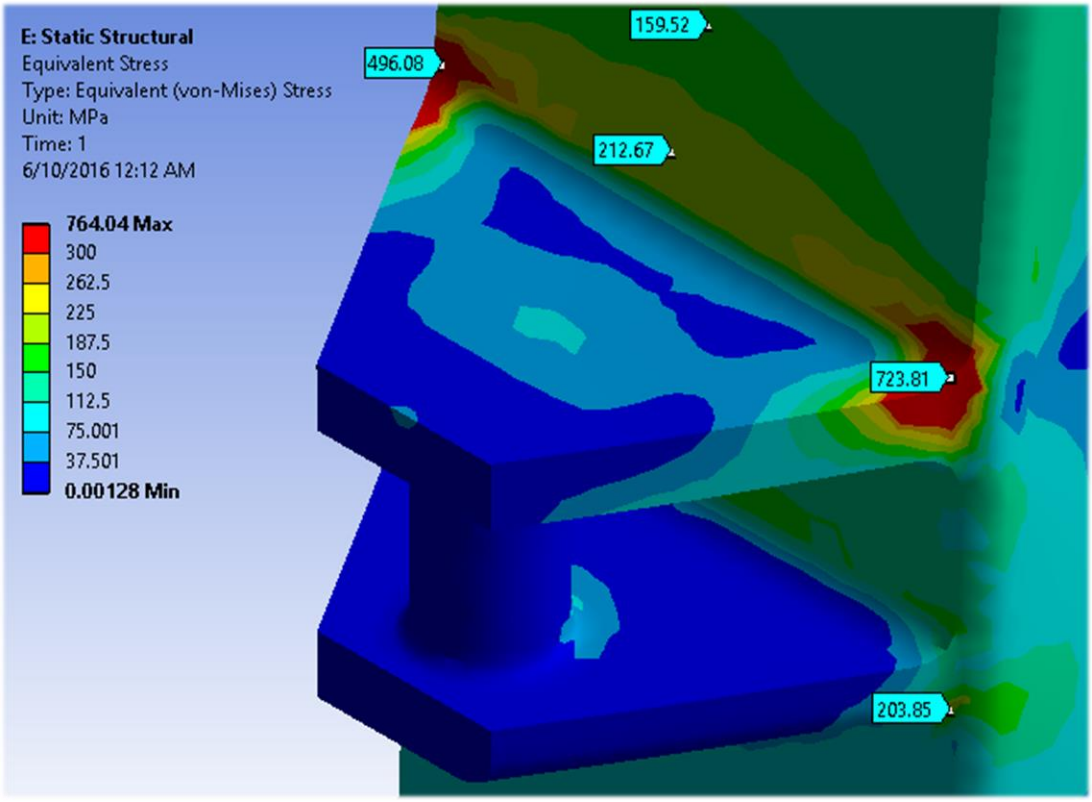

Figure 5-11 Image Showing Stress Levels on Initial Guy Cable Attachment Point

The high stresses on the SHS section directly above the attachment point, where the stress was approximately 220 were the most difficult to remove, and as such in the final design large rounds are required, extending up the post by approximately 100 mm. Figure 5.12 shows the final design and the result of its FEA simulation.

While the maximum stress levels are slightly in excess of the endurance limit of 153 MPa, this was not taken to be an issue, as this slight increase will not significantly affect the fatigue life of the fence post, which is likely to reach the end of its working life before reaching the cycle life associated with a stress value marginally greater than the endurance limit.

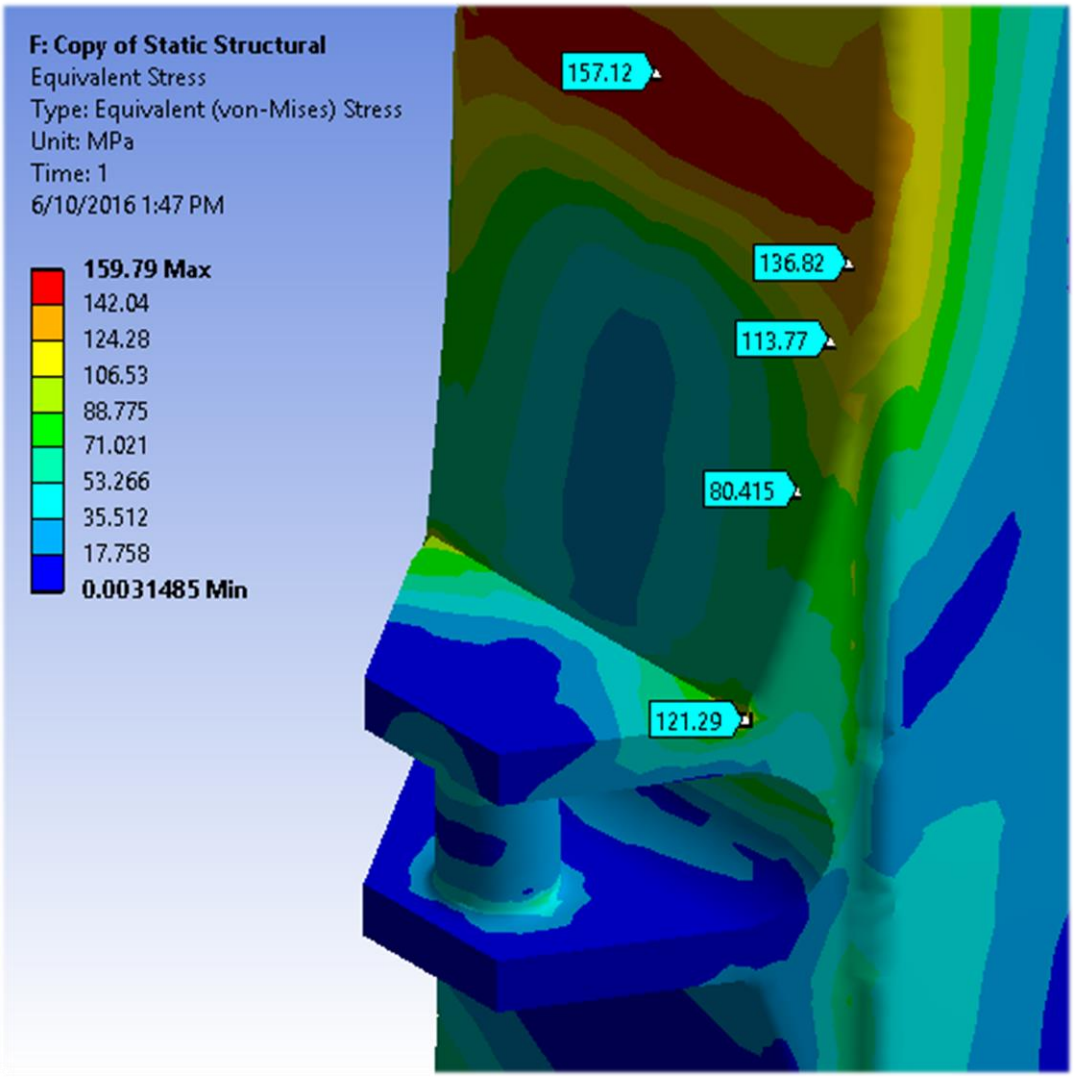

Figure 5-12 Image Showing Final Design and Associated FEA Results for the Guy Cable Attachment Point

5.1.9 Evaluation of Buckling Load

As was discussed in section 5.1.7 above, buckling is an important consideration in designing any long axially loaded column. Therefore, the loading condition which will result in buckling of the fencepost should be investigated to ensure the structural integrity of the fence design.

Classical buckling theory, first presented by Euler, uses the classical beam bending theory to determine the critical load at which a centrally loaded axial column will undergo buckling.

However, Euler's formula for column buckling is based upon the magnitude of the beam bending moment only arising from the compressive load multiplied by the horizontal beam displacement, as shown in figure 5.13 (Beer et. al.,2012).

As such it does not take into consideration the internal moments arising from eccentric loading, laterally applied loads or multiple axial loads. Equations exist to model eccentric loading cases, such as the Secant formula, and some formulas have been developed to model buckling loads with the presence of a lateral point load, however, analytical solutions are not available for loading cases with UDL's (Amir Javidinejad, 2012).

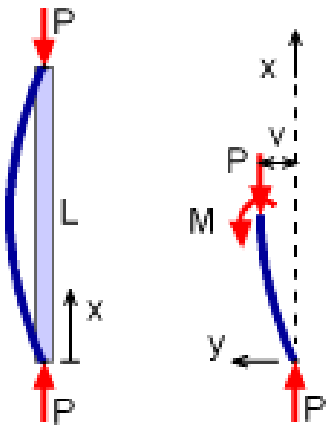

Figure 5-13 Image Showing Free Body Diagram of Euler Buckling (Kurt Gramoll, 2016)

Therefore, analysis of the critical buckling load had to be performed numerically. The FEA package ANSYS supports this functionality, and was used in this analysis. ANSYS utilizes linear elasticity in its buckling calculations, similar to the analytical approaches above, and as such it should be noted that this tends to produce unconservative results as imperfections and flaws are not accounted for (Sheldon Imaoka, 2007).

ANSYS linear buckling works by starting with a pre stressed model from a static FEA test. The loads on this model are then uniformly multiplied by a load 'load multiplier' progressively until the specified number of failure modes are identified. To investigate the validity of this approach to increasing the load, several FEA simulations were run with varying wind loading. It was found that regardless of the wind loading on the post, the force distribution between the guy wire and base supports remained roughly constant. Therefore, this 'load multiplier' is valid for this loading situation, and the load multiplier reported directly corresponds to the factor of safety against buckling at the maximum loading condition.

The loading conditions used in the buckling analysis was the same as used in the 3D FEA from section 5.1.5, with the exception of additional displacement constraints placed on the sides of the post where the mesh will be attached, which act only in the out of plane direction to the wind loading, parallel to the mesh. When the fence is assembled, the mesh and mesh attachments will serve as lateral restraints in that direction, and as such will retard buckling from occurring in that direction.

Because the onset of buckling is directly related to the stiffness of the column, the buckling simulations were only run at 500°C, as the reduced Young's modulus at that temperature will result in the lowest buckling load, giving the limiting state.

The buckling analysis conducted at 500°C revealed an interesting result. For the first three buckling modes identified, the entire column did not buckle, but instead local buckling occurred. The first two modes were located directly above the upper guy wire attachment point, at the site of the maximum identified stress in section 5.1.5, at a load multiplier of 3.135 and 3.195 respectively. These are shown in figures 5-14 and 5-15 below.

This is interesting, as being above both guy cable attachments, there is no compressive load directly applied. However, as this section of beam is effectively cantilevered, the bending stress will evidently result in local buckling at this location at that magnitude of load.

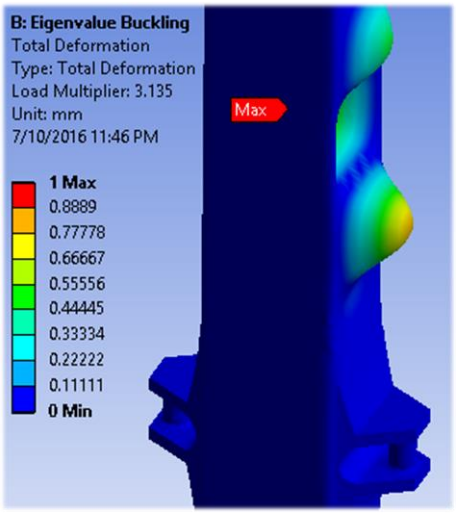

Figure 5-15 Image Showing a Buckling Mode of Fence Post at 500°C

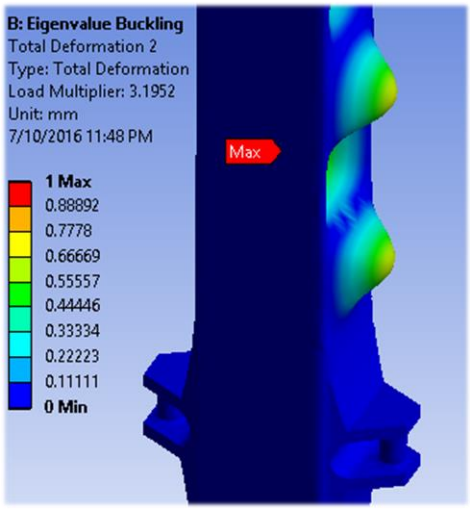

Figure 5-14 Image Showing a Buckling Mode of Fence Post at 500°C

However, as the section above the upper guy wire serves no major structural purpose other than to support the mesh above the guy cable support, this local buckling does not represent a complete failure of the entire fence, although should be avoided.

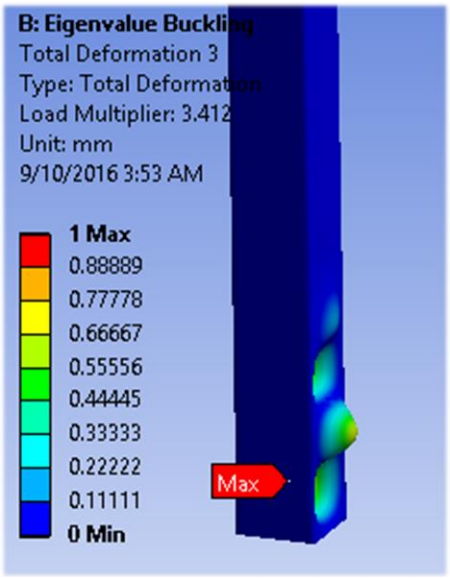

Figure 5-16 Images Showing a Buckling Mode of Fence Post at 500°C

The third mode induced was also local buckling of the post, however, this occurred just above the base attachment point. This happened at a load multiplier of 3.412, shown in figure 5-16 below. This local buckling however does likely represent a failure of the entire fence as a reduction in load capacity at this point will adversely impact the structural integrity of the entire fence.

These results indicate that for this particular fencepost sizing and arrangement, local buckling is more prevalent than global buckling. This is not

unsurprising; due to the selection of the lightest possible posts, the wall thickness is quite small with a large second moment of area, conditions generally associated with local buckling. However, given that all modes of buckling occur at load multipliers of 3 or more, the design in its current state was deemed acceptable.

5.2 Mesh Support and Fence Post Attachment

While the drag force acting on the mesh has been estimated at 177 N/m^2, the tensile force across the infill material will be much greater than this. In order to support the fine wire mesh across the fence post span, it was decided that the mesh would be attached to wire cables, the cables themselves being attached to the fence posts on either end and taking the high tensile loading. This approach is used in the design of wire mesh and cable net rock fall protection systems on cliffs and slopes, and has been shown to reduce the stress concentrations in the mesh (Sasiharan et. al., 2006).

This section will detail the process through which the design of the mesh infill of the fence was developed and the approach taken in the development of the fence design.

5.2.1 Mesh Attachment to Support Cables

Primarily, the factor that influences the number and spacing of the mesh support cables is the mesh strength itself. Due to the fact that the wind loading could come from either direction, the mesh needs to be attached to the support cables in such a way that equal support is provided in both directions.

The first problem posed was how to attach the mesh to the cables. The method of attachment has significant impacts on the levels of stress around the cable support in the mesh, and therefore should be properly designed to allow maximum cable support span.

Several key considerations were identified at this stage. These were:

- The clamp should attach to enough individual wire strands to keep stress levels to an acceptable level.
- The total clamp frontal area should also be minimized to avoid increasing the estimated drag level on the mesh much above what was determined in the design of 177 N/m^2.

- The maximum stress produced in the mesh should be kept to below 500 MPa. This stress value corresponds to a fourth of the predicted ultimate tensile strength of 2000 MPa for the wire, as calculated using equation 2.3.2.

A review of other mesh applications found that clamping the mesh was the most commonly implemented solution, used in applications such as security screen doors and windows, where large forces and impacts are not unexpected, shown in figure 5-15 (Crimsafe, 2016). Therefore, a clamping approach investigated as a method to restrain the mesh to the support cables.

Figure 5-17 Picture Showing Mesh Clamp Connection (Crimsafe, 2016)

Following this criteria, an initial clamp style design was modelled, and an FEA analysis performed with a quarter model using symmetry where possible to reduce computational costs.

To accurately simulate a full wind load on the mesh section without having to model a large area of mesh, extremely computationally expensive due to its fine size, the loading case was simulated as follows.

A small width of mesh section attached to the support/restraint was modelled, comprising of around 6 – 8 mesh cells. At the edges of the mesh where the modelling had been terminated, a displacement constraint was placed normal to the cut surface on each wire, simulating the restraint of the theoretically continuing wire. Also on these cut surfaces, the drag force load corresponding to the supported mesh area was applied parallel to the cut surface, simulating the internal shear reaction which would be present in the full mesh.

Using this approach, numerous different design geometries were trialled with differing loads corresponding to varying distance between clamp supports. However, no suitable design was identified which could keep the stress levels entirely below the specified limit of 500 MPa, as the transition zone between the clamped wires and unclamped produced a localized area of very high stress.

To determine if this high stress was in fact detrimental to the mesh integrity, simulations were performed with the wires in the high stress area ‘broken’ by removing a section,

simulating a failure of those particular strands. It was reasoned that if the stress levels in the neighbouring wires did not experience the same increase in stress than the design was workable. However, the stress concentration reoccurred, indicating a progressive 'tearing' style failure would likely occur.

As it was noted that the peak stress zone consistently occurred at the transition from supported wire to unsupported, it was reasoned that if the support was continuous up the entire length of the mesh this concentration could be eliminated. This was based upon the assumption that it was the large discontinuity between stiffness of the clamp; modelled out of two 2 mm steel sheet sections screwed together, and the wire mesh matrix which was responsible for the sudden increase in stress. By minimizing the jump in stiffness the major stress concentration could be avoided.

Taking inspiration from the way seams in fabric tend to stop the progress of tears, that is, fabric will tear up to the seam and then stop, a 'seam' of thin, narrow sheet metal was trialled on the mesh, running up the entire length of the modelled mesh, a 100 mm section. A thicker section mimicking the support cable attachment point was positioned on the back of the sheet metal and an analysis performed. While there were still significant stresses produced where the mesh attached to the sheet metal 'seam', the problematic stress concentrations were eliminated.

Several trials were then performed to determine the optimum seam dimensions and maximum spacing of the mesh supports while keeping the stress levels below the specified 500 MPa.

Using this configuration, the optimum area per mesh support was determined through simulation to be 0.66 m x 0.66 m, with a seam width of 10 mm and a thickness of 2 mm. This corresponds to 15 strips and 15 cables along the 10 metre length and height of the fence.

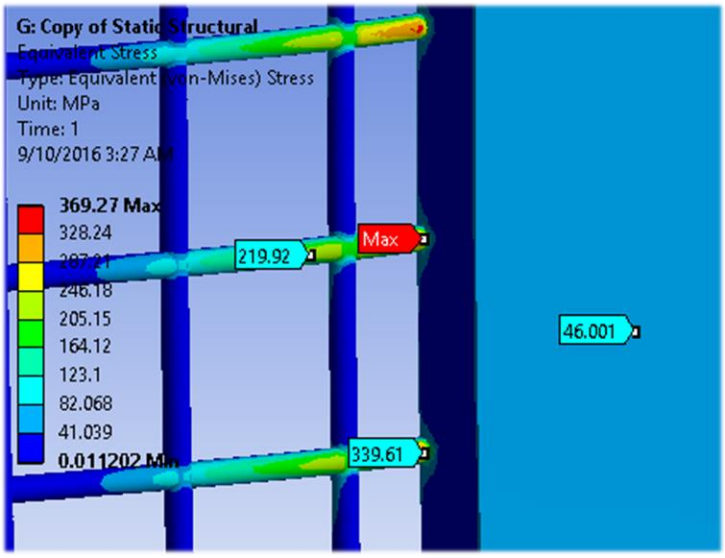

Figure 5-18 FEA Result of Wire Mesh Restraint Using Sheet Metal Seam

This configuration resulted in a peak stress of 369 MPa in the mesh, illustrated in the FEA results from the final mesh simulation shown in figure 5-18 at right.

Using 15 strips, each with a frontal area of 0.01 m x 10 m, the open space of the fence will be reduced by 1.5 m^2. Therefore, the additional drag force from this reduction needs to be considered. From Fox and McDonald's Introduction to Fluid Mechanics, the coefficient of drag for a square prism with an infinite aspect ratio is 2.05 for Reynolds numbers greater than 1000.

Therefore, using equation 2.5.1, at 28 m/s the additional drag force was estimated to be 1476.6 N. This represents an 8.34 % increase from the value of the mesh alone. While this is not an insignificant increase, it is well within the margin of error and safety factors used in the design and is therefore acceptable. Additionally, the actual increase in drag may in fact be less than this, as the 1.5 m^2 was initially included in the calculation of the mesh drag force.

As the mesh needed to be securely fastened to the sheet metal seam to be effective, clamping was not a valid option for the entire length. Therefore, alternative ways of attaching the mesh to the seam were investigated.

The method that was found to be most appropriate from a manufacturing perspective was roller welding the mesh to the sheet metal. Specialized welding equipment was found to be available which supported the welding of fine stainless steel wire mesh to both itself and to thin metal sheets, well suited to this application. An image showing this process is shown in figure 5-19 below.

Figure 5-19 Pictures Showing Welding of Wire Mesh to Sheet Metal (Sunstone Engineering, 2015)

As was mentioned above, the sheet metal seams will be welded along the entirety of the mesh, at 666 mm intervals. To attach the cables to the seam, it was decided that small eyelets fitted with grub screws would be welded to the seam at the specified 666 mm

intervals. While the stress of the mesh is quite high, the overall force at each attachment is not, and as such the design of these attachments has not been detailed.

5.2.2 Sizing of Mesh Support Cables

As wire cables cannot support a bending moment, the behaviour of the cables under a uniformly distributed load is quite complex. Through a literature review, it was found that the behaviour can be approximated using the follow formulas, which are derived from the cable equation (Buckholdt, 1999).

$$H = \frac{wL^2}{8d} \qquad 5.2.1$$

$$T = H\sqrt{1 + \left(\frac{4d}{L}\right)^2} \qquad 5.2.2$$

$$S = L\left[1 + \frac{8}{3}\left(\frac{d}{L}\right)^2 - \frac{32}{5}\left(\frac{d}{L}\right)^4\right] \qquad 5.2.3$$

Where H is the tension at the midpoint of the cable, w is the magnitude of the distributed load, L is the linear length between cable supports, d is the 'sag' or displacement of the centre of the cable from the line connecting the supports, T is the tension at the ends of the cable and S is the total length of the cable.

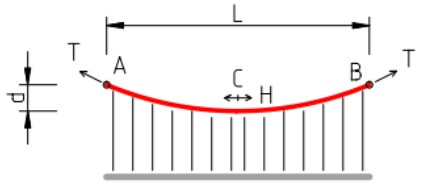

Figure 5-20 Image Showing Physical Meaning of Cable Equation Variables (Engineering Toolbox, 2016)

From equations 5.2.1 and 5.2.2, it is clear that the tension force experienced by the cables will be directly influenced by the sag in the centre of the span, with larger sags reducing the force. Equation 5.2.3 shows that the sag of the cable directly relates to the difference between the length of the cables and the true span between supports.

Note that the weight of the mesh and support cables themselves will not be considered in the loading case. As the mesh has a weight of 0.3 kg/m^2 and support cables are in the range of 0.05 to 0.124 kg/m, the imposed wind loading far exceeds the contribution from the weight.

While this gives a degree of control over the maximum tensile force developed by changing the level of 'sag', too much will result in the entire mesh sagging vertically when the wind is not at the maximum design load, which will likely be a majority of the time. This will reduce the efficacy of the fence, as the effective height is reduced.

Initial calculations showed that if minimal sag (15 mm) was allowed in the fence, the tensile force at the fence posts developed in each cable would be approximately 100 kN. Evidently, this was unworkable, and therefore the inclusion of some amount of sag is necessary.

To better understand this relationship between the cable extension, sag and tension, a graph was produced showing both the sag and cable tension force at the supports for any given cable elongation. This is shown in figure 5-21 below. Note that the additional drag force identified in section 5.2.1 has been included in these calculations, giving a total drag force per unit area of 191.8 N/m^2.

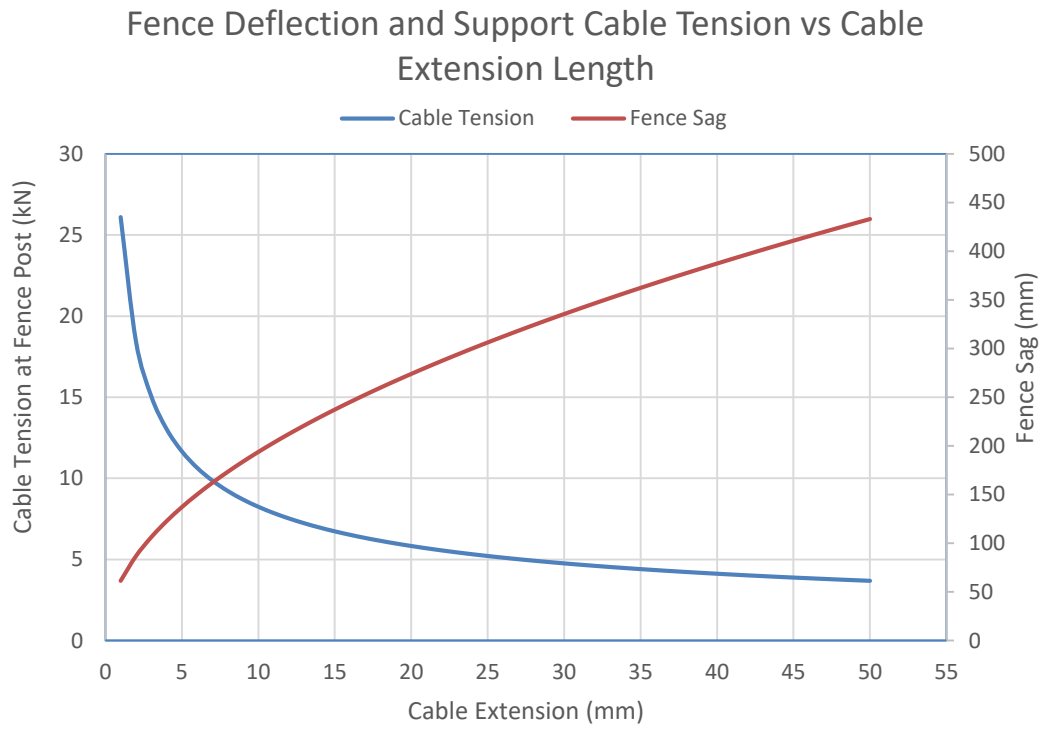

Figure 5-21 Graph Showing Relationship Between Tension, Cable Length and Fence Sag

This graphical representation clearly shows that there are large reductions in tension up to approximately 10 mm of cable extension, where the curve begins to plateau. This relationship is partially mirrored by the increase of fence sag, although less pronounced.

From the perspective of optimizing design by minimizing both tension and fence sag, between 20 to 25 mm of cable extension seems to be the optimum point, after which the sag grows much faster than the corresponding decrease in tension.

Given the relatively small elongation required to reduce the tension, two options are available for the design. Either the support cable lengths are of fixed length around 25 mm

longer than the span between the fence posts, meaning there is a constant sag in the mesh of around 300 mm; or each cable is fitted with a spring, which would take up the slack when the fence is not loaded and extend to relieve the tension when under heavy wind loading.

At a cable extension of 25 mm, the tension in the cable is approximately 5.22 kN; meaning that a simple extension spring would require a spring constant of 209 N/mm. Due to the nature of extension springs, the maximum load is available is smaller than for compression springs. As a result, a product search found no readily available extension springs with the required properties. While a design could be implemented using a compression spring in a similar fashion to a spring scale, the costs would outweigh the benefits in this application.

Therefore, it was decided that the design should simply have cables of fixed length. However, this design in particular is quite sensitive to proper spacing between the fence posts, requiring that the span be 10 metres exactly and the cables 25 mm longer. As shown in figure 5-21, if the slack in the cable decreases to 5 mm, the tension force will increase by over double to 11.7 kN.

To overcome this issue, one end of each cable will be fitted with a turnbuckle which in turn will be connected to the fence post attachment. This will allow for greater tolerances in the spacing of the fence posts, necessary to enable rapid fence assembly.

Figure 5-22 Picture Showing Turnbuckle with Jaw and Eyelet Ends Similar to the one Specified in the Design (Lifting Rigging, 2015)

Selecting a nominal cable extension of 25 mm, the maximum tension in each support cable will be 5.22 kN. From this, the size of cable and turnbuckle required by the design can be determined. Applying a safety factor of 3 gives a required strength of 15.66 kN. A product guide from 'Nobles', a Rigging and lifting equipment manufacturer, lists 6 mm diameter Grade 1570 Wire Rope Core cable as having a minimum breaking strength of 20.3 kN; the thinnest diameter wire to meet the requirement (Nobles, 2010).

Again from a 'Nobles' product guide, it was found that a grade 'P' M10 turnbuckle has a Working Load Limit of 0.6 tonnes; equivalent to 5.886 kN. As the maximum design tension in the cable is approximately 4.76 kN, this size of turnbuckle was selected in the design. Note that it is appropriate to size the WLL directly against the calculated maximum design load; because of the use of this equipment in lifting, a safety factor of 5 has already been included in the WLL (Nobles, 2010).

5.2.2 Design of Support Cable Post Attachment and Hoisting Mechanism

As was discussed in section 4.5, the method of fence assembly decided upon features constructing the fence posts first, followed by hoisting the mesh up between the two neighbouring posts.

Detailed above, mesh suspension and support is achieved through the use of thin wire cables suspended between the two fence posts. Therefore, the method of attaching these cables to the posts must be done in such a way that:

- The large tensile loads experienced by the support cables are safely transmitted through to the post.
- The attachment and hoisting process is quick and can be performed safely from the ground.
- Allow the mesh infill to be comprised of several different sections due to manufacture and portability restrictions.

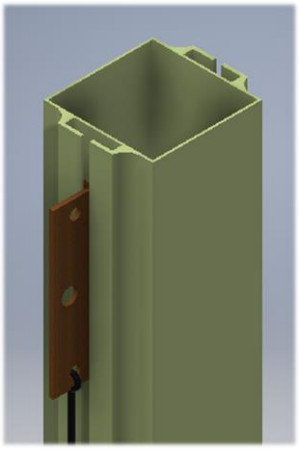

Figure 5-24 Image Showing Track and Runner Design

The most straightforward way in which these requirements could be achieved was reasoned to be the use of a sliding runner in a track extending up each side of the fence posts.

In this design, each end of the mesh support cables is attached to a 'runner'; a short piece of steel 'T' section, which is then positioned into the 'track'; two folded pieces of metal plate welded onto the side of the fence posts in a rectangular shape, with an opening for the base of the runner to protrude, shown at left in figure 5-23.

Figure 5-23 Picture of a Portable, Hand Operated 'Cable Puller' Type Winch (Harbor freight, 2016)

In addition to where the mesh support cables attach, each runner is also joined by a section of wire cable to the runner immediately above and below it at a spacing of 666 mm; corresponding to the spacing between of each of the support wires. Figure 5-25 shows an image of this arrangement.

Hoisting the runners and mesh up the fence posts is then achieved through a flagpole like setup. At the top of the fencepost, over both tracks a small pulley sheave will be mounted.

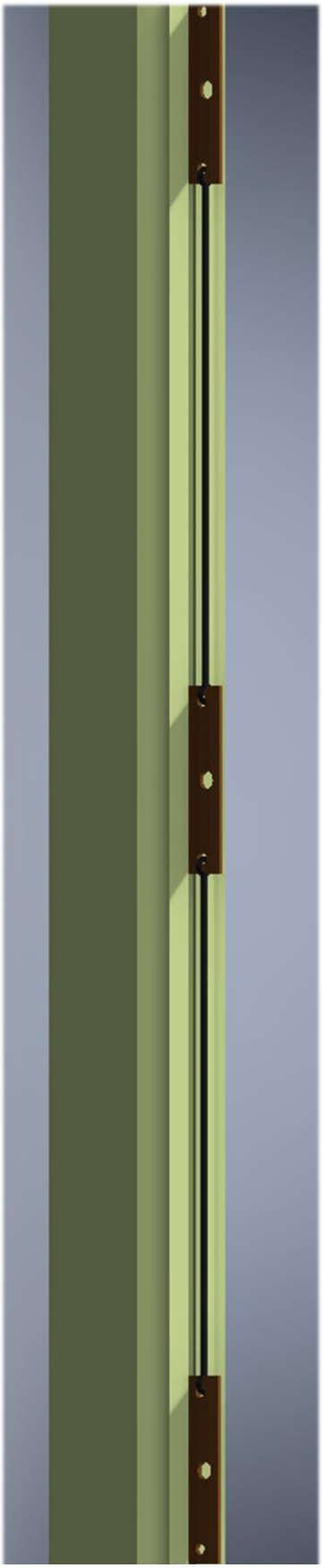

Figure 5-25 Image of Runner Hoisting Arrangement

Prior to the raising of the post while it is still horizontal on the ground, a wire cable connected on one end to a hand operated 'cable puller' winch (shown in figure 5-23) will be passed over the sheave and back down the track.

After the fencepost is then raised and secured, the free end of the cable will be attached to the first runner, and winched up. As the mesh is lifted, the successive runners are slotted into the track and drawn up until the mesh is fully raised; at which time the cable is secured to an eyelet on the fence base and the cable puller removed to be used on the next mesh section.

As the only vertical loading of the mesh, support cables and runners is from self-weight, plus the contribution of friction of the runners in the tracks during lifting, the loading anticipated on the vertical wires connecting the runners is low, and as such the sizing of these cables and lifting winch is not critical. For the sake of homogeneity throughout the design, the same cable used in the mesh support wires was specified.

The sizing of the 'T' section used for the runner and the thickness of the plate used for the track however, is critical, as the interaction between the post, track and runner is how the tensile force developed by the mesh in the support cables is transferred into the fencepost.

The primary reason for selecting a 'T' steel section for the runner was its well suited shape and common availability, thus avoiding the necessity for additional manufacturing. A review of available sizes found that the smallest was 40 mm x 40 mm x 4 mm (Handy Steel, 2016). This seemed ideal for the magnitude of loading and was therefore selected.

To size the track, FEA analysis of various track thicknesses were run in a loading situation simulating the actual loading

cases, both at 22°C and 500°C, until the stress levels were reduced to below 153 MPa. Note that in in order to keep ensure adequate strength in fire conditions, the materials specified for both the T section runner and the plate track was 450 Grade; maintaining homogeneity across the design.

The FEA analysis was performed on a short section of the track while it was attached to a half model of the fencepost; with symmetry constraints applied such that an accurate representation of the stresses developed in the fencepost could also be ascertained, not just the runner and track. Additionally, to accurately determine contact stresses between the runner and track, the runner and track were simulated as separate bodies in contact, rather than a single piece.

The applied load was equal in magnitude to that calculated for the tensile force in the mesh support cables in section 5.2.2.

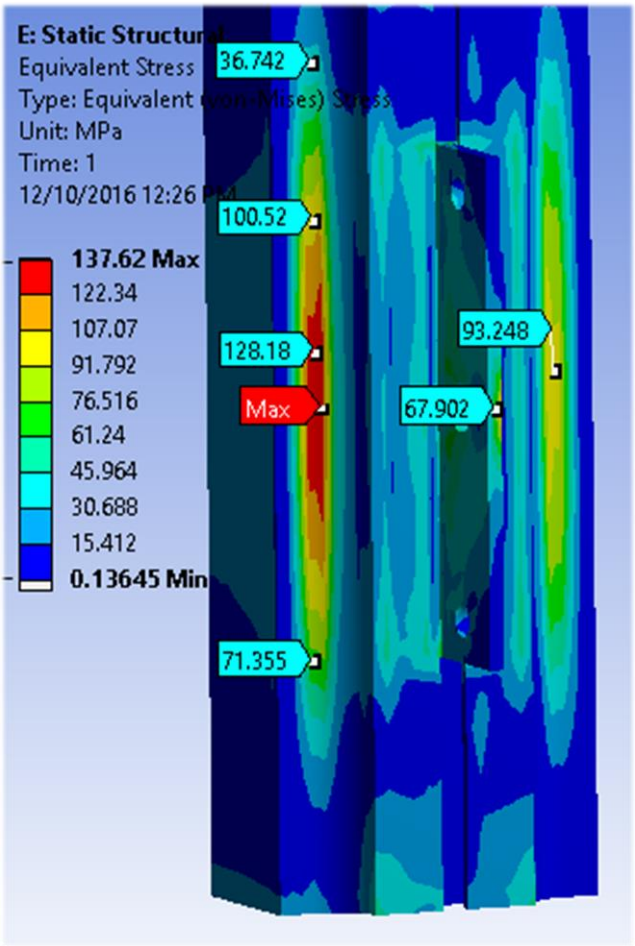

Figure 5-26 FEA Stress Results for Post, Runner and Track

After several FEA iterations, the design parameters found to keep the maximum stress below the specified 153 MPa and also minimize deflection at 500°C was a runner of length 150 mm, with a track plate thickness of 3 mm. The FEA results from the final simulation are shown in the figures below.

Detail design drawings of this assembly can be found in appendices C and D.

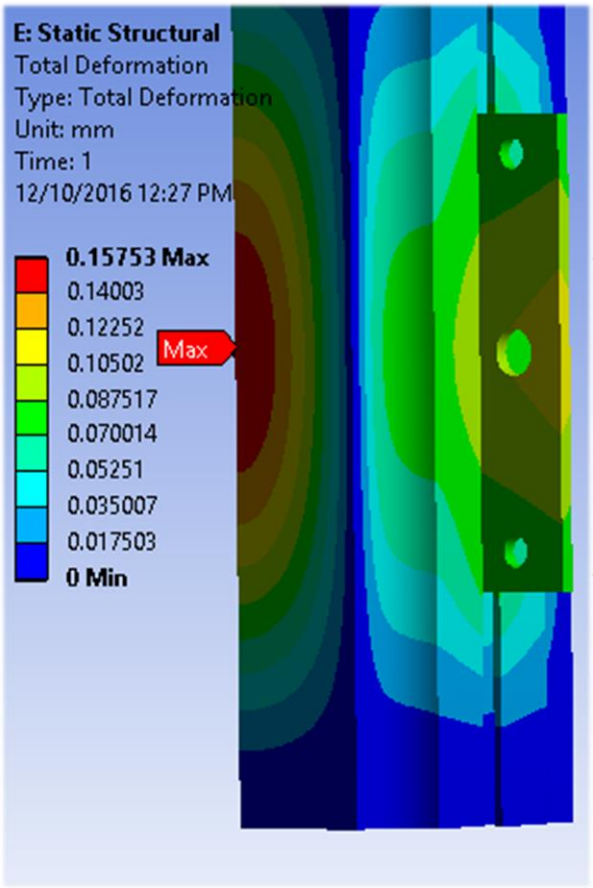

Figure 5-27 FEA Deformation Results for Post, Track and Runner at 22°C

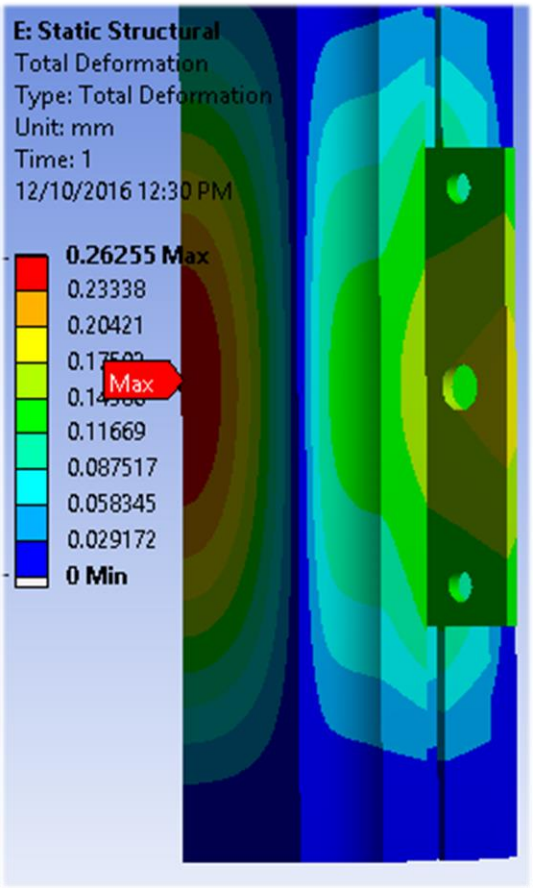

Figure 5-28 FEA Deformation Results for Post, Track and Runner at 500°C

5.3 Fence Base Design

The base for the fence posts serves several important functions in the design. These are:

- Provide a stiff and level support to evenly distribute the vertical load imposed by the fences weight and tension in the guy lines.
- Provide a frame to support the fence post and post lifting jig during post raising.
- Support the lateral drag force component acting at the fence post base.
- Provide support for the fence post to prevent tipping in the process of raising the post, securing the guy wires to the ground anchors and attaching and raising the mesh.

As with the other aspects of the design, weight, portability, assembly time and cost are all important factors. The sections below will detail the process through which the final design was developed.

5.3.1 Determination of Base Specifications

In order to achieve the necessary functions outlined above, several key parameters had to be identified. Primarily, these were:

- The magnitude of the vertical loading of the fence post.
- The magnitude of the horizontal loading at the base of the fence post.
- The magnitude of the overturning moment on the fence post due to wind drag prior to guy wire and mesh installation.

Reasonable estimates for the maximum loading caused by the post on the base in both the horizontal and vertical directions have been obtained from sections 5.1 and 5.2. The methodology of how the magnitude of the overturning moment acting on the unsupported post was determined is explained below.

Given that the major source of external loading acting upon the post during its assembly stage will be drag force from any wind present, the magnitude of the drag force acting on a 100mm x 100mm SHS section was estimated.

This was done using equation 2.5.1, the drag force equation, shown below:

$$F_D = \frac{1}{2} C_d . \rho . A . V^2 \qquad 5.3.1$$

To apply this equation to the post, an appropriate coefficient of drag for the post had to be determined. Note that as it is a square section, both the area and drag coefficient is the same for all directions, meaning that care does not have to be taken to determine the direction of highest drag force.

From Fox and McDonald's Introduction to Fluid Mechanics, the coefficient of drag for a square prism with an infinite aspect ratio is 2.05 for Reynolds numbers greater than 1000. Note that this a reasonable approximation as the actual aspect ratio of the post is 100, with an estimated Reynolds number of 192,370 at a wind speed of 28 m/s.

While it is unlikely and certainly inadvisable for the construction of the fence in 28 m/s winds, designing for this wind speed allows for the possibility of sudden wind gusts of high velocity, as well as also providing additional security against unforeseen loads and incidences.

Using the value of air density of 1.225 kg/m^3 as was used in the calculation of mesh drag, along with the post frontal area of 1 m^2, the drag force was calculated to be 984.41 N.

To obtain an estimate of the overturning moment on the post, the drag force was approximated as a point load, acting at the centroid of the post, 5 metres above the base. While this method will slightly underestimate the moment as the drag force will cause a minor deflection in the post, creating an additional moment from the weight offset from over the centre, this deflection was found to be minor and was thus neglected.

Therefore, the overturning moment calculated was calculated as such:

$$Overturning\ Moment = 5 \times F_D \qquad 5.3.2$$

This gave a result of 4922.05 N.m. A summary of the maximum applied loads on the base is presented in the table below.

Maximum Vertical Post Loading	**14604 N**
Maximum Horizontal Post Loading	**3644.1 N**
Maximum Overturning Moment	**4922.1 N.m**

Table 5-3 Table Showing Imposed Loads on the Fence Post Base

5.3.2 Sizing of Base Ground Anchors

As was discussed earlier in sections 5.1.4 and 5.1.5, it is intended that the horizontal component of the wind loading that acts at the base of the fencepost is balanced by the

frictional force between the base and the ground. Using the lowest anticipated value for the coefficient of friction between steel and silty sand/gravel of 0.25 in conjunction with the vertical reaction of the base identified through FEA analysis also in section 5.1.5, it was found that the two forces are approximately equal.

However, as the magnitude of the frictional force is subject to a high level of uncertainty due to factors such as variability in the coefficient of friction, decreased normal reaction force at the base due to improper positioning/shallow angling of the guy wires and the potential for sudden, dynamic type wind loading, additional ground anchors are required to secure the base to the ground.

To ensure an adequate safety margin at all times, the ground anchors used must be sufficient to restrain the base of the fencepost against the horizontal load without any contribution from the aforementioned frictional force. By designing the ground anchors to bear the horizontal load exactly without additional capacity, the entire fence base will have a safety factor of 2; measured against a conservative coefficient of friction of 0.25.

Two approaches were identified for using ground anchors to restrain the base. These were using the anchors to directly support the horizontal force by pegging them into the ground and being loaded in a lateral manner; or to use a similar approach to the guy cables and load them in tension, tying the base down and increasing the normal and thus frictional force.

As explained in section 4.3.3; ground anchors develop most of their strength in tension only, and are limited in their lateral strength. Due to this, no suppliers of screw earth anchors give lateral strengths of their products.

While lateral loading is a valid approach, and simpler to execute than loading the anchors in tension, its difficulty to quantify means that it was not nominally selected for use in the design, although if demonstrated to be suitable could be substituted without issue.

Using equation 5.1.6, with a base horizontal reaction of 3644.1 N, identified in section 5.1.5, the required normal reaction of the base is 14576.4 N.

Assuming a total of four base legs, each with a ground anchor, the required tensile strength of each ground anchor is 3644.1 N. Consulting load charts available from one supplier of suitable ground anchors, Spirafix, it was found that in class ‘7’ soils, such as soft clay and very soft silts, their 50 mm diameter, 630 mm long ground screw could support approximately 3.9

kN tensile load (Spirafix, 2016). Therefore, four of this size anchor was specified for the base restraint. The load chart used in this selection is available in appendix B.

5.3.3 Base Geometry and Steel Section Sizing

Having determined the size of the ground anchors required to restrain the base against the horizontal reaction, the next stage was to determine the shape and sizing of the base itself.

The first parameter that was evaluated was the required length of the base arms away from the centre of the post required to support the maximum overturning moment of post caused by the drag force prior to mesh installation found in section 5.3.1.

Assuming that all four legs of the base were to be equal distances away from the centre in all directions, and the downforce at each leg end was 3600 N; the load required for each leg found in section 5.3.2, the minimum *perpendicular* length away from the base centre of each leg was identified. The value identified was 0.34 metres, meaning that the base had to have a minimum footprint area of at least 0.68 m x 0.68 m.

In order to minimize the amount of material required for use in construction of the base to reduce the weight, several different design geometries were investigated. Of these, an 'X' cross style design was chosen, as it was found that this used the least material to achieve the required footprint. It was also found to produce lower bending moments than an 'I' style design, as the vertical load from the fencepost is supported by two beam sections rather than just one. An image of the design is shown in figure 5-26.

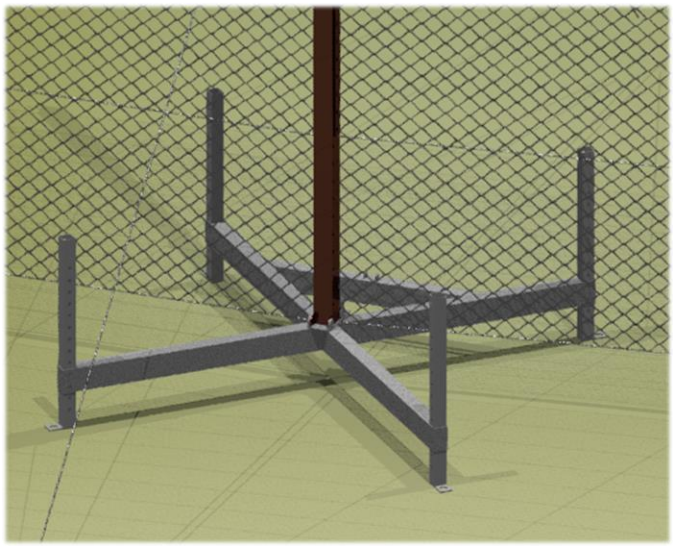

Figure 5-29 Image Showing 'X' Style Base Design

To reach the required base footprint with an 'X' cross, the base arms have to be longer than the perpendicular length from the centre, as per the Pythagorean theorem. As the legs are separated by 90° from one another, it was calculated that the minimum leg distance was 0.48 metres. Doubling this value for the sake of redundancy against

overturning gives a value of 0.96 metres, which was rounded up to an even metre.

Similar to the methodology used in sizing the fencepost, to size the steel 'beam' sections of the base, a 2D beam analysis was performed in ANSYS, with the vertical load applied being taken as 14604 N as was identified in section 5.1.5.

From this, the maximum bending moment in either beam was found to be 3658.5 N.m. Using equation 5.1.3 and a maximum value of stress of 153 MPa; the endurance limit of CL450L0 identified in section 5.1.3, a suitable size of RHS section was determined. Note that RHS was selected for this application as bending is not an issue in both directions, therefore, RHS offers greater strength for the same weight as compared to SHS.

With an elastic section modulus of 27.0 x 10^3 mm^3, a 125 mm x 75 mm x 2 mm RHS section (6.07 kg/m) was selected, giving an estimated maximum bending stress of 135.5 MPa. A 3D model was then created and subjected to a 3D FEA analysis with the same loading conditions. This simulation found that the peak Von-Mises stress was approximately 65 MPa. As such, this sizing was selected and used in the design.

5.3.3 Post Attachment Assembly Sizing

In order for the base to fulfil its design requirements outlined at the beginning of this section, the assembled fencepost needs to be securely connected to the base such that loads applied to the post are successfully transmitted into the base and its associated restraints. It also needs to be quick and easy to engage and also support the post through the lifting process.

The simplest method devised to meet the above criteria is through the use of opposing butt hinge style assemblies on either side of the fencepost. This type of arrangement was deemed to offer significant advantages; it is easily put together and deconstructed, all rigid body motion in all directions is restricted when both side are pinned, while assembly of only one of the hinges would create a pivot point from which to raise the post.

As all of the loads imposed upon the post is transmitted to the base solely through the two hinge pins, which are loaded predominantly in shear. This results not only in the creation of large shear stresses in both hinge pins but also large bearing stresses on the hinge 'barrel' sections of the post and base respectively.

In order to determine an appropriate size for the hinge pins and barrel sections, the maximum load applied to this assembly had to be determined. Of the loads identified in table 5-3, the overturning moment will produce the largest forces in the connection.

In the posts assembled state, this overturning moment will be transferred to the base through a force couple created by the hinges. As these forces are developed between the post and base section of the hinge, the total magnitude of can be calculated using the following formula:

$$M = F.d \qquad 2.5.4$$

As the distance between the line of action of the forces is the width of the fence post, 100 mm, the force required on each side of the fencepost was calculated as 49221 N. This load is shared between the hinges on either side; therefore, the maximum force experienced by any one part of the hinges is half of this value, 24610.5 N.

As mentioned above, the hinge pins are loaded in shear. For a uniformly applied load, such as the horizontal or vertical reaction on the post, they would be loaded in double shear; as the load could be borne by both sides of the hinge. However, in the event of the overturning moment, found to give the largest force, the hinge pin becomes loaded in single shear. Therefore, the average shear stress created in the pin can be found by:

$$\tau = \frac{F}{A} \qquad 2.5.5$$

Where t is the average shear stress, F is the applied force and A is the cross sectional area of the pin.

In order to minimize the required diameter of hinge pins, a high strength steel was specified. A review of data from various steel manufactures found that grade 4140 steel is a commonly used material for general engineering applications requiring reasonable strength, such as load bearing pins. It features a minimum yield strength of 480 MPa and minimum ultimate tensile strength of 700 MPa (Interlloy, 2011).

As no data is provided as the ultimate shear strength of 4140 round bar, a value was estimated from the ultimate tensile strength. Juvinall and Marshek (2012) report that for steel, a rough estimate of the ultimate shear strength of steel is 80 % of ultimate tensile strength. Therefore, the ultimate shear strength of 4140 grade bar stock was estimated as 560 MPa.

As the strength reduction factors identified in the literature review focused mainly on yield strength, to accommodate the reduction in strength associated with the elevated temperatures a safety factor of 4 was applied in calculating the required pin diameter. It should also be noted that the load itself represents a good safety factor, as the forces associated with the overturning moment should never be experienced during a fire event, only during fence construction.

Therefore, using equation 2.5.5, the required pin diameter was found to be 14.96 mm. As such, a 15 mm diameter was specified for the hinge pin.

Finally, the width of the hinge barrel sections required sizing. As the hinge section of the post was specified to extend the entire width of the post to help with installation alignment, only the bearing area of the base hinge sections required sizing.

As with the mesh track and runners, the hinge material specified was a 450 Grade plate, with a guaranteed minimum yield strength of 450 MPa. Therefore, taking the value of yield reduction calculated in section 5.2.1 of 264.13 MPa, a safety factor of 2 was applied, giving a maximum design bearing stress of 132 MPa.

Average bearing stress can be calculated using the following formula:

$$\sigma = \frac{F}{d \times t} \qquad 2.5.6$$

Where d is the pin diameter and t is the thickness of the bearing area. Therefore, using the values from above, the required thickness found was 12.43 mm. This was rounded down to 12 mm due to plate availability reasons. It should be noted that this slight reduction increased the stress by less than 1 MPa.

Note that as the width of the RHS sections used in the base are less than required for mounting the hinges, a base plate of 10 mm thickness was specified to be attached to the top of the base. Detail drawing of this entire assembly attached to the base can be seen in appendix E.

5.3.4 Design of Base Ground Anchoring Arrangement

Identified in section 5.3.2, as a redundancy to prevent the base from sliding under the full design load, each arm of the base requires an additional earth anchor attachment to provide

a vertical downforce to supplement the normal force in the event of poor soil friction coefficients or improper guy wire placement.

It was found that the easiest was to achieve this was to connect the underside of the base to the ground anchor with a vertical cable which could be adjusted to increase the tension. Theoretically, this cable should be preloaded to the specified tension of 3.64 kN; however, in practice, provided the initial tension is sufficient to eliminate any slack, minor sliding of the base will increase the tension until equilibrium is established.

As was specified in the sizing of the mesh support cables, turnbuckles are a cheap and easy way of adjusting the cable length and providing the initial preload tension. As the WLL of the 'P' grade M10 turnbuckle is 5.886 kN, it was specified in the design. Note that while a smaller turnbuckle would likely also be appropriate, M10 is the smallest available which is rated (Nobles, 2010).

For a detailed view of the base, complete with ground attachment lugs, see appendix E.

5.3.5 Design of Base Legs

Due to the requirement to construct the fence is varying locations, consideration had to be given to construction on unlevel ground. The natural solution to this problem was to specify adjustable length legs so the base could be levelled over sloping terrain. As part of the design process, a maximum hill inclination of 20^{o} was specified, corresponding to a gradient of approximately 36 %. Basic trigonometry was used to determine the maximum variation of leg length required; 0.5 m.

To achieve this, 'telescoping' sections of SHS were selected for the legs. By affixing a short female section perpendicular to the end of each base arm, the male SHS section comprising the leg can be slid to the required length, where it is then secured with pins in discretely positioned holes in the leg.

As the width of the RHS base arms is 75 mm, the outer telescoping SHS section attached to the base was also 75 mm to allow neat, easy attachment. As the associated male section for the 75 mm section is 65 mm, a wall thickness of 3.5 mm was selected, as this would give a

total clearance of 3 mm, 1.5 mm on either side of the leg. The leg section comprised of 65 mm x 65 mm x 4mm, the thickness determined through FEA analysis described below.

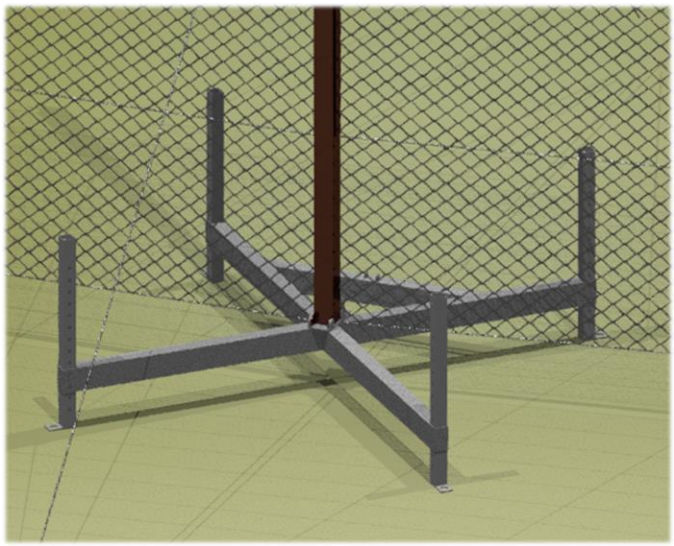

Figure 5-30 Image Showing Orientation of Fence Base to Fence

To prevent the legs of the fence from interfering with the mesh when the full leg length is not used, the orientation of the post to the 'cross' axis of the base is shifted by 45°, shown in figure 5-19.

This creates a complex loading situation involving the locking pins and the bearing area of the base and leg holes, as the transmission of the horizontal load is not normal to axes of the locking pins. In addition, the distance between the base and the ground will create a moment which needs to be supported.

As 15 mm diameter 4140 Grade round stock is already specified in the design, suitable for loads of up to 24.6 kN as demonstrated in section 5.3.3, the locking pins were specified as this size dependent upon FEA validation. Note that to support the moment created by the height of the base, two locking pins were specified per leg.

The applied loads used in the FEA simulation were a result of the 'worst case' scenario, a horizontal force of the design load 17.7 kN and vertical force of 14.6 kN was applied at the fence post attachment point. A 3.64 kN vertical force was also applied at the ground anchor attachment points as discussed in section 5.3.4.

Additionally, to best capture the behaviour at the connection between the legs and base, the legs and base were simulated as separate bodies in contact with a third separate body, the locking pin. As such, the loading case and model closely approximates the true situation.

The FEA results for both 22°C and 500°C are shown in the figures on the next page.

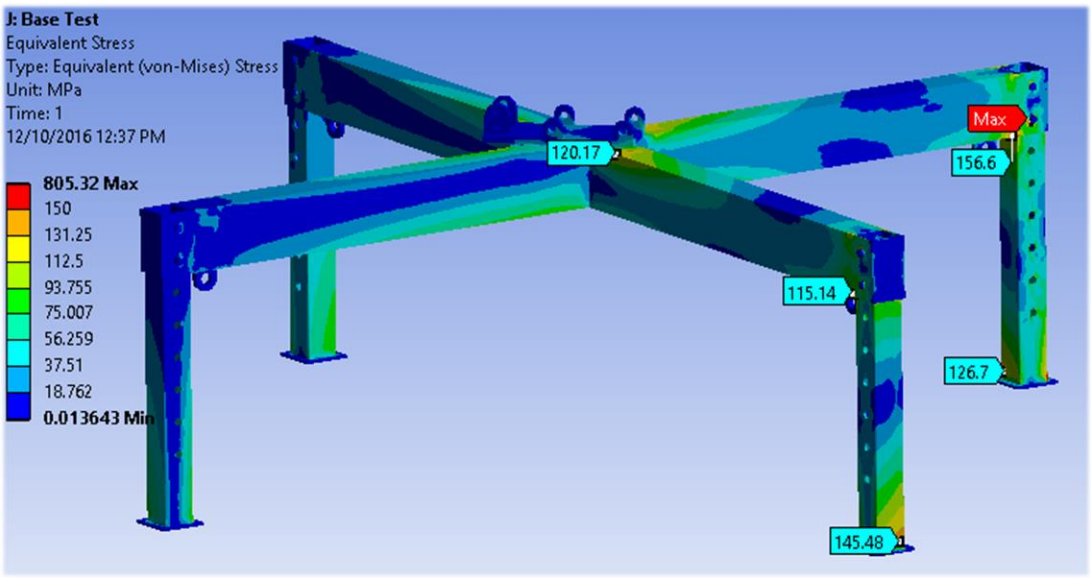

Figure 5-31 FEA Stress Results of Fence Base Model Under Maximum Loading Conditions

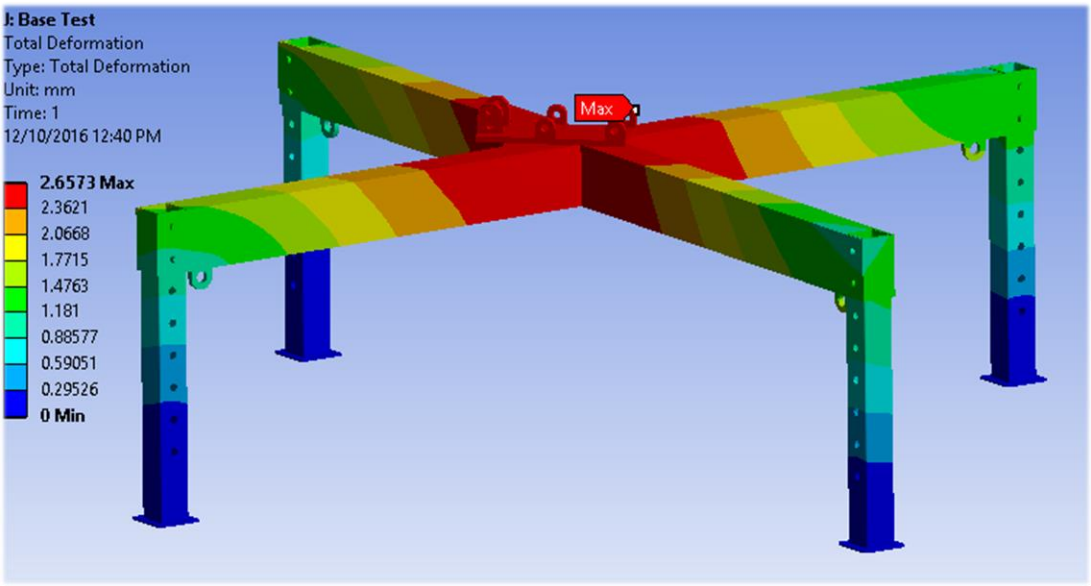

Figure 5-32 FEA Deformation Results of Fence Base Model at 22°C Under Maximum Loading Conditions

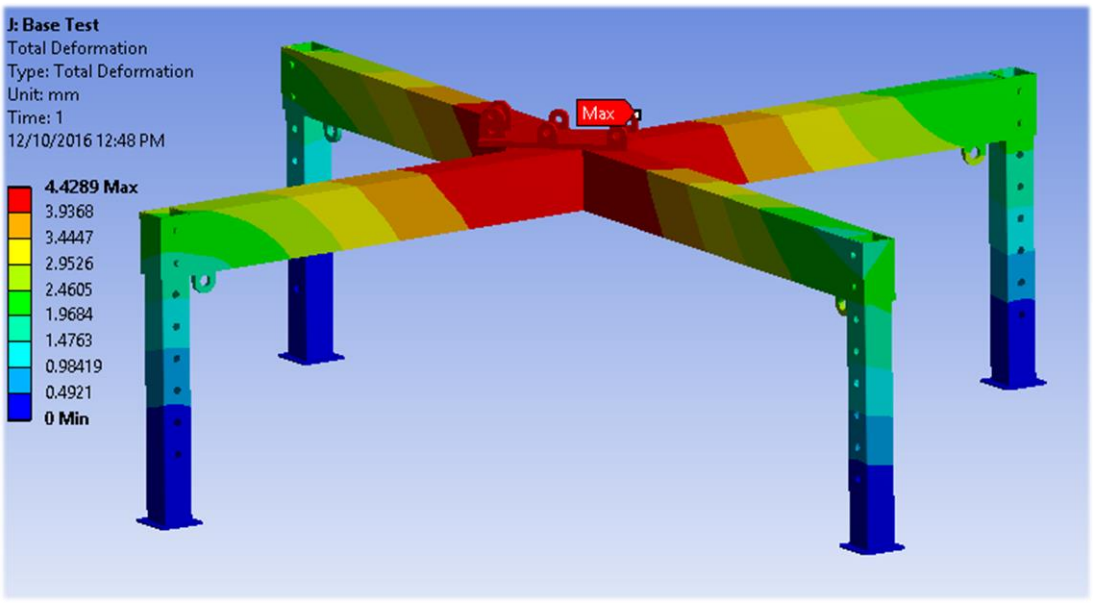

Figure 5-33 FEA Deformation Results of Fence Base Model at 500°C Under Maximum Loading Conditions

While the maximum stress level is very large, over 800 MPa, closer investigation identified that this was likely an artefact of the simulation process, as it occurred on a tiny section of the contact between the load pin and bearing surface. A cut section showing the area in question is shown in the figure below.

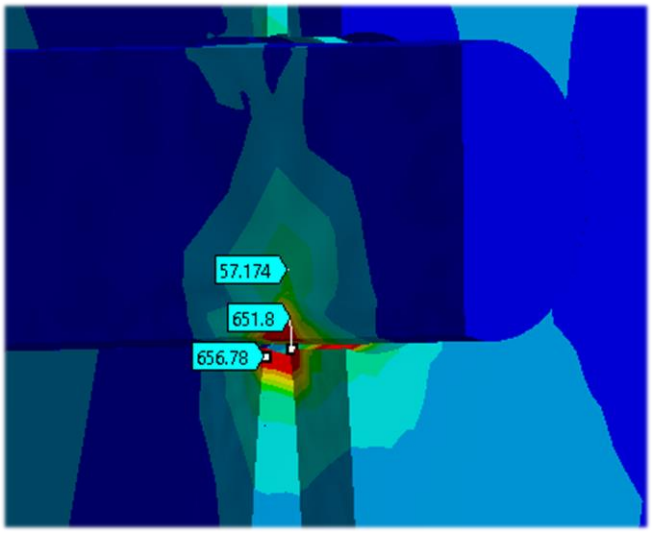

Figure 5-34 Close-up of FEA Stress Concentration in Pin

This shows that the peak stress is coming from the corner of the leg and lower pin. It was noted that the upper pin was not carrying any load, thus all the load was on the lower pin.

In reality, minor localized yielding at the leg and lower pin would redistribute the load between the two much more evenly. However, as this is a purely linear elastic simulation, this behaviour is not captured and thus a stress peak is caused.

Therefore, from the results, it was concluded that the arrangement was suitable, as the stress levels in the SHS sections was below 153 MPa, determined to be the endurance limit, and only around 60 MPa on average in the pins.

5.3.6 Design of Post Lifting Jig

Due to the heavy weight and large height of the fence posts, mechanical assistance will be required to raise them into position. However, as explained in section 3.1.3, the design aims preclude the use of heavy machinery.

Several different approaches were considered for raising the fence posts, such as telescoping type fencepost arrangement or the use of a hand operated jack. Ultimately, it was decided that the easiest approach to implement was to use a detachable winch mounted on a frame to hoist the post up about a pivot point on the fence base. Figure 5-28 shows an image of the lifting arrangement.

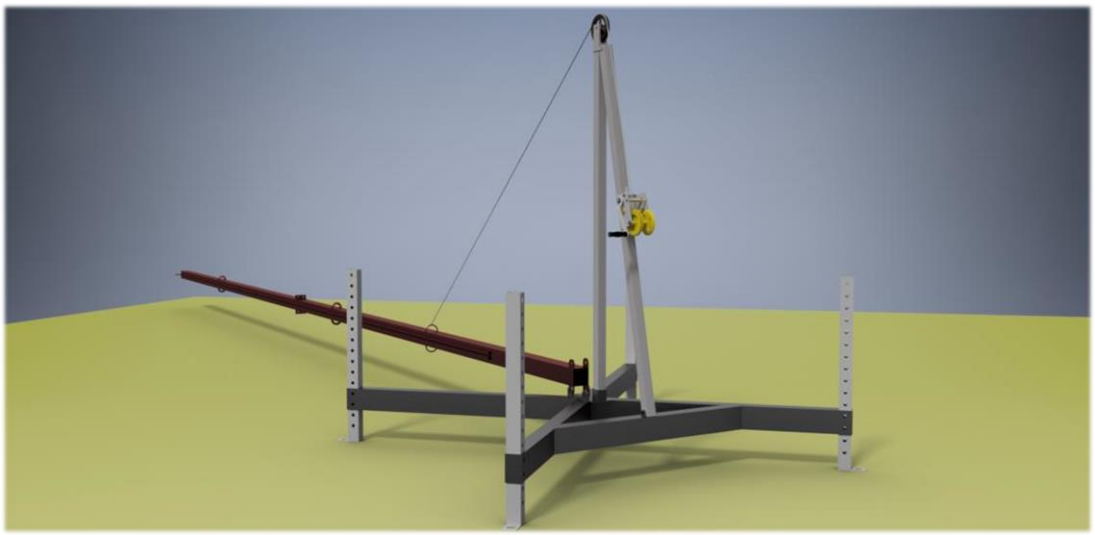

Figure 5-35 Image Showing Post Winching Concept

Comprising of a simple frame, the main post provides a lever arm for the tension force developed in the winch cable to create a moment on the fencepost, raising it up. The second angled section balances the forces acting at the top of the main post, avoiding the generation of a bending moment in the main post. As this structure is only required during post assembly, it has been designed to be removable, and is connected to the base through the use of pins.

Because of the angle offset between the fencepost and the base arms described in section 5.3.5 above, an additional RHS section had to be added spanning between two of the base arms to provide a location for the lifting post support strut to be attached. In order to minimize the angle of the support strut, this additional horizontal section was positioned at the ends of the arms.

In order to determine the capacity of the winch, the size of steel sections and the thickness of the locking pins required, in addition to the forces and reactions of the base, a basic calculator was developed in Excel which computed the maximum winch cable tension, main post compression, support strut tension, fence post pivot reactions and base ground reactions, based upon the mass of the fence post, the height of the lifting post and the angle of the support strut.

Using a main lifting post height of 1.5 metres, a support strut angle of approximately 65^{o} and a post mass of 100 kg, roughly the final weight of the assembled fencepost, the following results for the maximum forces during lifting were obtained:

Winch Cable Tension	**4690 N**
Support Strut Tension	**3091 N**
Lifting Post Compression	**10353 N**
Front Ground Reaction	**-3021 N**
Rear Ground Reaction	**4016 N**

Table 5-4 Table Showing Results of Post Lifting Analysis

As the maximum forces created in this configuration are less than the forces that are imposed on the base during operation at the maximum loading condition, this arrangement was selected. Additionally, while there was a large negative reaction at the front feet of the base, meaning a downwards force is required, this load is well within the specified ground anchors capabilities.

Converting the winch cable tension from Newtons to kilograms; the common method of representing winch capacity used by the industry, the required winch size was found to be 478 kg. This size capacity of hand winch is readily available on the market and was therefore a particular model is not specified here.

The major consideration in the sizing process of the lifting jib was then ensuring that the large compressive force on the long, relatively unconstrained lifting post did not cause buckling.

Therefore, to size the main lifting post, a required second moment of area formula was calculated for the post, determined through rearrangement of Euler's column buckling formula, shown below (Juvinall and Marshek, 2012):

$$P_{cr} = \frac{\pi^2 EI}{Le^2} \qquad 2.5.7$$

Where P_{cr} is the critical buckling load, E is Young's Modulus, I is the second moment of area and Le is the equivalent length of the post configuration.

In the proposed design, the bottom of the main lifting post will be pinned in place, however, as the top will effectively be a 'free' end in the direction normal to the support strut, two pins will be used, similar to in the base leg attachment to provide additional moment support.

Therefore, the combination of a fixed and free column end corresponds to an effective length of twice the actual measured length (Juvinall and Marshek, 2012). Using a value of E of 200 GPa and critical load equal to the maximum post compression, a required I value of 47.2 x 10^3 mm^4 was found. Given the small size of the result, a safety factor of 4 could be included for little cost; as such the specified I value for the post was 188.82 x 10^3 mm^4.

Nominating a SHS section for the post material, design tables were consulted, which showed that a 50 mm x 50 mm x 3 mm section has a second moment of area value about both axes of 195 x 10^3 mm^4 (Onesteel, 2011). After confirming buckling indeed would be the limiting failure mechanism by calculating the axial stress, this size was specified for the main lifting post.

The method used to connect the main lifting post to the base is the same as other connection on the fence, using steel plate section on either side of the lifting post and locking it in place with two pins.

Given that 15 mm diameter 4140 grade round bar stock has been specified for numerous other locking pin applications on the fence, it was again specified for the reasons of homogeneity throughout the design. This is largely over designed, as this size was sized for the post base connection force of 24.6 kN at 500°C in section 5.3.3. As such, the stress levels are not calculated here.

Likewise, for the plate sections, in order to minimize the variation of plate sizes required in the design, 12 mm 450 grade plate used in the base-post hinge was also used. Again, this is overdesigned for this application and thus the bearing stress is not calculated here.

As can be seen in figure 5-28, at the top of the lifting post a pulley sheave is required to support the winch cable. For a winch in the 500 kg capacity range, wire diameters of between 4 and 5 mm are typically used (Manutec, 2016). The recommended minimum pulley to cable diameter advised to minimize bending stresses on the cable and prolong

service life is given as 16:1; therefore, for a 5 mm cable, the pulley diameter should be 80 mm (Bridon, 2010).

As the lifting jig design features the winch mounted on the support strut, the maximum force transmitted through the strut section will be between the fence base and the winch mount, where both tension forces are carried. This gives a sum of 7781 N, and thus this value was used in the design calculations.

For a purely tensile load of the above magnitude, the overall section size is not a limiting factor as the average stress developed is not large enough to be of concern. The bearing at the pin connection to the base, in particular, was reasoned to be the area of highest stress and thus the section was sized in accordance.

Again specifying a 15 mm diameter locking pin, the required section size of SHS was calculated with equation 2.5.6 for average bearing stress; rearranged to solve for the thickness associated for a maximum design stress of 150 MPa, a third of the yield stress of the sections.

This gave a required wall thickness of 1.73 mm; therefore, a 35 mm x 35 mm x 2 mm SHS section was nominated. 35 mm x 35 mm was chosen as it would neaten the attachment of the support strut to the main lifting post.

Detailed design drawings for the lifting jib are available in appendix F and G.

6.0 Evaluation of Final Design

This chapter evaluates the standing of the current design developed in the second part of this report against the performance criteria developed in section 3.2. This aims to set a benchmark against which future designs and improvements to the current design can be qualitatively assessed.

6.1 Fence Weight Per 100 Metre Length

To assess the total fence weight per 100 metres, a table of each component used in the fence construction, their weight, and the number used per single 10 metre span was created. This is shown in table 6-1 on the following page.

Component	Mass	Number Used
Lower Post	50.44 kg	1
Upper Post	50.93 kg	1
Base	38.4 kg	1
Base Legs	4.98 kg	4
Guy Cable Anchors	3 kg	4
Base Anchors	2.5 kg	4
Mesh Support Runners	0.347 kg	32
Mesh + Seams (Total)	42.5 kg	1
Mesh Cables (Per cable)	1.24 kg	16
M10 Turnbuckles	0.28 kg	20
Mesh Hoisting Sheave	1.41 kg	2

Table 6-1 Table of Component Weights and Quantities Used in Design

Note that 'one off' components such as the post lifting jig, ground anchor installer etc. have not been included as their individual contribution is minimal once larger fence spans are considered.

Summing the values in table 6-1 to give an approximate mass of the entire fence assembly per 10 metres span gives a result of 263.6 kg. Multiplying this number by 10 gives the total fence weight per 100 metres, estimated here to be 2.64 tonnes per 100 m.

6.2 Fence Assembly Procedure and Estimated Assembly Time

To develop an estimate of the speed with which the current design can be assembled, the assessment procedure outlined in section 3.2.4 was followed. Therefore, listed in appendix B is all of the tasks required for assembly of a single fence span, accompanied by estimates of each task time. It should be noted that in most cases, the estimates presented are based upon engineering reasoning and judgement, and no actual timing of tasks has been

performed. As such, the following times are a guide at best. It was also assumed that only one person was working on a task at a time, unless otherwise specified.

Summating all of the task times in appendix B indicates that the estimated total work time for assembling a 10 metre section of the fence is around 41 – 42 minutes. As the fence is intended to be constructed by a team, ideally a four-man crew, the actual elapsed time will be less than this, as many of these tasks can be completed in parallel.

Following the procedure in 3.2.4, a precedence table was developed from the list of tasks, and a network diagram was created; located in appendices B and C respectively.

Using critical path analysis on the network diagram, an estimate for the assembly time for one fence section was obtained; a time of 23.5 minutes. Converting this time to hours and dividing 10 by the result to give the assembly time in metres per hour yields a result of 25.5 metres / hour. Therefore, a 200 metre section of fence would take nearly 7.8 hours to construct.

This seems like a poor result, however, not considered in this basic analysis of construction time is the requirement to continue to repeat the process for successive sections of fence.

For example, the critical path tasks E through M take up 12.5 minutes and generally only require a one or two people; as such, the two workers performing task C and D have substantial downtime, and are somewhat underutilized in the current arrangement. If they continued on to perform task A and B on the next post the assembly time would decrease considerably; as task B is a major bottleneck.

To develop a second assessment of the assembly time to attempt to better utilize the workers, an assumption will be made that tasks A and B are pre completed, and as such removed from the analysis.

This yields a critical path time of 15.5 minutes per 10 metre fence span, an 8-minute reduction. Converting this to the designated unit of metres per hour gives a result of 38.7 m/h, a 65.9 % increase in assembly speed. At this estimate, a 200 metre fence could be constructed in 5.17 hours, work-breaks not included.

Again, this result is still slightly lower than ideal, however, it represents a starting point for both optimization of the fence design to feature faster installation and further work studies and time assessments on the currently proposed method to ascertain the optimum result.

However, as the times listed are purely theoretical values, their usefulness is limited and obtaining better data is essential for further work.

7.0 Conclusions and Recommendations for Further Work

7.1 Summary of Work Undertaken

As part of the requirements towards the awarding of a Bachelor of Engineering (BENH) degree at the University of Southern Queensland, a research project was performed investigating the design of a portable bushfire attenuation fence.

The project was broadly split into three main sections: review of the current understanding of the performance of fine aperture wire mesh against major methods of bushfire propagation; Determination of appropriate parameters for the construction of a portable bushfire attenuation fence; and the development of a preliminary design for such a fence.

In the first section, it was identified that fine wire mesh aids in attenuating bushfire spread through two major methods; reducing firebrand transmission across the mesh and reducing radiant heat flux from the fire front across the mesh. Reduction in firebrand transmission was found to be a function of aperture size, while radiant heat flux attenuation was a result of porosity.

In the second section, the requirements for a first generation bushfire defence fence were developed, with a strong focus on simplicity, portability and ease of construction. Developing on this, a criterion for assessing bushfire fence performance characteristics was also developed to allow evaluation of the final design as well as qualitative comparisons of future designs. As such, appropriate design aims were developed, and through feasibility analysis using basic engineering calculations, basic parameters for the final fence design were determined.

In the final major section, a design process was undertaken to develop a preliminary design for the manufacture of a prototype bushfire attenuation fence. Consideration was given to all the factors determined to be relevant, and the design was validated through the use of appropriate computational analysis using the ANSYS FEA package. As the final stage in the project, the fence performance metrics of weight per 100 metre span and assembly time per 100 metre span was estimated as per the criterion developed earlier in the project.

7.2 Summary of Results

Investigation into conditions associated with bushfires lead to the selection of a maximum design wind speed of 28 m/s (100.8 km/h), with a maximum peak temperature of 500°C.

Additionally, investigation into the conditions leading to the spread of bushfires found data indicating that a minimum fence height of 10 metres would be required to aid in preventing the spread of fire across tree tops.

Based on these results, the maximum drag force per unit area on three different types of bushfire mesh at 28 m/s was estimated. Of these results, it was determined that only the lowest porosity mesh (76%), with a maximum drag force of 177 N/m^2 could be implemented with any real practicality.

Initial feasibility analysis carried out on various fence restraint methods found that of all investigated, only the use of ground anchors with supplementary guy wires would provide suitable restraint to the fence. Basic engineering calculations based on available ground anchor capacities subsequently lead to the selection of a 10 metre fence height with a 10 metre fence post support span.

Based on calculation of strength and stiffness reduction associated with high temperatures, in conjunction with fatigue life calculations, a main fencepost size of 100 mm x 100 mm x 2 mm SHS was determined and validated using FEA analysis. A base material size of 125 mm x 75 mm x 2 mm was also used in the design.

Basic computational analysis performed on the support and loading of the wire mesh found that and restraint of the fine mesh should be continuous along a single piece of mesh in order to avoid the generation of significant stress risers.

Basic analysis of the total weight for the final design lead to an estimated mass of 2.64 tonnes per 100 metre span, with two different estimates for construction time per 100 metres, ranging from 25.5 to 38.7 metres fence per hour.

7.3 Recommendations for Further Work

From this project, it is the authors opinion that the concept of a portable bushfire attention fence has merit, and is both feasible and economic to implement. However, areas which

were identified as lacking in available data which would aid in the development process of such a fence are listed below:

- Further study and detailed investigation into required fence height for different applications. In this project, a 10 metre fence height was selected, however, this was based off of research intended for other applications and as such the results have been extrapolated. This could be divided into application as well, e.g. required fence height for typical home defence may be substantially lower than required for retarding the progress of an entire bushfire. This would prevent overdesigning a fence for a given application and likely lead to optimized outcomes.

- Further study is also recommended into the material properties of fine wire mesh under high wind loading and high temperatures. It was predicted from prior research that the wires used would have a tensile strength on the order of 2000 MPa, however, it is uncertain the reduction that would occur at high temperatures. Physical testing of roller welded mesh to sheet metal is also recommended prior to any attempt to build the prototype design detailed here, as there were significant assumptions about material properties, bonding conditions and loading used in the mesh FEA modelling. Thus, physical investigation and validation is highly recommended.

8.0 References

All Lifting 2016, Australia, Viewed 24th September 2016 https://www.alllifting.com.au/

ANCA Structural Anchors, 2016, Sheffield, UK, Viewed 5th August 2016 http://www.structuralanchors.com/

Anderson, H. 1969, *Heat Transfer and Fire Spread,* USDA Forest Service, Utah, Viewed 23rd May 2016 http://www.fs.fed.us/rm/pubs_int/int_rp069.pdf

Australian Institute of Criminology, 2009, *Cost of Bushfires,* Australian Government, Canberra, Viewed 25th February 2016 http://www.aic.gov.au/publications/current%20series/bfab/41-60/bfab060.html

Balston, J.M. and Williams, A. 2014, *Modelling bushfire changes for South Australian regions*, Department of Environment, Water and Natural Resources South Australia, Adelaide, South Australia. pp.88

Bridon Oil and Gas 2010, *Steel Rope Technical Information,* Bridon The Ropes Group, UK. Viewed 4th October 2016 http://www.bridon.com/china/x/downloads/steel_technical.pdf

Block Division 2013, *Swivel Eye – Single Sheave,* Block Division, Viewed 25th September 2016 http://www.blockdivision.com/Swivel-eye-pulley-blocks-1-single-sheave-stainless-steel-zinc-movable-pulleys-system/

Buchholdt, H. 1985, *An Introduction to Cable Roof Structures,* Thomas Telford, Scotland

CFA Victoria, 2012, *About Black Saturday,* CFA Victoria, Victoria, Viewed 25th February 2016 http://www.cfa.vic.gov.au/about/black-saturday/

Chen, J., Young, B., and Uy, B. (2006). *Behavior of High Strength Structural Steel at Elevated Temperatures J. Struct. Eng.*, 10.1061/(ASCE)0733-9445(2006)132:12(1948), 1948-1954.

Crimsafe 2016, Crimsafe Security Systems Pty. Ltd. Viewed 28th September 2016 https://crimsafe.com.au/

Demar, P., Adshead, D. 2011, *Blue Gum Plantation Fuel and Fire Behaviour Guide,* Department of Agriculture, Fisheries and Forestry, Canberra, Viewed 18th August 2016 http://www.ghd.com/PDF/BlueGumFuelandFireGuide.pdf

Dixon, J.C. 2007 *The shock absorber handbook*, 2nd edn. Chichester, England: Wiley-Blackwell.

Ellis, P. 2012, *A Review of Empirical Studies of Firebrand Behaviour,* Bushfire CRC, Canberra, Viewed 15th May 2016 http://www.bushfirecrc.com/sites/default/files/managed/resource/attachment_b_fuelbed_ignition_lit_review_1.pdf

Fact or Fiction, 2016, Guidance on workplace lifting regulations, WorkSafe Australia, Canberra, Viewed 19th August 2016 http://www.safeworkaustralia.gov.au/sites/SWA/media-events/safety-month/Documents/fact-or-fiction-questions.pdf

Ferdinand P. Beer, 2012. *Mechanics of Materials* 6th International edition McGraw Hill Higher Education.

Fox, R. W., Pritchard, P. J., & McDonald, A. T. (2010). *Fox and McDonald's introduction to fluid mechanics*. United Kingdom: John Wiley & Sons.

Hashempour, J., Sharifian, A., Billingsley, J., 2015, *Experimental measurement of direct thermal radiation through single-layer square-cell plain woven screens,* ASME Journal of Heat Transfer

Hubble 2016, *Chance Anchors Catalogue June 2016,* Chance Anchors, Viewed 1st September 2016 http://www.hubbellpowersystems.com/catalogs/anchoring/04-Anchors.pdf

Image of Ground Penetrating Anchors, 2016, Rittenhouse, Viewed 1st September 2016 http://mkrittenhouse.com/media/catalog/product/cache/2/image/9df78eab33525d08d6e5fb8d27136e95/p/e/penetrator_tro_300x_zoom.jpg

Imaoka, S. 2007, *Sheldon's ANSYS.NET Tips and Tricks: Buckling in WB Simulation,* ANSYS Systems Pty. Ltd., Viewed 29th September 2016 http://ansys.net/ansys/tips_sheldon/STI0705_Buckling.pdf

Interlloy 2011, *4140 High Tensile Steel,* Interlloy Pty Ltd, Viewed 26th September 2016 http://www.interlloy.com.au/our-products/high-tensile-steels/4140-high-tensile-steel/

Institute for Steel Development and Growth 2011, India, Viewed 24th September 2016 http://www.steel-insdag.org/

Insurance Institute for Business and Home Safety, 2016, *Simulated Firebrand Attack on a House,* Insurance Institute for Business and Home Safety, Florida, Viewed 10th May 2016 https://disastersafety.org/wildfire/research-center-demo-wildfire-2011/

Javidinejad, A. 2013. *Buckling of Beams and Columns under Combined Axial and Horizontal Loading with Various Axial Loading Application Locations,* Journal of Theoretical and Applied Mechanics, 42(4), pp. 19-30. Retrieved 11 Oct. 2016, from doi:10.2478/v10254-012-0017-9

*Journal of the Australian Steel Institute, '*Specification of threaded bar in structural applications', Volume 47 Number 1 – July 2014

Juvinall, R.C. and Marshek, K.M. 2012, *Fundamentals of machine component design*. 5th edn. United States: Wiley, John & Sons.

Kraft, S, 2013. *The Characterization of the Effects of Stress Concentrations On the Mechanical Behaviour of a Micronic Woven Wire Mesh*, Electronic Theses and Dissertations. Paper 2552. http://stars.library.ucf.edu/etd/2552

Kreith, F., Manglik, R. M., & Bohn, M. S. (2010). *Principles of heat transfer, Si edition* (7th ed.). Stamford, CT: CENGAGE Learning Custom Publishing.

Manzello, S. 2016, *Reduced Ignition of Building Components in Wildland-Urban Interface (WUI) Fires Project,* NIST, Maryland, Viewed 10th May 2016 https://www2.nist.gov/programs-projects/reduced-ignition-building-components-wildland-urban-interface-wui-fires-project

Manutech 2010, *Hand Winches,* Manutech Pty. Ltd., Viewed 28th September 2016 http://www.manutec.com.au/webmedia/prodinfo/hand%20winches%20and%20whches%20parts%20page27-32.pdf

Mason, G. L., Burhman Q. Gates, Victoria D. Moore, *Determining forces required to override obstacles for ground vehicles*, Journal of Terramechanics, Volume 49, Issues 3–4, June–August 2012, Pages 191-196, ISSN 0022-4898, http://dx.doi.org/10.1016/j.jterra.2012.04.001.

McGinnis, R. 2012, *Zero to Sixty,* Viewed 20th August 2016 http://rickmcginnis.blogspot.com.au/2013/07/how-to-build-racetrack.html

Nobles 2010, *Nobles Rigging Screws & Turnbuckles,* Nobles Pty. Ltd. Viewed 3rd October 2016 http://www.nobles.com.au/getattachment/Products/Lifting-Rigging/Rigging-Screws-and-Turnbuckles/Turnbuckles-Jaw-Eye/Care-In-Use-Rigging-Screws-Turnbuckles.pdf.aspx

O'Neill, J 2003, *Aftermath of the 2003 Eastern Victorian Alpine Bushfires,* Viewed 23rd May 2016 https://en.wikipedia.org/wiki/Bushfires_in_Australia#/media/File:2003_Bushfires_aftermath,_Big_River_near_Anglers_Rest.jpg

OneSteel 2012, *Design Capacity Tables for Structural Steel Hollow Sections*, OneSteel, Queensland, Viewed 2nd October 2016 http://www.onesteel.com/images/db_images/productspecs/DCT_CF.pdf

Poon, S. 2003, *Predicting Radiation Exposure from an Advancing Bushfire Flame Front,* Warrington Fire Research, Victoria, Viewed 23rd May 2016 http://www.timber.net.au/bushfire/common/general/PDFs/radiation.pdf

Samuel L. Manzello, Seul-Hyun Park, Sayaka Suzuki, John R. Shields, Yoshihiko Hayashi, Experimental investigation of structure vulnerabilities to firebrand showers, Fire Safety Journal, Volume 46, Issue 8, November 2011, Pages 568-578, ISSN 0379-7112, http://dx.doi.org/10.1016/j.firesaf.2011.09.003.

Sasiharan, N., Muhunthan, B., Badger, T.C., Shu, S., Carradine, D.M. 2006, 'Numerical analysis of the performance of wire mesh and cable net rockfall protection systems', *Engineering Geology* 88 (2006) 121–132

Sharifian, A. and Hashempour, J. 2015, *The combined effects of woven wire screens and buffer zone in mitigating risks associated with firebrand showers,* University of Southern Queensland, Toowoomba

Spirafix 2016, Newport, South Wales, Viewed 30th September 2016 http://www.spirafix.com/

Stainless Steel Wire and Mesh, 2016, Stainless Steel Wire and Mesh, Viewed 10th May 2016 http://www.sswm.com.au/Stainless-Steel-Bushfire-Mesh

Standards Australia 2009, *Construction of buildings in bushfire-prone areas,* AS 3959-2009, Standards Australia, Sydney, Viewed 26th February 2016

Standards Australia 2009, *Temporary fencing and hoardings,* AS 4687-2007, Standards Australia, Sydney, Viewed 26th February 2016

Soil Density, Argonne National Laboratory, Viewed 2nd August 2016 http://web.ead.anl.gov/resrad/datacoll/soildens.htm

Zhejiang Guanming Power Transmission Material Corporation, 2016, Shaoxing, China, Viewed 3rd September 2016 http://www.galvanizedsteelcable.com/sell-power_tower_stay_wire_astm_a_475_or_bs_183-3949378.html

Appendix A

ENG4111/4112 Research Project

Project Specification

For:	Bradley Fell
Title:	Design of a Dismountable Bushfire Attenuation Fence
Major:	Mechanical Engineering
Supervisor:	Ahmad Sharifian
Enrolment:	ENG4111 – ONC S1, 2016 ENG4112 – ONC S2, 2016
Project Aim:	To identify key design parameters required for a wire mesh fence to withstand bushfire conditions, develop assessment criteria for evaluating the performance of a portable bushfire attenuation fence and develop a preliminary design of such a fence through computational modelling.

Programme: Issue B, 19th September 2016

1. Research the factors affecting the propagation behaviour of bushfires to determine the necessary design parameters of a portable bushfire attenuation fence for feasibility, practicality and effectiveness.
2. Develop a series of assessment criteria against which any particular bushfire attenuation type fence can be evaluated, creating a benchmarking tool for prospective future designs.
3. Through the use of relevant engineering theory and data, evaluate the feasibility of various fence design options, determine the most appropriate available options and develop a preliminary design overview.
4. Develop a computer model of the proposed fence and through an appropriate simulation method identified, investigate the relationship between design parameters and structural loads and performance.
5. Develop a computation model using the Finite Element Analysis Software ANSYS to determine design parameters such as maximum stress, deflection and support forces and reactions, refining and detailing the preliminary design further.
6. Evaluate the final design developed against the assessment criteria previously created to assess the success in which the final design met the design goals.

If time permits:

7. List recommendations for the direction which further work in this area should be directed, based upon the findings and information gained through the course of the research project.

Appendix B

- Base positioning, leg attachment and levelling: 2.5 minutes total
- Base ground anchor installation: 2 minutes each
- Attachment and tensioning of ground anchors to base: 2 minutes total
- Positioning and installation of guy cable earth anchors: 2 minutes each
- Attaching lower fence post to base with hinge pin: 0.5 minutes
- Bolting together fence post sections: 2 minutes
- Positioning mesh hoisting cable over pulley sheave: 0.5 minutes
- Attaching guy cables to the fencepost: 0.5 minutes
- Attaching lifting jig to fence base and winch cable to post: 2 minutes
- Winching post into vertical position and pinning in place: 3.5 minutes
- Detaching lifting jig from base: 1 minute
- Attaching guy cables to earth anchors and tensioning: 4 minutes
- Unrolling mesh infill and attaching runners to cable ends: 4 minutes
- Hoisting mesh into position (requires two people): 3 minutes

Task Code	Task Description	Predecessors
A	Base Positioning & Leg Attachment	None
B	Base Ground Anchor Installation	None
C	Guy Cable Ground Anchor Installation	None
D	Unrolling Mesh Infill and Attaching Runners to Support Cables	None
E	Attachment and Tensioning of Base Ground Anchors	A,B
F	Attaching Lower Fence Post to Base Hinge Joint	E

G	Bolting Together Fence Post Sections	F
H	Positioning Mesh Hoisting Cable Over Sheave	G
I	Attaching Guy Cables to Fencepost	G
J	Attaching Lifting Jib to Fence Base	E
K	Winching Post into Position	H,I,J
L	Detaching Lifting Jig	K
M	Attaching Guy Cables to Earth Anchors & Tensioning	C,K
N	Hoist Mesh Into Position	D,M

Appendix C

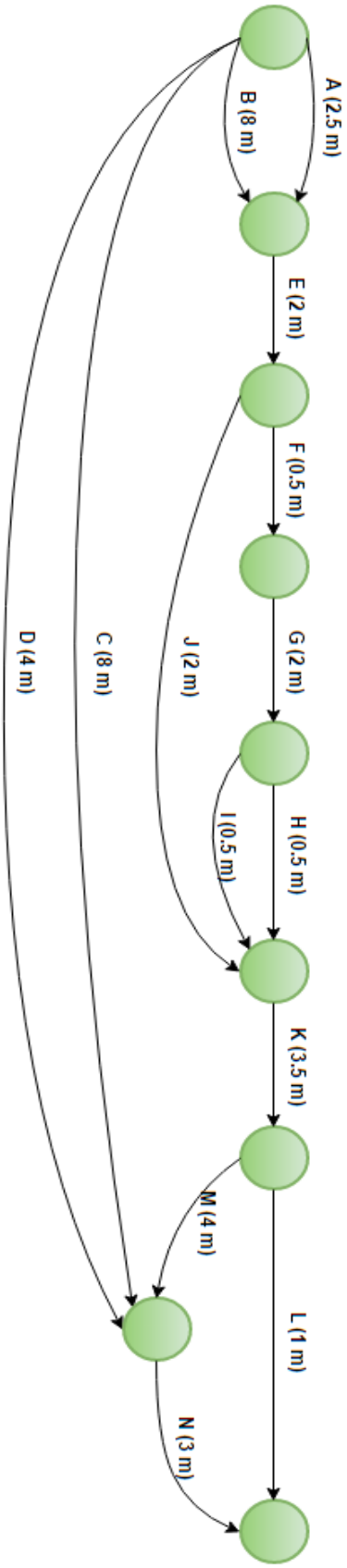

Figure 0-1 Network Diagram for Fence Assembly

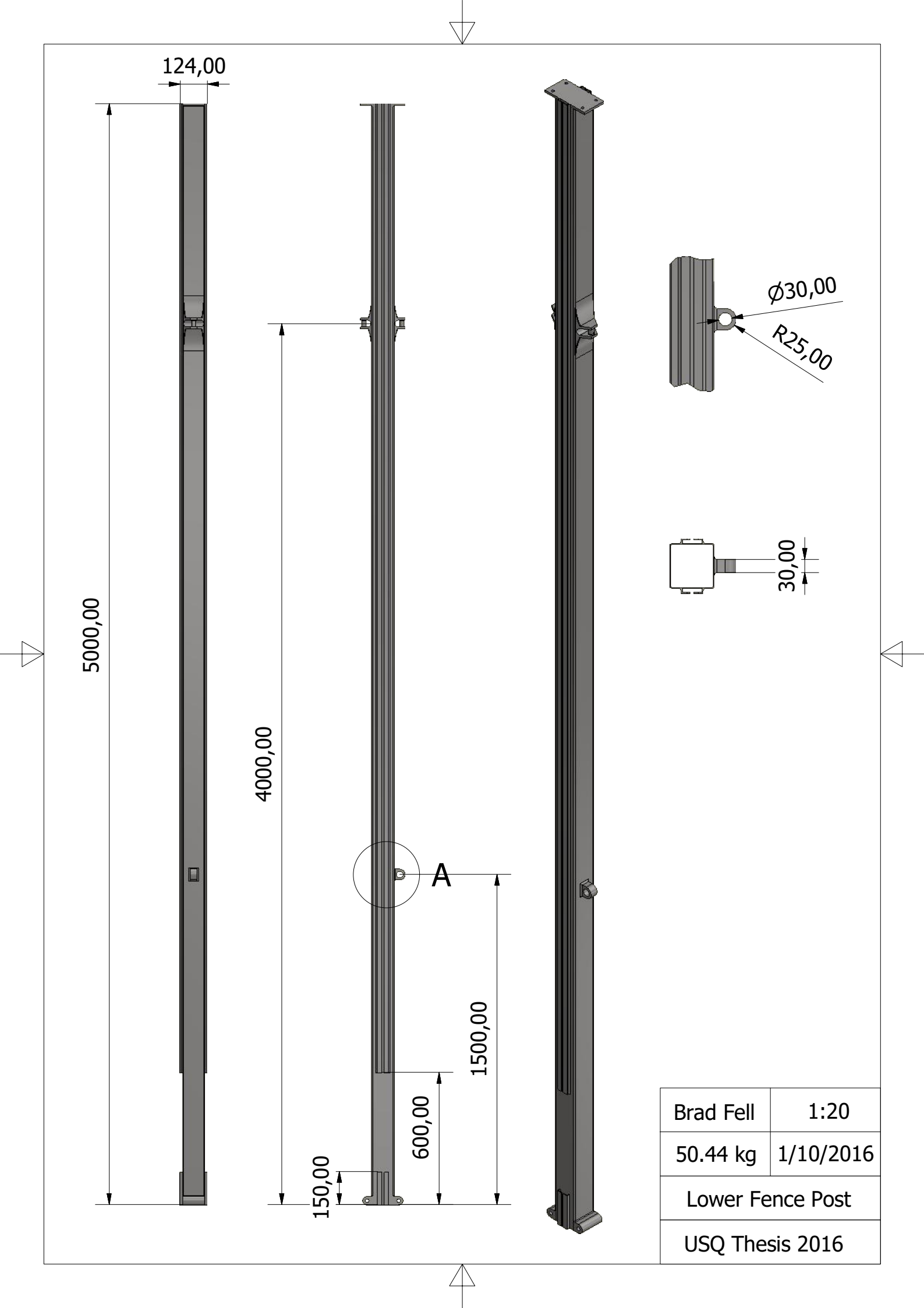

Brad Fell	1:20
50.44 kg	1/10/2016
Lower Fence Post	
USQ Thesis 2016	

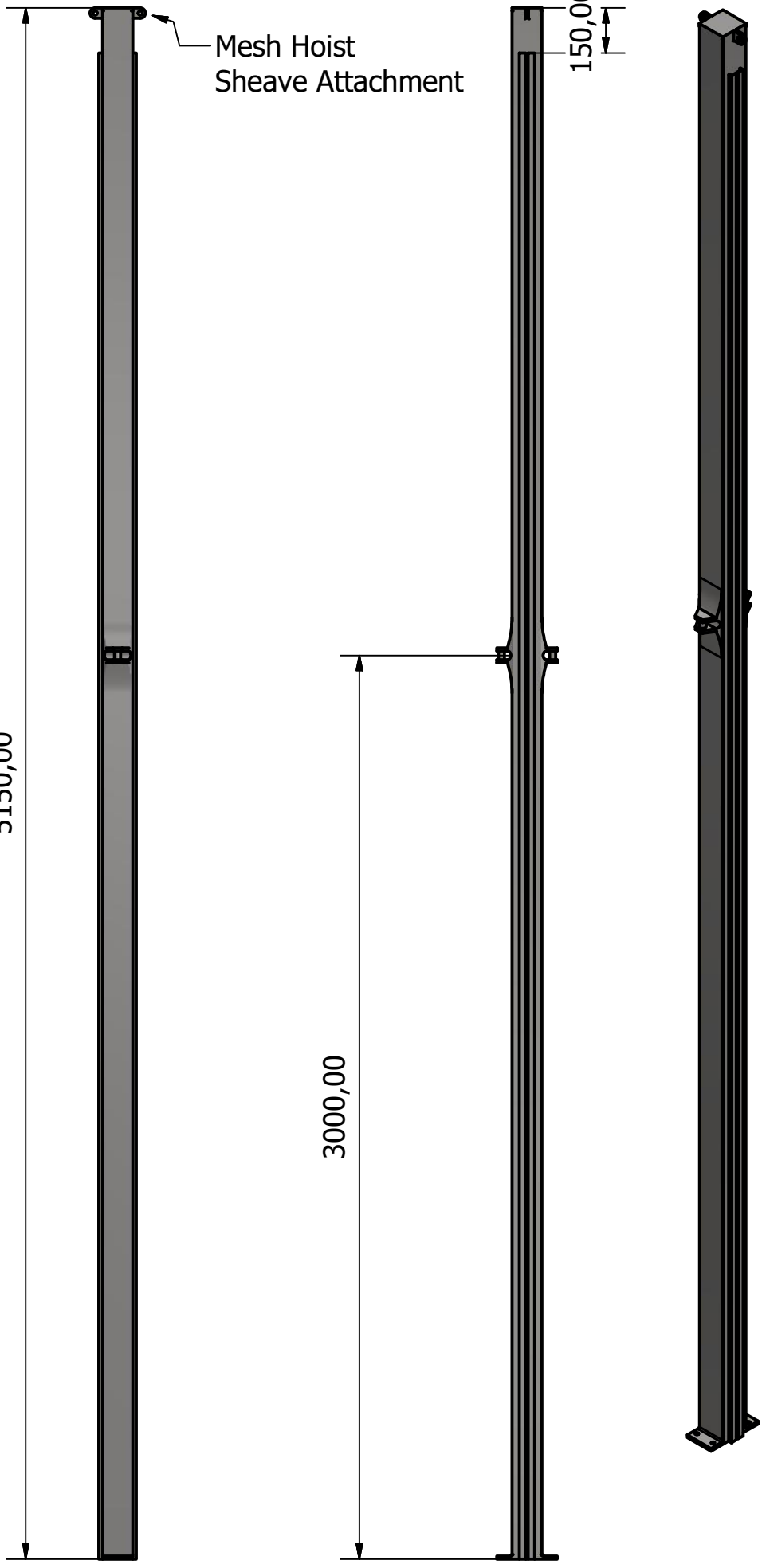

Brad Fell	1:20
50.93 kg	2/10/2016
Upper Fence Post	
USQ Project 2016	

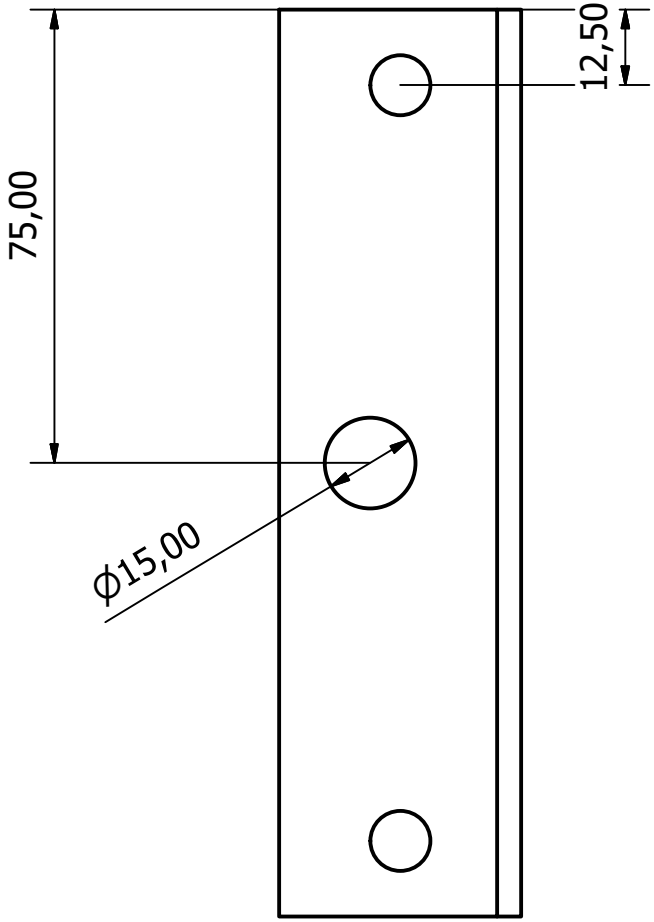

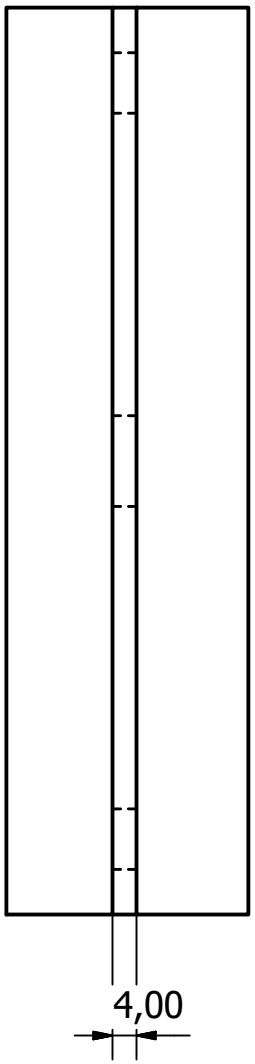

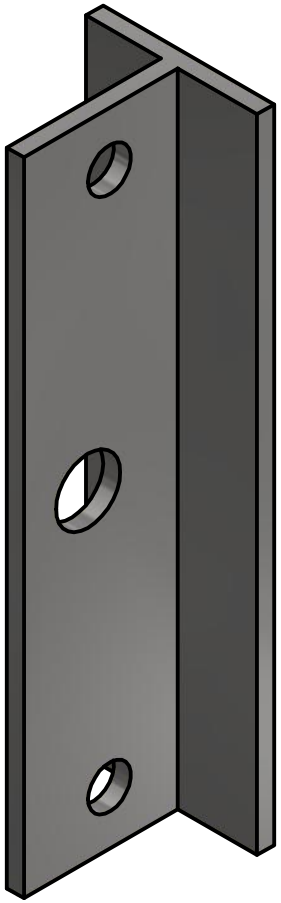

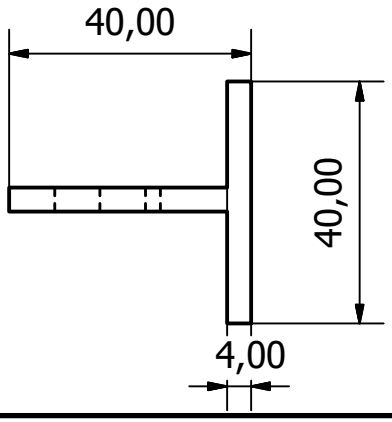

Brad Fell	1:1.25
0.347 kg	3/10/2016
Mesh Support Runner	
USQ Project 2016	

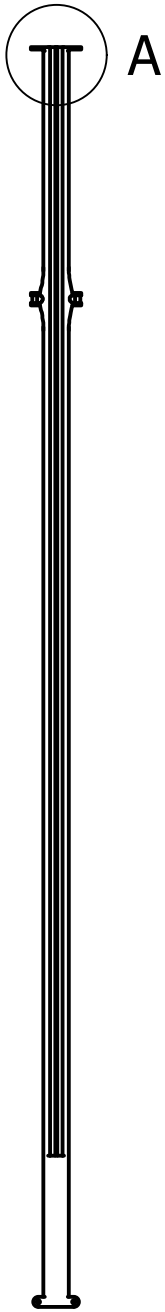

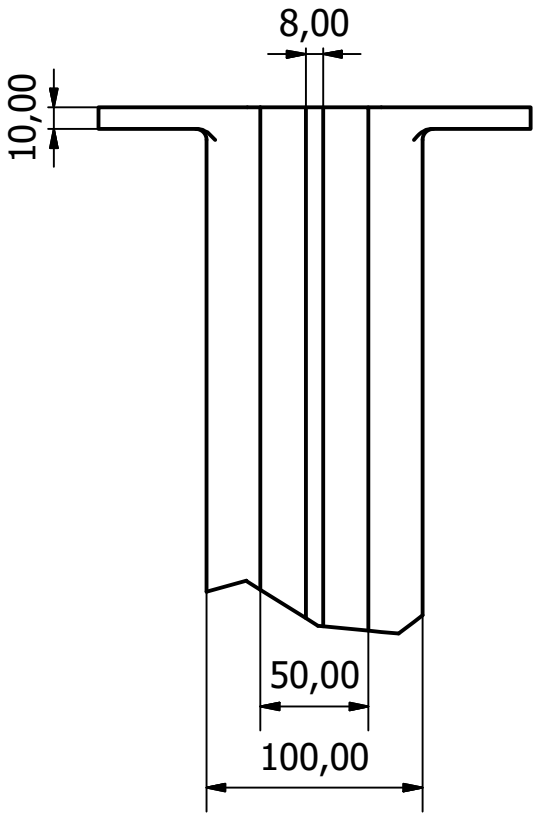

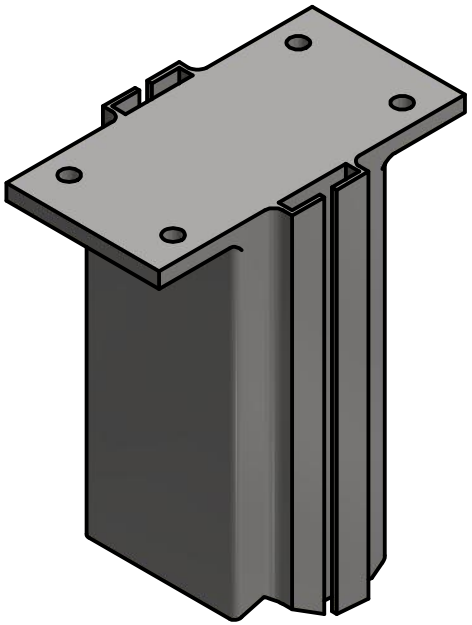

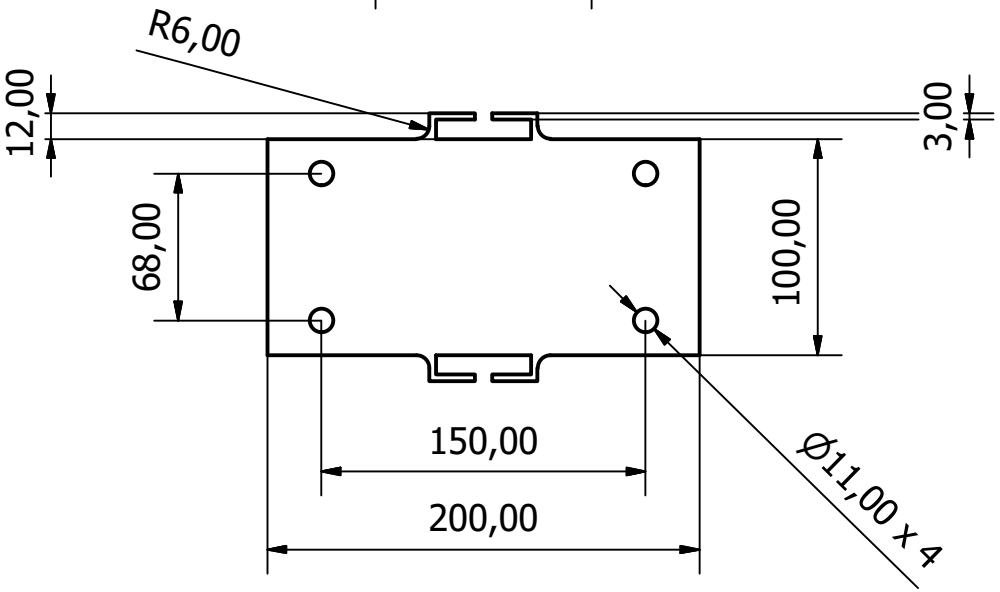

Brad Fell	1:3.5
	1/10/2016
Lower Post Joint	
USQ Project 2016	

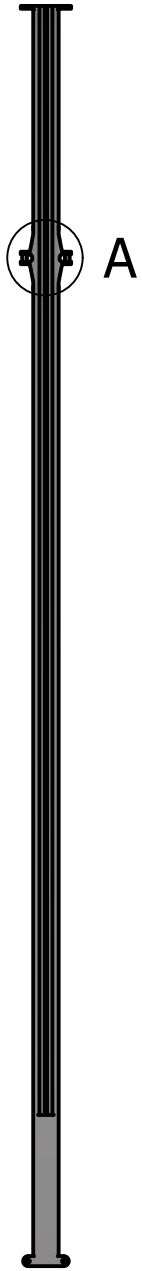

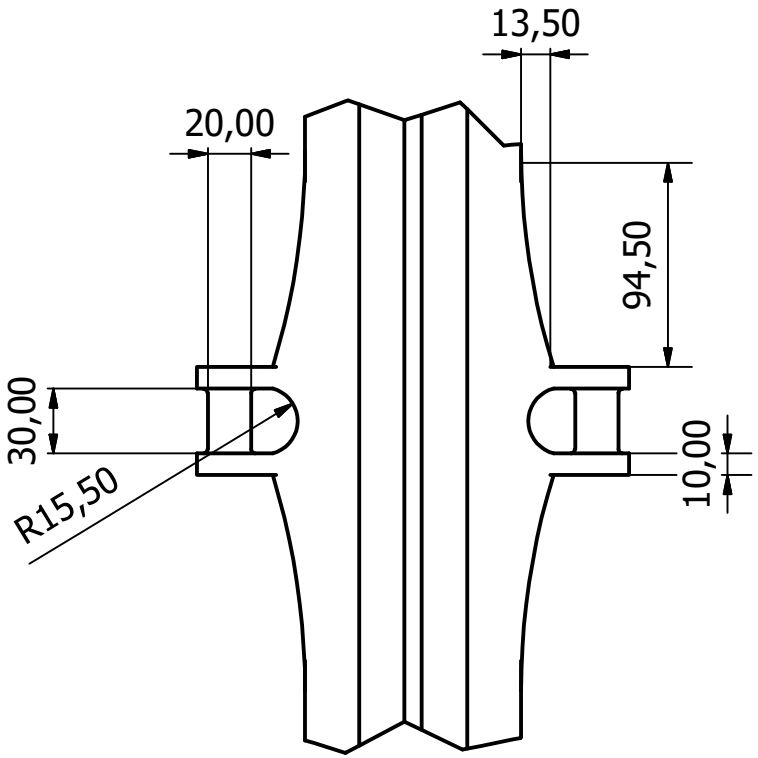

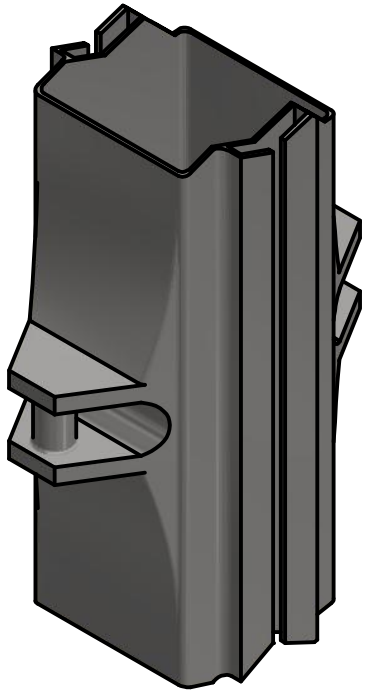

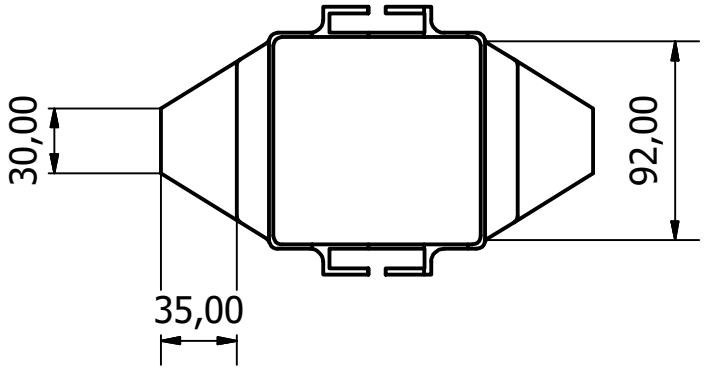

Brad Fell	1:3.5
	1/10/2016
Upper & Lower Guy Cable Attachment Point	
USQ Project 2016	

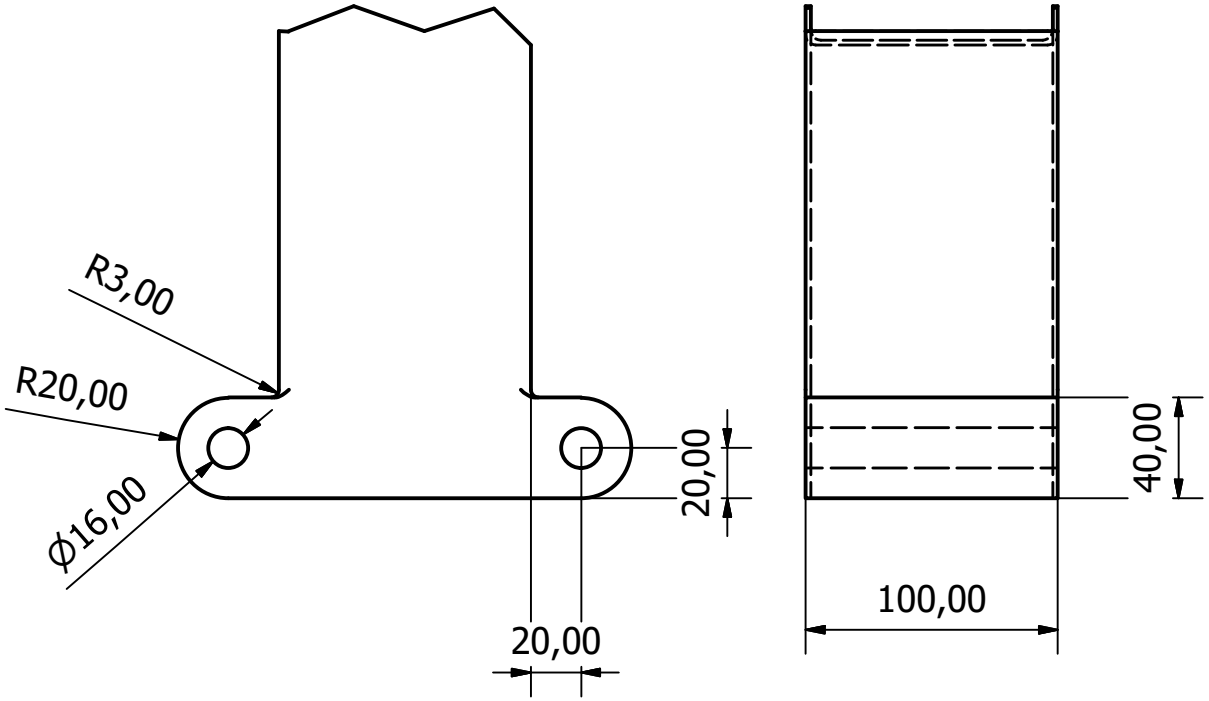

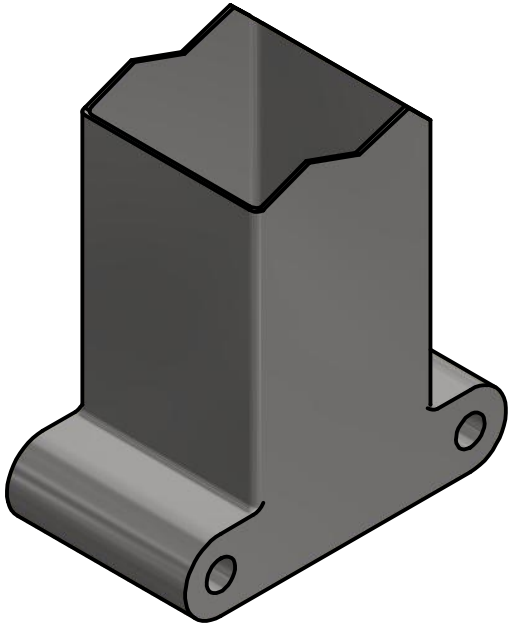

A

Brad Fell	1:3
	1/10/2016
Post Base Connection Hinges	
USQ Project 2016	

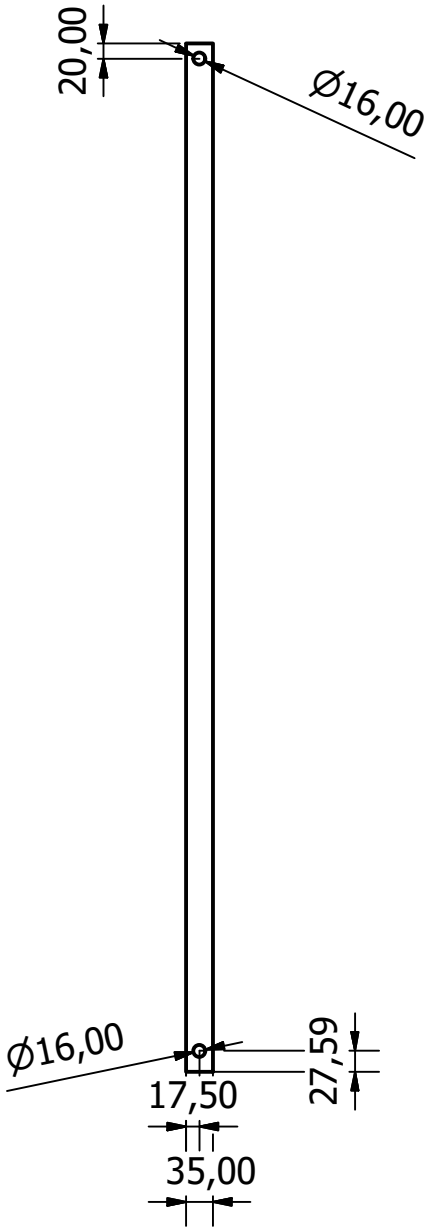

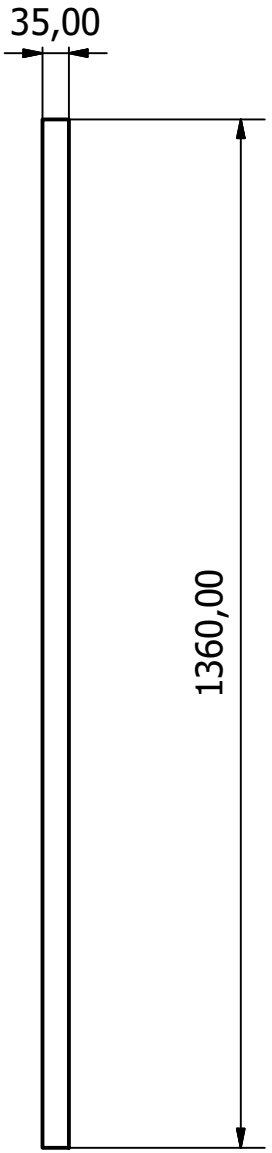

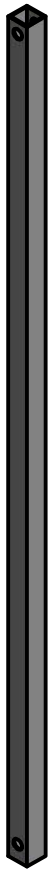

Brad Fell	1:10
	6/10/2016
Winch Support Strut	
USQ Project 2016	

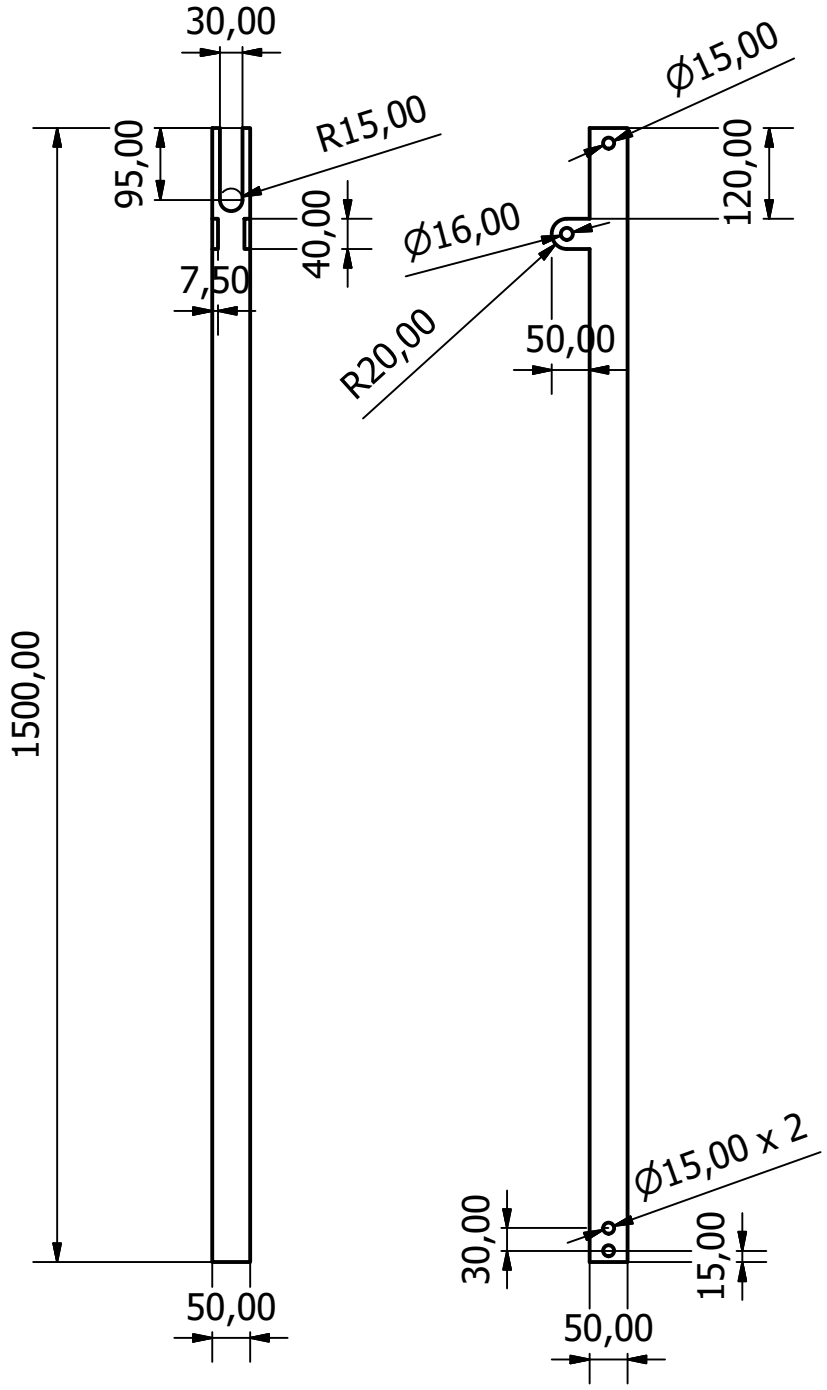

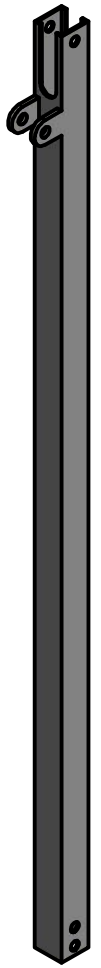

Brad Fell	1:10
	6/10/2016
Main Winch Post	
USQ Project 2016	

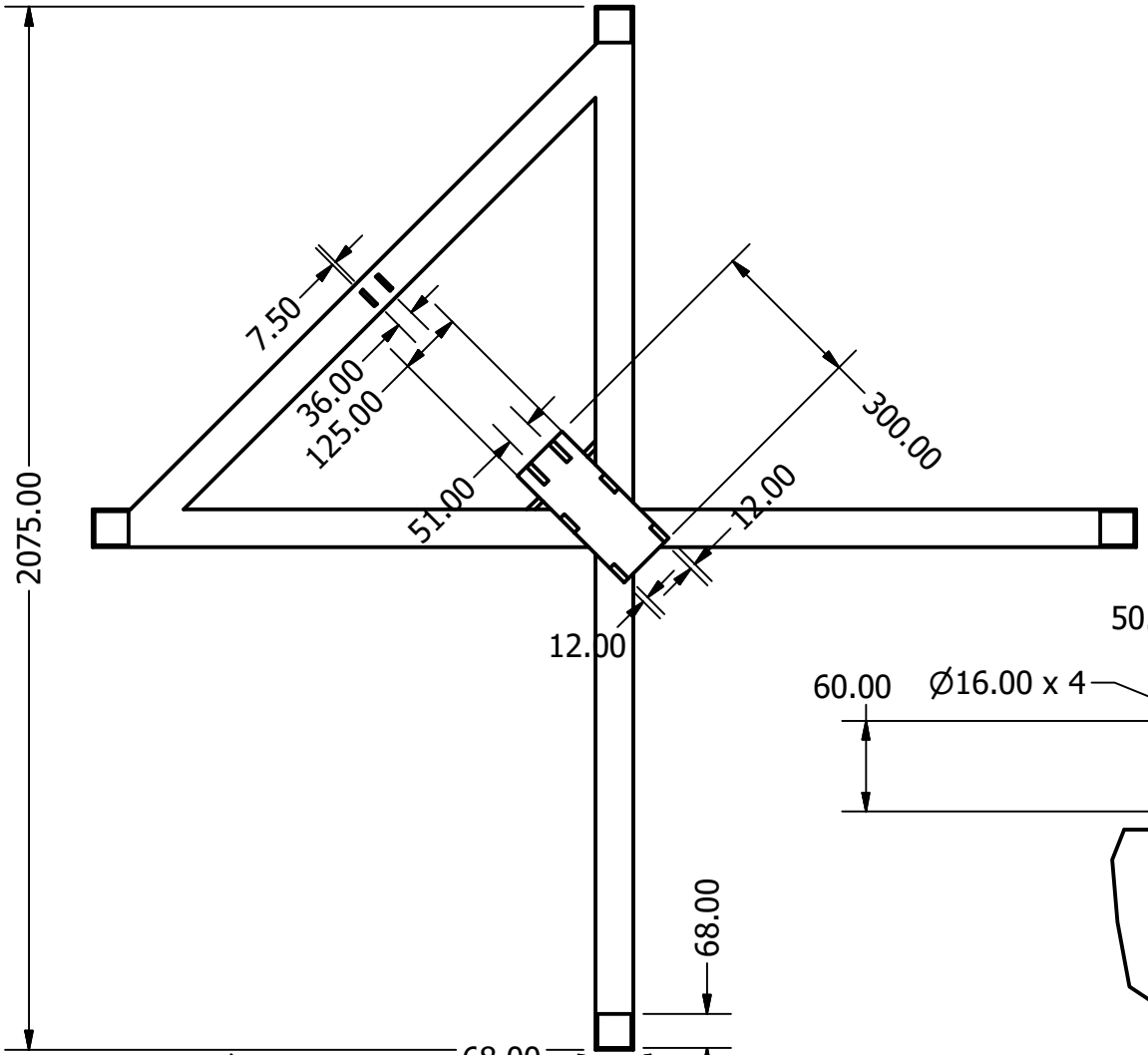

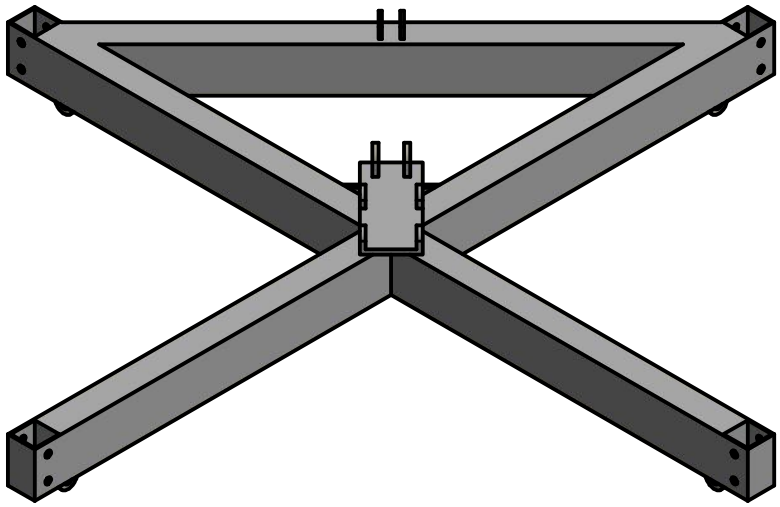

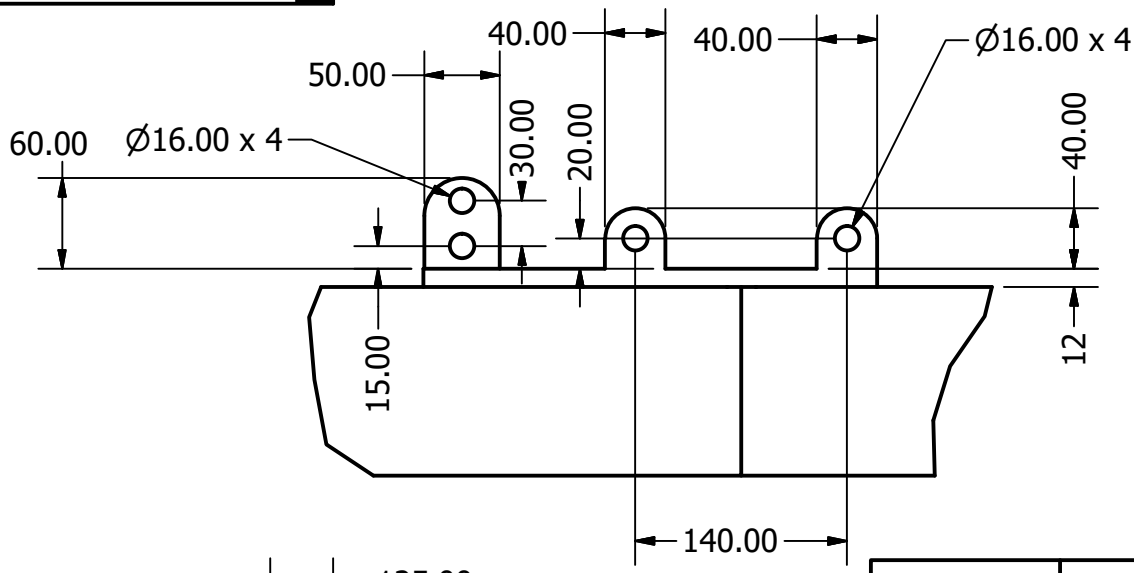

Brad Fell	1:15
33.47 kg	4/10/2016
Fence Base	
USQ Project 2016	

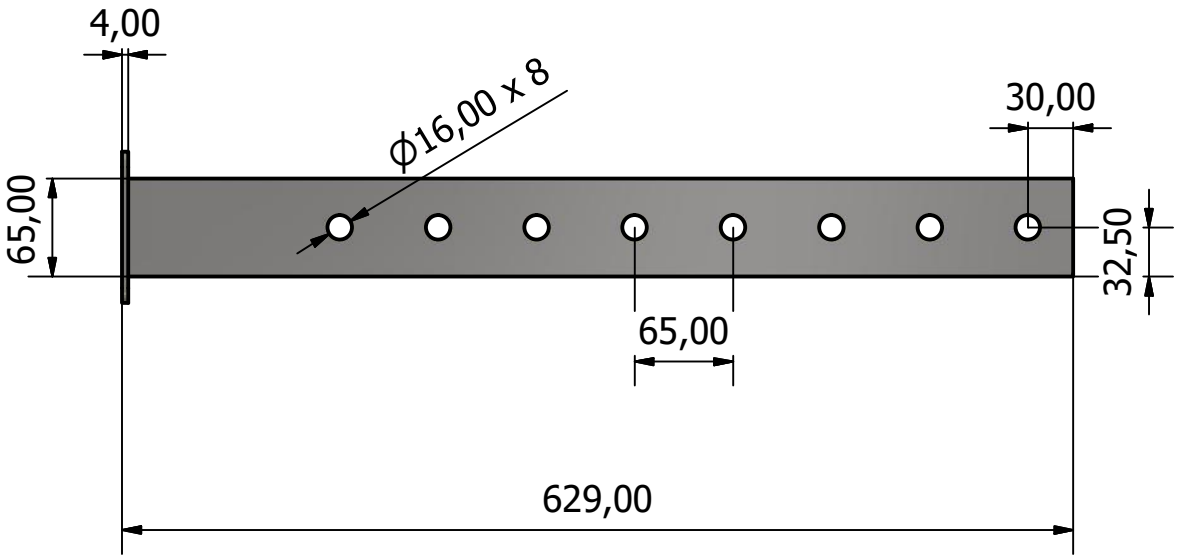

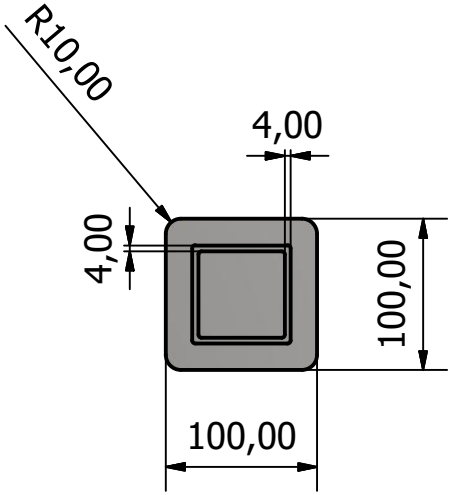

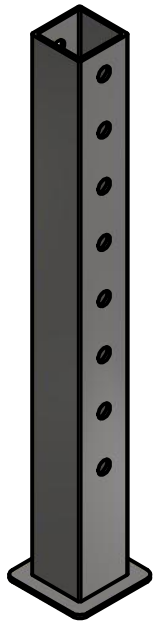

Brad Fell	1:5
4.98 kg	4/10/2016
Fence Base Leg	
USQ Project 2016	

50mm Spirafix™ Ground Anchor Load Chart

Spirafix Limited
Unit 3 Wern Industrial Estate, Rogerstone
Newport NP10 9FQ United Kingdom
Tel: +44 (0)1633 890910
Email: sales@spirafix.com Website: www.spirafix.com

Designed & Manufactured In Britain

50mm Diameter Spirafix™ Vertical Maximum Working Tensile Loads

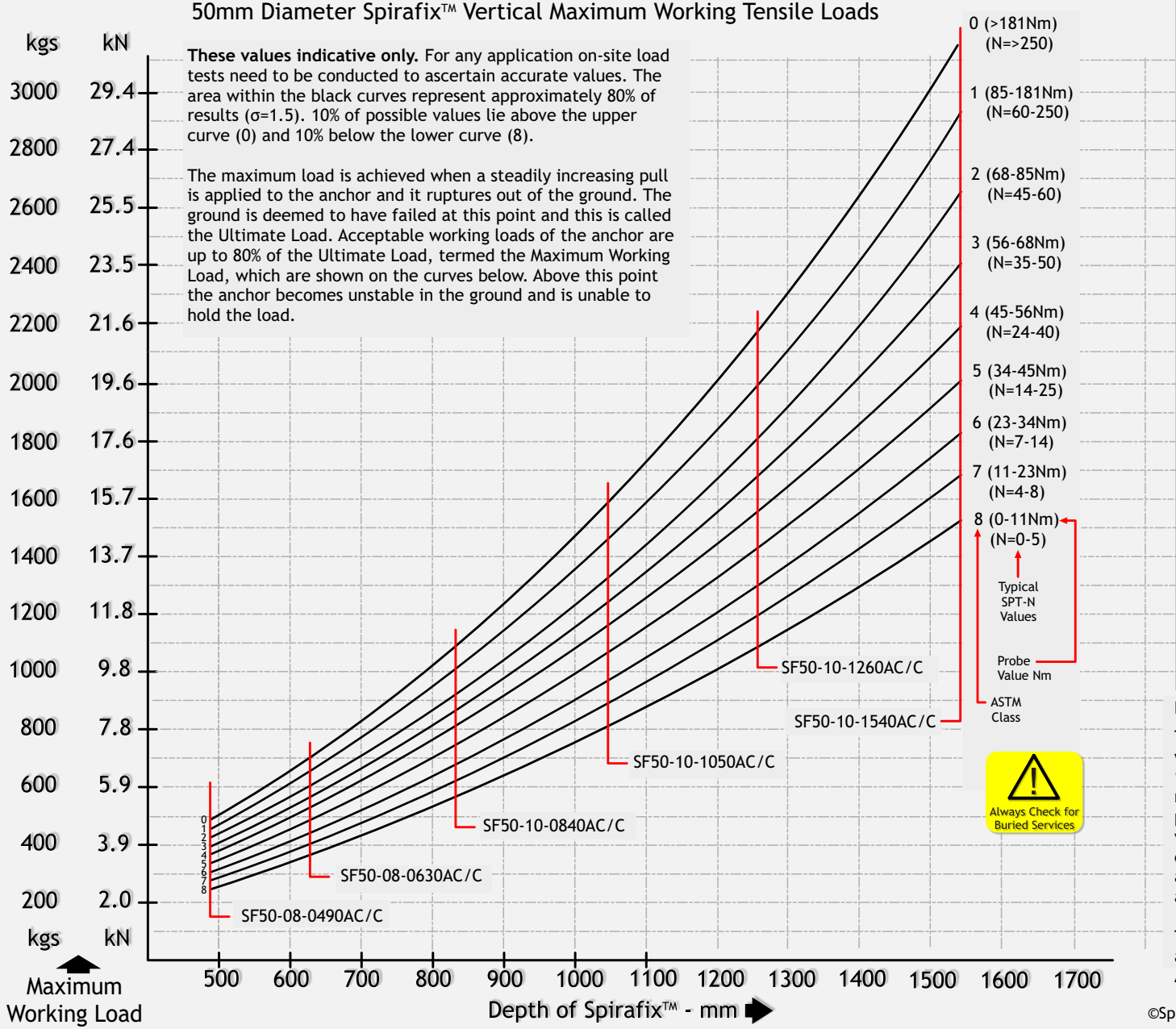

These values indicative only. For any application on-site load tests need to be conducted to ascertain accurate values. The area within the black curves represent approximately 80% of results (σ=1.5). 10% of possible values lie above the upper curve (0) and 10% below the lower curve (8).

The maximum load is achieved when a steadily increasing pull is applied to the anchor and it ruptures out of the ground. The ground is deemed to have failed at this point and this is called the Ultimate Load. Acceptable working loads of the anchor are up to 80% of the Ultimate Load, termed the Maximum Working Load, which are shown on the curves below. Above this point the anchor becomes unstable in the ground and is unable to hold the load.

Soil Classification

Basic Soil Type	Sub Group	Compaction/ Strength	SPT-N	ASTM Class
Sands	Sand	Very Loose	0-3	8
		Loose	3-8	5
		Compact	8-30	3
		Cemented	30-58	1
	Sandy Clay/ Sandy Silt	Soft	3-8	5
		Firm	8-30	3
		Stiff	30-58	1
Silts	Silts	Very Soft	7-14	6
		Soft	14-25	5
		Firm	25-60	4
	Silty Clay	Soft	7-14	6
		Firm	14-25	5
		Stiff	25-60	4
Clays	Clay	Very Soft	0-5	8
		Soft	4-8	7
		Firm	7-14	6
		Stiff	14-25	5
		Very Stiff	35-60	3
		Hard	>60	1
Peats	Organic Clay Silt or Sand	Firm	0-5	8
	Peat	Spongy	0-5	8
		Plastic	0-5	8
Chalks	Very Weak		0-25	6
	Weak		25-100	2
	Moderately Weak		100-250	1
	Moderately strong to very strong		>250	0

Notes:

The above classifications are outlined in BS 5930 with the exception of chalk and the “Sands” and “Clays” sections have been expanded. Also chalk is not covered in the ASTM classification, but for the purposes of predicting loads it has been assigned values. The range of pull out loads in strong chalks can be considerably higher than shown on the chart and field tests need to be carried out to obtain accurate values.

The Standard Penetration Test (SPT) N values quoted above are in accordance with BS1377:1990 Part9, ASTM Standard D1586-84 and AS 1289.6.3.1-1993

 DS1412